Norwegian University
of Life Sciences

Master's Thesis 2019 60 ECTS
Faculty of Chemistry, Biotechnology and Food Science

Characterization of a thermostable exolytic alginate lyase from hot vents in the Arctic Mid-Ocean Ridge

Bjørn Pedersen
Biotechnology

ACKNOWLEDGEMENTS

The present work was carried out at the faculty of Chemistry, Biotechnology and Food Science at the Norwegian University of Life Sciences (NMBU) from August 2018 to May 2019, with Vincent Eijsink, Magnus Øverlie Arntzen and Lasse Fredriksen as supervisors. The research was funded by Foods of Norway.

First of all, a huge thanks goes out to my supervisors for guiding and helping me during the work with this thesis. I would like to thank my main supervisor Vincent for the opportunity to work on this subject and for providing very helpful inputs and feedback. Thank you to Magnus for all your help in the lab and for the guidance along the way. Thank you to Lasse for your supervision in the initial parts of the work.

I would also like to thank the other people in the Protein Engineering and Proteomics (PEP) group who have been very kind and helpful. Thanks also to my family for their support and encouragement, and to my fellow master's students at the lab for fruitful discussions and good company.

Ås, May 2019

Bjørn Pedersen

Sammendrag

Verdens behov for petroleumsprodukter øker stadig, men minkende oljereserver og miljøproblemer gjør at det bør prioriteres utvikling og bruk av alternative, fornybare ressurser. Bioraffinering dreier seg om å bruke biomasse som karbonkilde for produksjon av energi og nyttige kjemikalier/materialer. Makroalger er et eksempel på en biomasse med egenskaper som gjør den relevant for bruk i framtidige bioraffinerier. Denne studien undersøker egenskapene til et rekombinant enzym, Apl17-2, som depolymeriserer alginat, som er en viktig bestanddel av brune makroalger.

Ved bruk av 3,5-dinitrosalisylsyre (DNS) metoden for deteksjon av reduserende ender, ble det fastslått at Apl17-2 er aktiv på alginat, poly mannuronat (M) og poly guluronat(G). Aktivitetstesting av to tyrosin til alanin mutanter, Y251A og Y446A, viste at Tyr251 er viktig for enzymets aktivitet, mens Tyr446 ikke er det. Apl17-2 ble videre karakterisert med alginat som substrat, og det ble funnet at enzymet foretrekker 0.3 M NaCl, og har optimal pH og temperatur på omtrent henholdsvis 4.8 og 60 °C. Som et eksempel på termisk stabilitet, beholdt enzymet 100% relativ aktivitet etter 24 timers preinkubasjon på 60 °C.

Enzymets virkemåte ble undersøkt ved dyptgående produktanalyse ved hjelp av high performance anion exchange chromatography with pulsed amperometric detection (HPAEC-PAD), UV-absorpsjon og matrix assisted laser desorption time of flight (MALDI-TOF) mass spectrometry (MS).

Basert på resultatene fra HPAEC-PAD analyse, ble det bestemt at Apl17-2 er en eksolytisk alginat lyase som jobber fra ikke-reduserende ende av substratet og kan bryte ned dimerer og lengre kjeder av substrat med metta- eller umetta ikke-reduserende ender. Alginat med umetta ikke-reduserende ender genereres av aktiviteten til endolytiske alginat lyaser. Apl17-2 genererte monomerprodukt kontinuerlig og lagde intermediære kjeder med umetta ikke-reduserende ender. Monomerproduktet absorberte UV-stråling på 235 nm med avtagende verdier i løpet av 24 timer. Disse resultatene tyder sterkt på at Apl17-2 er en oligo-alginat lyase (EC 4.2.2.26) som opererer i tråd med den konvensjonelle β-eliminasjons mekanismen til polysakkarid lyaser (PL). Sammenlignet med andre oligo-alginat lyaser som har blitt funksjonelt karakterisert, er Apl17-2 blant de mest termostabile og har lavest pH-optimum, som kan være nyttig for anvendelser i industrielle bioprosesser.

Abstract

The world's demand for petrochemicals is rising, but depletion of oil reserves and environmental concerns encourage the utilisation of alternative, renewable resources. Biorefineries are based around the concept of using biomass as a carbon source for generating energy and useful chemicals/materials. Macroalgae (seaweed) have properties that make them and interesting and relevant biomass for use in future biorefineries. This study investigates the properties of a recombinantly produced enzyme, Apl17-2, that depolymerises alginate, which is a major component of brown macroalgae.

Using the 3,5-dinitrosalisylic acid (DNS) method for detection of newly generated reducing ends, Apl17-2 was found to be active on alginate, poly mannuronate (M) and poly guluronate (G). Two tyrosine to alanine point-mutants, Y251A and Y446A, were also tested for activity, showing that Tyr251 is important for activity whereas Tyr446 is not. Using alginate as substrate, Apl17-2 was further characterized, showing that the enzyme prefers 0.3 M NaCl, and has pH and temperature optima for activity of approximately 4.8 and 60 °C, respectively. As an example of thermal stability, the enzyme retained 100% relative activity after 24 hours of pre-incubating at 60 °C.

The enzyme's mode of action was analysed by in-depth product analysis using high performance anion exchange chromatography with pulsed amperometric detection (HPAEC-PAD), UV-absorption and matrix assisted laser desorption time of flight (MALDI-TOF) mass spectrometry (MS).

Based on the results of HPAEC-PAD-analysis, Apl17-2 was found to be an exolytic alginate lyase that operates from the non-reducing end of the substrate and is capable of breaking down dimers and longer chains of saturated and unsaturated substrates. Unsaturated alginate, i.e. alginate with an unsaturated sugar at the non-reducing end, is a product of the activity of endotype alginate lyases. The enzyme continuously generated monomeric products and intermediate chains with unsaturated non-reducing ends. The monomeric product was found to be UV-active at 235 nm with decreasing absorption over 24 hours. These findings strongly indicate that Apl17-2 is an oligo-alginate lyase (EC 4.2.2.26) that operates in accordance with the canonical β-elimination mechanism of PL-enzymes. Interestingly, compared to other functionally characterized oligo-alginate lyases, Apl17-2 has the lowest pH optimum and is among the most thermostable, which may be useful in bioprocess applications.

Abbreviations

CAZY	Carbohydrate-Active Enzymes
DEHU	4-deoxy-L-*erythro*-5-hexoseulose uronic acid
DNS	3,5-dinitrosalisylic acid
G	α-L-guluronic acid
GE	Glucose Equivalent
HPAEC-PAD	High Performance Anion Exchange Chromatography with Pulsed Amperometric Detection
LB	Lysogeny Broth
LIC	Ligation Independent Cloning
M	β-D-mannuronic acid
MALDI-TOF	Matrix Assisted Laser Desorption Time of Flight
MS	Mass spectrometry
PCR	Polymerase Chain Reaction
PL	Polysaccharide Lyase
SDS-PAGE	Sodium Dodecyl Sulfate–Polyacrylamide Gel Electrophoresis
SOE-PCR	Splicing by Overlap Extension – Polymerase Chain Reaction
TB	Terriffic Broth
WT	Wild Type
w/v	weight/volume
Δ	4-deoxy-L-*erythro*-hex-4-enopyranuronate (monomer)

Table of contents

1 Introduction

1.1 Towards greener fuels and materials

Environmental problems and decreasing amounts of fossil resources calls for a transition to more sustainable alternatives for production of energy, fuels and other chemicals and materials that are produced by the petroleum industry today. Biorefineries aim to utilise biomass to produce products that can replace those produced by oil refineries today. In the broadest terms, these products can be divided into energy products and chemical/material products. They may be identical to those produced from fossil sources, or different-, but with similar functions (Cherubini, 2010).

The majority (84%) of the 102.4 billion litres of bioethanol produced worldwide in 2017 came from American corn (58%), and Brazilian sugar cane (26%) (Renewable Fuels Association, 2019). At least one third of all the corn produced in the US. in 2018 was used to produce bioethanol (USDA, 2019). Lignocellulose is an important alternative to food crops that have seen a promising development in recent years with regards to the efficiency of cellulose depolymerization to fermentable sugars and utilization in a biorefinery concept. Macroalgae (seaweed) and especially brown seaweed provide another promising alternative and the enzymatic conversion of macroalgal polysaccharides is the main topic of this study.

1.2 Seaweed

Seaweed are macroalgae that grow along coastlines and shallow banks where sufficient sunlight can reach them to enable photosynthesis. Some species, such as *Sargassum natans* and *S. fluitans* even drift freely at the surface of the open sea. Seaweeds create the foundation of many marine ecosystems and provide food and shelter for an abundance of organisms. They can be divided into three main taxonomic categories that do not have a common multicellular ancestor: red-, green- and brown seaweeds. The following paragraphs will focus on brown seaweed since alginate, which is the most relevant component for the subject of this thesis, is only found in brown seaweed.

The main carbohydrates in brown seaweed are alginate, cellulose, laminarin, mannitol and fucoidan. Alginate is an unbranched co-polymer of mannuronic- and guluronic acid and will be discussed in more detail later. Cellulose and laminarin are both glucose polymers, but with different linkages, β-1,4 in

cellulose and β-1,3 in laminarin. Laminarin consist of two types of glucose-polymer chains where G-chains are pure glucose and M-chains have a mannitol residue at the reducing end. Mannitol is a sugar alcohol that is produced as one of the main primary products in photosynthetic organisms and which are abundant in brown macroalgae. Fucoidan is a complex sulphated polymer where L-fucose is the main component, and may in addition contain small fractions of galactose, mannose, xylose, glucose or glucuronic acid. Alginate, cellulose and fucoidan are structural carbohydrates that are found within the cell walls and in the extracellular space. Together they contribute to maintain the seaweed's shape and physical properties. Laminarin and mannitol are storage carbohydrates that provide a source of carbon and energy when needed (Stiger-Pouvreau et al., 2016). Polyphenols are found mainly in brown seaweed stipes and are of interest to pharmaceutical and nutritional companies (Scheiner et. al, 2015).

The amount of the different components in seaweed varies between species and within the body of the individual organism. Stipes generally contain substantially more alginate than the fronds, which are richer in metabolic carbohydrates i.e. sugars like mannitol and laminarin (McKee et al., 1992; Schiener et al., 2015). In addition, there is seasonal fluctuation for several of the components, although alginate and cellulose are relatively stable compared to mannitol and laminarin (Schiener et al., 2015). Table 1 is based on the findings of Schiener and co-workers (Schiener et al., 2015) and lists the occurrence of selected components in the brown macroalgae *Laminaria hyperborea* and provides information about seasonal variation.

Table 1: Selected components of *L. hyperborea*.
The table is based on data collected by (Schiener et. al, 2015) and represent the average composition of L. hyperborea through seasonal variation from August 2010 to October 2011. The samples were harvested along the Scottish coast outside of Clachan at 56°N.

	Average amount of dry mass [%]	Seasonal variation
Alginate	33.2 ± 3.8	(Relatively stable)
Mannitol	17.5 ± 7.4	max. 25%, min. 7%
Cellulose	11.1 ± 1.0	(Stable through the season)
Laminarin	7.4 ± 8.0	max. 25%, min. 2%
Protein	6.8 ± 1.3	max. 8.1%, min. 4.3%
Polyphenol	0.15 ± 0.04	max. 0.23%, min. 0.10%
(Water)	(87.2 ± 2.2)*	

**percentage of total, undried mass.*

Commercial use of seaweeds constitutes a large industry with global annual value exceeding 6 billion US $, with about 85% of the value being generated from food products for human consumption, and most of the remaining part being obtained from various uses of extracted carbohydrate polymers like alginate, agar and carrageenan (FAO, 2018; Roesijadi et al., 2010). The carbohydrates alginate, agar and carrageenan belong to a class of compounds called phycocolloids and have a range of applications in for example paints, lotions, food products, pill capsules, agar culture plates, as bioink in regenerative medicine and many more (Axpe & Oyen, 2016; Pomin, 2012). Alginate is extracted from brown seaweed while agar and carrageenan originates from red seaweed (Pomin, 2012). In contrast to land-based alternatives, seaweed does not require land area, fresh water, fertilizer or pesticides. In 2015, 1.1 million tonnes of seaweed were harvested and 29.4 million tonnes were farmed in aquaculture with well over 90% of the farmed seaweed produced in Asia (FAO, 2018).

There are different ways of utilizing seaweed for energy and materials. When it comes to harvesting the internal energy of the seaweed, there are two main categories: 1) those that require drying (combustion, pyrolysis, gasification and transesterification) and 2) those that can work on the wet biomass (hydrothermal treatment, fermentation to e.g. bioethanol or biobutanol and anaerobic digestion methane (Milledge et al., 2014). Since the water content of raw seaweed is very high; 80-90%, either low energy drying or other methods should be used to avoid significant negative impact on the energy return on investment (EROI) (Milledge et al., 2014). High drying temperature has been shown to negatively affect the subsequent enzymatic saccharification, with the optimal drying temperature determined to be 30 °C for the brown seaweed *Saccharina latissima* (Sharma & Horn, 2016). However, since seaweed doesn't contain lignin which complicates the utilization of land based alternatives in biorefineries (Kumar & Sharma, 2017), simple pre-treatment like milling and leaching may be sufficient to increase the availability of carbohydrates for depolymerization and fermentation (Enquist-Newman et al., 2014; Wargacki et al., 2012).

More detailed investigation of profitable processing pipelines for brown macroalgae have been conducted by Svein J. Horn (Horn, 2009), Enquist Newman et al. and Bio Architecture Lab Inc. in collaboration with Harris Group Inc. (Washington, U.S.A.) and EcoShift Consulting (California, U.S.A.) (Enquist-Newman et al., 2014).

1.3 Alginate

Alginate is a structural carbohydrate in the cell walls of brown macroalgae as salts of calcium, magnesium and sodium (McHugh, 2003). It has been found to comprise up to 40% of the dry mass of *Laminaria hyperborea* (Horn et al., 1999). It is also produced by some species of bacteria of the genera *Azotobacter* and *Pseudomonas*. Alginate is a linear co-polymer of β-D-mannuronic acid (M) and α-L-guluronic acid (G) with 1-4 linkages (Figure 1). Within physiological pH-ranges, the majority of M and G residues are deprotonated to mannuronate and guluronate, but both terms are generally used to refer to the alginate residues, in the literature and in this thesis. M and G are C5-epimers of each other, which means that the only structural difference between them is that they have the carboxyl group facing in opposite directions. Since they have the carboxyl group on different sides, M and G have opposite chair conformations as the carboxyl group will be in the energetically favoured equatorial state (Gacesa, 1988). It follows that M-M bonds are equatorial and G-G bonds are axial (Figure 1).

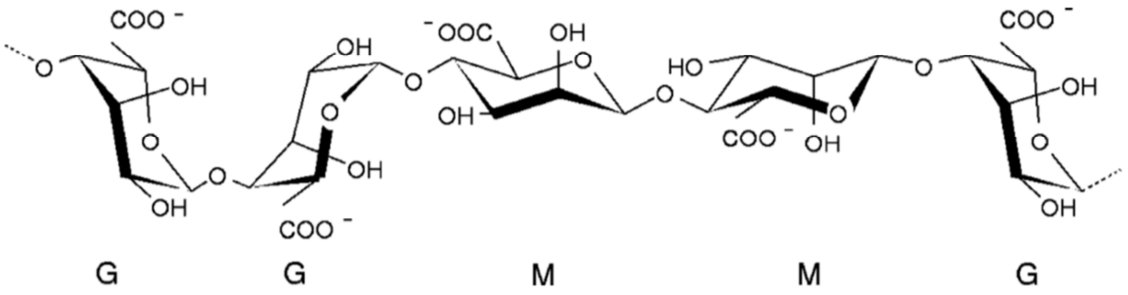

Figure 1: **Geometries of G and M residues in alginate.** The scheme shows how the different bonds are structurally arranged. The axial configuration of the G-G bonds means that blocks of poly G will have a denser and different structure from blocks of poly M and alternating MG residues. The figure is reused from (Sikorski et al., 2007) with permission from the American Chemical Society.

The alginate polymer is composed of blocks of poly M, poly G and blocks of strictly alternating M- and G residues (Haug et al., 1967). As mentioned above, alginate content varies greatly between different species of brown seaweed, the same applies to the ratio of M to G and the distribution of the different block-types, which are important for the properties of the alginate polymer (Lee & Mooney, 2012). This variation means that alginate is not a single compound with defined properties, but rather a group of polymers with similar building blocks and 1,4-glycosidic bonds. The alginate content also depends on the growth conditions. Seaweeds that grow in turbulent areas have higher alginate content to help them withstand the forces and keep them intact (McHugh, 2003; Pomin, 2012).

The viscosity of alginate is affected by the pH of its environment, chelate-binding of divalent cations, polymer length, but not so much on temperature. Lower pH increases the degree of protonated uronic acids, and thereby increase the ability of polymeric chains to form hydrogen bonds and create more viscous solutions. This effect is maximized in the pH range 3-3.5 (Lee & Mooney, 2012). Viscosity is also affected by the presence of ions, and especially divalent cations like Ca^{2+} and Mg^{2+}. While all blocks of alginate are polyanionic in solution and can form ionic bonds to cations (Gacesa, 1988), studies indicate that in alginate, only the G-blocks can coordinate divalent cations in chelate binding and promote gelation. A similar effect was not observed for poly M-blocks or MG-blocks (Grant et al., 1973). The addition of Ca^{2+} ions to solubilised alginate, displaces sodium ions and lead to gel-formation (McHugh, 2003). Thus, alginate rich in poly G, are able to form more rigid gels than those with low poly G content (Smidsrød et al., 1972). Based on their investigation of bond angles in the chelate coordinated poly G-blocks by circular dichroism, and previously known coordination geometries, Grant and co-workers proposed an "egg box model" (Figure 2) for how the G-residues coordinate the calcium ions (Grant et al., 1973).

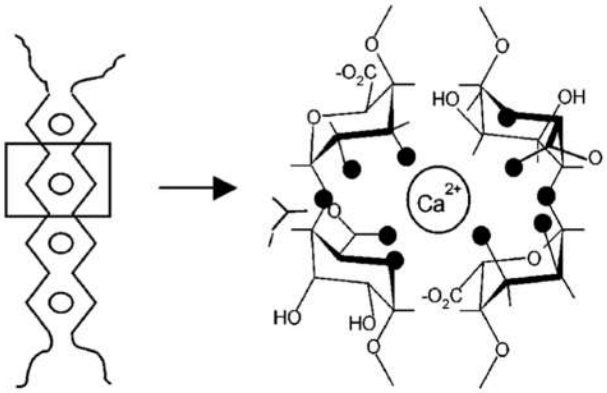

Figure 2: **Illustration of the "egg box model" of Ca^{2+} binding by poly G.** The figure shows how Ca^{2+} ions are thought to hold chains of alginate together by interacting with poly G residues in a manner that resembles an egg box. The black dots represent the oxygen atoms involved in the coordination of the Ca^{2+}-ion. The figure is reprinted from (Braccini & Pérez, 2001) with permission from the American Chemical Society.

The size of the polymers is also important with regards to viscosity. The molecular weight of commercial sodium alginates (as were used in this study) varies from 32000 to 400000 g/mol (Lee & Mooney, 2012). This translates to polymer lengths of about 170 to 2280 residues. In contrast to gels of agar, agarose or carrageenan, alginate forms thermostable gels that can maintain stability at temperatures over 100 °C (Gacesa, 1988). Since the value of whole alginate is largely dependent on the strength of its gelling properties, alginates with high poly G content are extra valuable because of their ability to form chelate bonds with divalent cations and promote gel formation (Gacesa, 1988;

McHugh, 2003). Poly G-rich alginates may be obtained by the activity of exolytic M-lyases (Wang et al., 2018) or by C5-epimerases that act stereospecifically to turn mannuronic acid residues into guluronic acid. C5-epimerases may also be used more selectively to finetune alginate composition for highly valuable ultrapure, defined alginate products (Ertesvåg, 2015).

1.4 Bacterial alginate

Bacterial alginate synthesis was first discovered in *Azotobacter vinelandii* (Gorin & Spencer, 1966) and *Pseudomonas aeruginosa* (Linker & Jones, 1966). *P. aeruginosa* is a common bacterium that is present throughout nature, but it is also an opportunistic pathogen that infect the lungs of vulnerable individuals and is the major cause of death in cystic fibrosis patients. It is hypothesised that the alginate produced by the bacterium plays a vital role in its resistance to the host immune system and antibiotics by forming a protective biofilm barrier around the bacteria (May et al., 1991). *A. vinelandii* is a nitrogen-fixing soil bacterium that form protective cysts where alginate is a major component (Sabra et al., 2001).

Spontaneous alginate-producing mutants have been isolated from *Pseudomonas fluorescens*, *P. putida* and *P. mendocina*. The fact that these mutants were generated spontaneously, indicates that the alginate-producing genes are present in these bacteria, but have been repressed (Govan et al., 1981). Bacterial alginate is characteristically dissimilar to algal alginate, and the differences go beyond the variation between algal species. In contrast to algal alginate which is not acetylated, bacterial alginate is O-acetylated at the O2 and O3 positions of only mannuronate residues (Linker & Jones, 1966; Skjåk-Bræk et al., 1986). The O-acetyl groups can readily be removed by alkaline treatment using 0.1 M NaOH, 25 °C for 20 min, and are therefore not present in bacterial alginates obtained by alkaline extraction (Gacesa, 1988; Linker & Jones, 1966). O-acetylated mannuronate residues are protected from C5-epimerisation and from the action of some alginate lyases (Davidson, I. et al., 1977; Ertesvåg, 2015), as bacterial alginate is synthesised as poly M before selective epimerisation to give block segments analogous to algal alginate (Pindar & Bucke, 1975). Acetylation also increase the viscosity and the water-binding capacity of the alginate (Ertesvåg, 2015; Skjåk-Bræk et al., 1989).

Bacterial alginate is not produced commercially today. If it was, it would likely be extra valuable since a defined bacterial monoculture would produce predictable amounts of alginate of consistent composition (Sabra et al., 2001).

1.5 Applications of alginate

Because of its low toxicity and gelling properties, different variants of alginate polymers and oligomers are used in a wide range of applications from food- and textile industry to medical industry (Lee & Mooney, 2012; McHugh, 2003; Szekalska et al., 2016). To the authors knowledge, there is no current commercial use of alginate monomers, but there are indicators of potential for future production of a broad variety of products with the use of microbial digestion and fermentation. A few examples are reported later in the introduction, and possible future aspects will be further addressed in the discussion.

1.6 Alginate lyases

Alginate lyases are enzymes that depolymerise alginate. They have been found in a range of organisms such as bacteria, marine fungi, animals, algae and viruses (Wong et al., 2000). They are categorised under the polysaccharide lyase (PL) class in the carbohydrate active enzyme (CAZy) database. The CAZy database groups enzymes that cleave, modify or create glycosidic bonds into classes, families and subfamilies based on sequence similarity of their functional domains (Lombard et al., 2010).

The majority of alginate lyases are classified into PL families 5, 6, 7, 14, 15, 17, and 18 (Peng et al., 2018). There are currently three types of alginate lyases: Mannuronate-specific that cleave M-M and M-G bonds (EC 4.2.2.3), guluronate-specific that cleave G-G and G-M bonds (EC 4.2.2.11) and oligo-alginate lyases that can exolytically degrade the unsaturated oligomers produced by endolytic alginate lyases (EC 4.2.2.26). Alginate lyases can be divided into two categories with regards to function; endolytic- and exolytic alginate lyases. Terms like endotype and exotype are also used and also endolyase and exolyase (Preiss & Ashwell, 1962a). Most endolytic alginate lyases are found in PL5 and PL7 while exolytic ones are only found in PL6, PL7, PL14, PL15 and PL17 (Zhu & Yin, 2015). Endolytic alginate lyases break glycosidic bonds within the polymer chain while exolytic ones cleave off monomeric residues from the end of the chain. While endolytic alginate lyases may be of great use in enzyme cocktails for degrading the polymers, exolytic lyases will be necessary to achieve saccharification which is essential for further digestion and fermentation by microbes. Depending on their properties, endolytic lyases convert alginate to di-, tri-, tetra- or pentamers (Ertesvåg, 2015), while exolytic lyases may have similar limitations for catalysing such small oligomers, they continuously generate monomers from polymers. Saccharification can also be achieved by thermochemical means, but enzymatic conversion is generally considered more sustainable (Horn et al., 2012).

Most of the identified alginate lyases are endolytic, but at least twelve exolytic alginate lyases have been found: A1-IV from *Sphingomonas sp*. A1 (Miyake et al., 2003), Atu3025 from *Agrobacterium tumefaciens* (Ochiai et al., 2006), AlgL from *Sphingomonas* sp. MJ-3 (Park et al., 2012), Alg17c from *Saccharophagus degradans* 2-40 (Kim et al., 2012), AlyA5 from *Zobellia galactanivorans* (Thomas et al., 2013), OalA, OalB and OalC from *Vibrio splendidus* (Jagtap et al., 2014; Wargacki et al., 2012), OalS17 from *Shewanella* sp. Kz7 (Wang et al., 2015), OAL from *Stenotrophomonas maltophilia* KJ-2 (Shin et al., 2015), ZH0-IV from *Sphingomonas* sp. ZH0 (He et al., 2018) and TcAlg1 from *Thalassotalea crassostreae* (Wang et al., 2018). At the time of writing, the structure of only two exolytic alginate lyases have been determined: Alg17c from PL17 (Park et al., 2014) and Atu3025 from PL15 (Ochiai et al., 2010). Alg17c is the only enzyme in the PL17 family whose structure has been resolved.

1.6.1 Catalytic mechanism

All enzymes of the polysaccharide lyase group, including both endolytic and exolytic alginate lyases, cleave the glycosidic bonds of uronic acid-containing polysaccharides by a process called β-elimination (Lombard et al., 2010). In β-elimination, the glycosidic bond is broken between C4 and O4 and the overall mechanism can broadly be summarised in three steps as hypothesised by Gacesa in 1987: The first step is the neutralisation of the negative charge of the carboxyl group. This decreases the pKa of the C5-hydrogen and makes it easier to separate from the carbon which is what happens in the next step: a proton-abstracting base removes the hydrogen on C5 to create a resonant enolate anion intermediate. Lastly, there is a β-elimination of the C4-O4 bond to form a double bond between C4 and C5 (Gacesa, 1987; Garron & Cygler, 2010). A Brønsted base, and -acid is needed to remove the H5 hydrogen and to donate a proton to the oxygen of the broken glycosidic bond (Garron & Cygler, 2010). The overall β-elimination results in a new reducing end and a C4-C5 unsaturated residue on the other side of the bond cleavage; at a new non-reducing end. The actual β-elimination itself is an $E1_{cb}$ reaction that proceeds via an anion transition state (Yip & Withers, 2006). Because the various substrates of PL-enzymes (including M and G) have different stereochemistry, the exact details of the mechanism will vary between the PL-enzymes with regards to which residues that are involved and exactly how the bond breakage is done. However, some interesting commonalities have been reported; according to Garron and Cygler (2010), PL-enzymes can be divided into two categories with regards to the carboxyl-neutralising agent and the catalytic Brønsted base and -acid. In one group, the anionic carboxyl is neutralised by a metal ion (Ca^{2+} or Mn^{2+}) with water as the catalytic base and lysine or arginine as the catalytic acid. In the other group, asparagine/glutamine or protonated aspartate/glutamate neutralise the negative charge on the substrate-carboxyl, while tyrosine or histidine acts as the catalytic base and

tyrosine as the catalytic acid (Garron & Cygler, 2010). The large majority of identified alginate lyases are part of the latter group, but PL6 alginate lyases are an exception.

There are two subcategories of β-elimination: *syn* and *anti*-elimination. The type is dependent on the conformation of the monomeric residue in the active site; whether the H5-hydrogen and O4-oxygen are on the same (*syn*) or opposite sides (*anti*) (Figure 3) (Lombard et al., 2010).

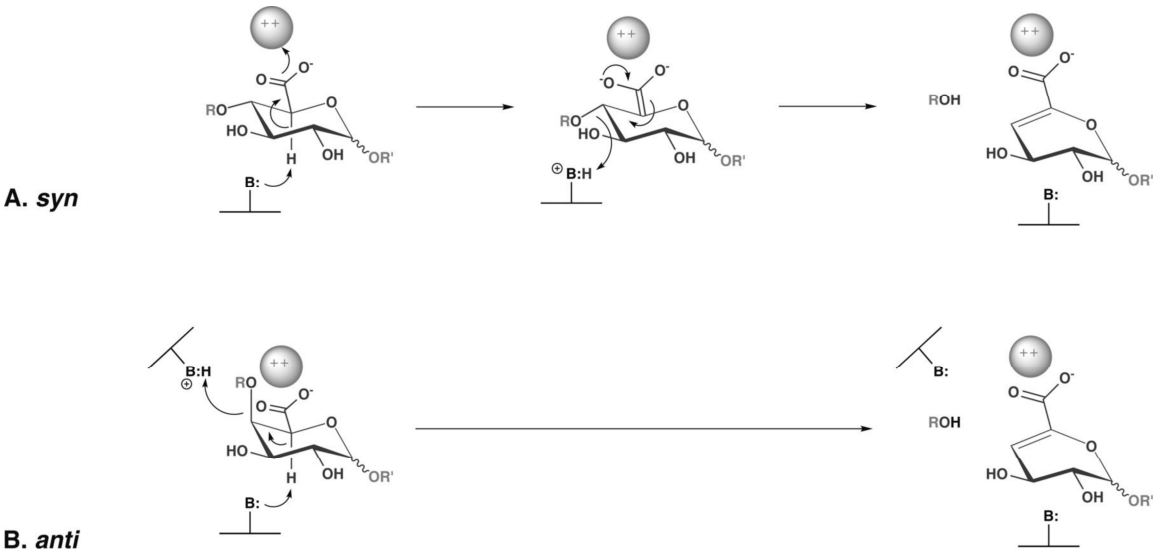

Figure 3: **Mechanisms of *syn*- and *anti*-elimination.** The figure illustrates the difference between syn- and anti-elimination. In syn-elimination, the same residue or external molecule may act as both the catalytic base and acid. In anti-elimination, two distinct acid-/base agents are needed. The substrate in the scheme represent a general uronic acid, and not G or M specifically. The figure is reprinted from (Lombard et al., 2010) with permission from Portland Press.

Studies on different *syn*-eliminating enzymes have shown that they commonly use a single residue as the catalytic base and acid, and that the residue is often tyrosine (Lunin et al., 2004; Yip & Withers, 2006). Enzymes capable of degrading substrates containing C5-epimers like alginate, are indicative of an ability to utilize both *syn*- and *anti*-elimination and the presence of His/Tyr-containing active site, although this is not always the case (Garron & Cygler, 2010). C5-epimerases which change the stereochemistry on the C5-carbon, act by the same mechanism as alginate lyases except for the final step where the epimerase replace the hydrogen on C5, changing the stereochemistry according to the enzymes specificity (Gacesa, 1987).

1.6.2 Products of alginate lyase activity

When an endolytic alginate lyase cleaves a glycosidic bond, it will generate a new reducing end of either G or M and a new C4-C5-unsaturated non-reducing end. The newly formed double bond eliminates the stereogenic centre at C5, which means that the C5-epimers G and M yield the same unsaturated product: 4-deoxy-α-L-*erythro*-hex-4-enopyranuronosyl at the new non-reducing end (Davidson, I. W. et al., 1977) often referred to as Δ. Exolytic alginate lyases may attack the end of saturated- and/or unsaturated poly- or oligomers, depending on their specificities. There seems to be a consensus that when exolytic alginate lyases attack saturated substrates, the product of the first cleavage is a saturated monomer with a newly formed reducing end (Miyake et al., 2003; Ochiai et al., 2010; Park et al., 2012). As the lyase works its way along the chain and break of monomers, it continuously generates unsaturated ends on the residue upstream of the cleavage point identical to the residues generated after endolytic activity (4-deoxy-α-L-*erythro*-hex-4-enopyranuronosyl). This means that all the following monomers that are cleaved off are unsaturated. The unsaturated monomeric product, 4-deoxy-L-*erythro*-hex-4-enopyranuronate, is eventually rearranged by ring opening and tautomerization to an α-keto acid; 4-deoxy-L-*erythro*-5-hexoseulose uronic acid (DEHU or DEH). DEHU was first discovered by Preiss and Ashwell (Preiss & Ashwell, 1962a). There is some ambiguity concerning the terms for the immediate circular 4,5-unsaturated monomeric product and linear DEHU, sometimes DEHU is used to refer to both compounds. In this study, the circular, unsaturated monomeric product will be referred to as Δ, while the linear α-keto acid will be called DEHU.

The UV-properties of the alginate products require some additional background information: Pectin is another abundant uronate polysaccharide and is found in the cell walls of terrestrial plants. Enzymes that degrade pectin also utilise β-elimination, and after exolytic activity end up with a monomeric product that is very similar to DEHU; 4-deoxy-L-*threo*-5-hexosulose uronic acid, also called 5-keto-4-deoxyuronate (DKI). After saccharification by an exolytic pectin lyase, it was found that the absorption at 230 nm increased, as expected when intermediate 4,5-unsaturated oligomers are formed (Preiss & Ashwell, 1962a), but the UV-absorption was unstable and eventually decreased. It was suggested that as the exolytic enzyme cleaved the glycosidic bonds, 4,5-unsaturated monomers formed that were UV-active but spontaneously rearranged to UV-inactive 4-deoxy-L-*threo*-5-hexosulose uronic acid (Shevchik et al., 1999). This hypothesis seems to have been accepted as the current explanation for what is seen in the saccharification of both pectin and alginate by PL enzymes (Hobbs et al., 2016; Wargacki et al., 2012).

To summarise; both the unsaturated end from endolytic cleavage and the free unsaturated monomer absorbs UV at λ_{max} = 235 nm (Gacesa, 1987). While the unsaturated end of oligomers remain

UV-active, the monomer is spontaneously rearranged to DEHU which does not absorb UV at 235 nm (or 230 nm) (Preiss & Ashwell, 1962a). Experiments conducted by Hobbs and co-workers (2016), have shown that the enzyme KdgF catalyses the conversion of 4,5-unsaturated monomers of alginate and pectin to DEHU and DKI respectively. For organisms that use alginate as a carbon source, the *in vivo* utilisation of KdgF facilitate effective metabolism of alginate by the host organism so it does not have to wait for spontaneous rearrangement to metabolizable DEHU (Hobbs et al., 2016).

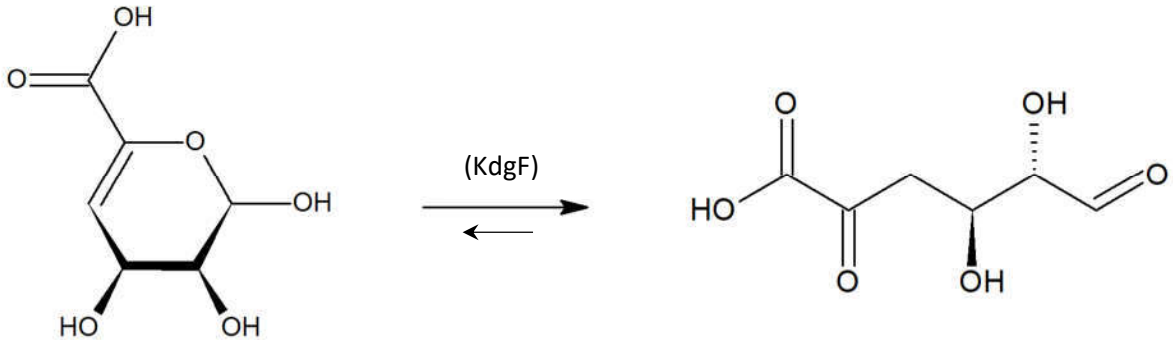

Figure 4: **Monomeric products of enzymatic saccharification of alginate.** The picture shows the protonated versions of the products generated from exolytic enzyme activity on alginate. On the left side is the 4,5-unsaturated monomer which is obtained from both G- and M-residues and absorbs UV at λ_{max} = 235 nm. The circular monomer rearranges to DEHU by the help of the enzyme KdgF, but also spontaneously at a slower rate, and does not absorb UV at 235 nm.

To my knowledge, no exolytic alginate lyase that cleaves off monomers has been discovered that attack a substrate chain from the reducing end; such an enzyme would not likely yield an unsaturated product (Preiss & Ashwell, 1962a) and would probably have to use a different mechanism. No enzyme that cleaves the linkages of alginate by a hydrolytic mechanism seems to have been found, but several hydrolytic pectin lyases (EC 3.2.1.15) have been discovered and characterized.

1.6.3 The structure of alginate lyases

According to Zhu et al. (2015), alginate lyases can be divided into three structural categories; a β-helix family, a $(\alpha/\alpha)_6$ barrel (-toroid) family and a jelly-roll family (Zhu & Yin, 2015). The two currently structurally resolved exolytic alginate lyases to date; Atu3025 of PL15 and Alg17c of PL17 (Figure 5), consist of a α_6/α_6-barrel and a C-terminal linked arrangement of antiparallel β-sheets (Park et al., 2014). In addition, Atu3025 has 100 residues at the N-terminal with respect to Alg17c that form seven β-strands. Both these lyases belong to the topical class of multidomain $(\alpha/\alpha)_n$ toroids (Garron & Cygler,

2010; Park et al., 2014). Topology is the spatial arrangement of secondary structure elements in a protein. Even though the lyases have very similar structures, they only share 13% sequence identity.

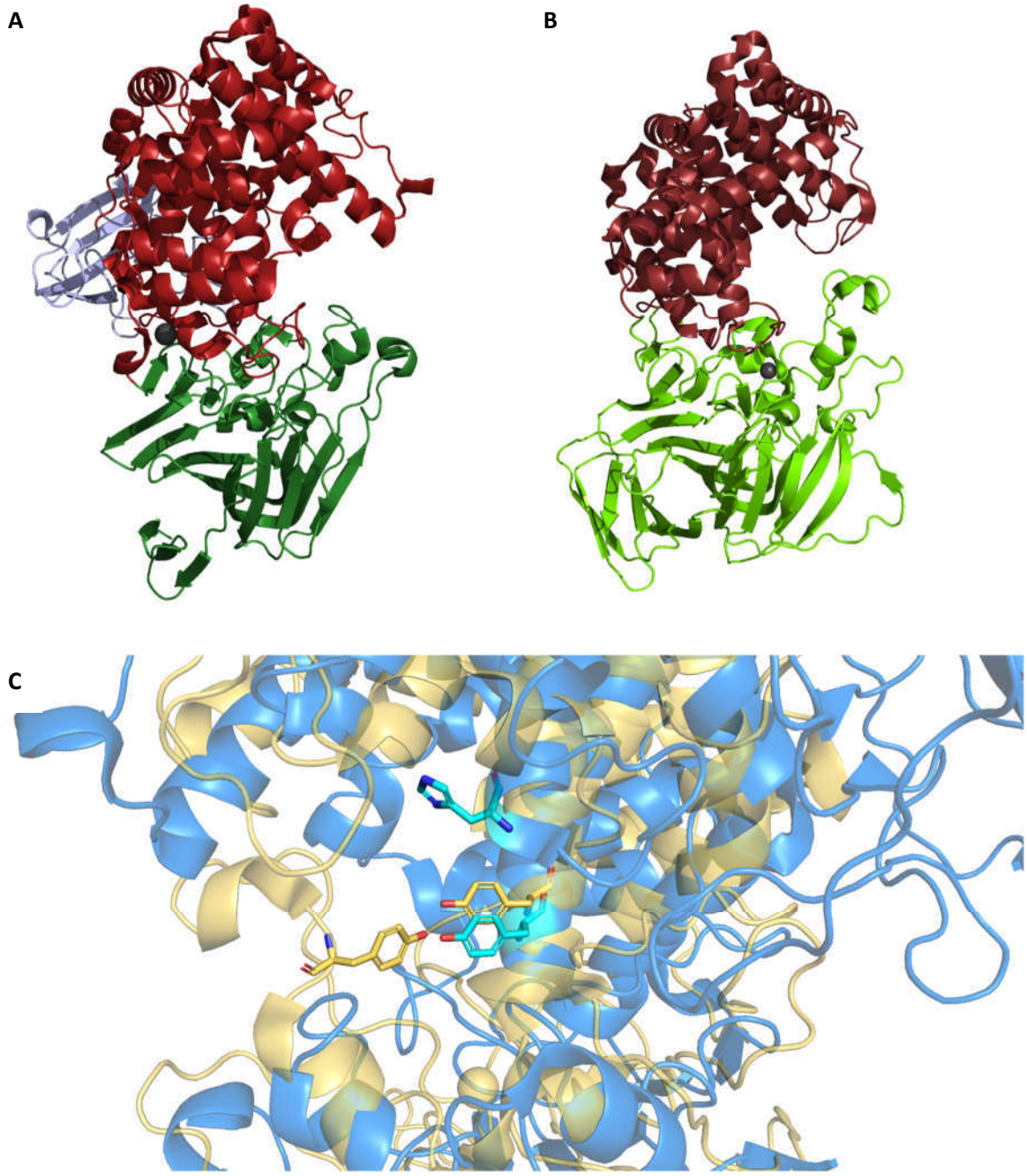

Figure 5: **Crystal structures of Atu3025 and Alg17c.** (A) Atu3025 with the N-terminal β-strand domain in light blue, the α_6/α_6 -barrel domain in red and the C-terminal β-sheet domain in green. The Cl^- ion is shown as a black sphere. (B) Alg17c with the α_6/α_6 -barrel domain in red and the C-terminal β-sheet domain in green. The ostensible Zn^{2+} ion is represented by a black sphere. (C) Structural alignment of Atu3025 (blue) and Alg17c (beige) with focus on the catalytic base and acid of each protein. The figure is rotated horizontally almost 180° with regards to the structures in A and B.

Ochiai and co-workers (2010) determined the structure of Atu3025 and found evidence that suggested that a histidine residue acted as the proton-abstracting base, and a tyrosine residue was the catalytic

acid. Two arginine residues contribute to stabilising the carboxyl anion at subsite -1 and +1 correspondingly. Atu3025 has a deep catalytic pocket that is suggested to open and close in a series of steps during activity. First, the active site is open to facilitate binding of the substrate with the residue at the non-reducing terminal in the innermost position at subsite -1, before closing and bringing the active residues within working range and breaking the glycosidic bond between subsites +1 and -1. Then the enzyme would open again to release the free monomer and enable new binding of the polymer chain. This would then continue in an open/close-fashion as the enzyme works along the chain. For both Atu3025 and Alg17c, structural alignment of enzyme structures with- and without bound substrate, revealed that substrate binding induced a 10° to 12° fixed rotation of the β-sheet domain that caused a necessary conformational shift in the active residues, arranging them for catalytic interaction with the substrate. (Ochiai et al., 2010; Park et al., 2014).

Park and co-authors (2014) point out that the sequence of all exolytic alginate lyases of PL17 are conserved throughout the secondary structures and indicate that the overall 3D-structure of the PL17 Alg17c should be representative for all alginate lyases within this family. Results from X-ray crystallography revealed an electron dense area within the enzyme structure that was surrounded by residues and solvent molecules in octahedral coordination. Based on the coordination geometry and bond length, it was assigned to be a Zn^{2+}-ion. It was further assumed to only play a structural role as it is located relatively far (>15 Å) from the active site. There is a Cl^--ion in Atu3025 which is also located far from the active site and is not likely to have direct interaction with the substrate. By investigation of the protein structure and by activity-testing of different mutants, it was determined that the catalytic base was a tyrosine residue in position 450, while the catalytic acid was a tyrosine residue in position 258. A structure with bound substrate suggested that an asparagine at 201 and a histidine at 202 worked as stabilisers of the negative charge on the C6-carboxylate group. This means that Alg17c and Atu3025 falls into the category of PL-enzymes with purely amino acid-catalysed mechanism as mentioned above, with amino acids corresponding to the roles outlined by Garron and Cygler in 2010 (Garron & Cygler, 2010), with the exception of a histidine residue contributing in the stabilising of the anionic substrate carboxyl in Alg17c, and arginine residues doing the same in Atu3025. Interestingly, the catalytic acid of each protein is located at very similar sites in the structures (Figure 5), while the bases are located very differently. Yet, they are still arranged at opposite sides of the substrate in the respective proteins, allowing for *anti*-elimination to occur.

It was found that Alg17c elutes as a dimer even at low concentrations in analytical size exclusion chromatography. It was also observed intersubunit interaction in the crystal structure. Based on these results, it was suggested that the active form of Alg17c is a homodimer (Park et al., 2014).

1.7 Microbial digestion of alginate

Alginate lyases are found in organisms that produce alginate and those that utilise it as a carbon source (Wong et al., 2000). However, no alginate lyases have been found in brown macroalgae (Ertesvåg, 2015), but several have been found in microorganisms associated with the surface of these algae and microorganisms have become the most important source when it comes to discovering novel alginate lyases (Wang et al., 2017). Alginate lyases have been found in the genes of all identified alginate producing bacteria (Ertesvåg, 2015), and evidence suggest that the alginate lyases are crucial for the survival of the bacteria. In mutants lacking the associated alginate lyase, toxicity was corelative to the amount of alginate produced and eventually lead to overaccumulation of alginate in the periplasm and subsequent cell lysis (Bakkevig et al., 2005; Jain & Ohman, 2005).

Organisms that use alginate as a carbon source, may have a range of different alginate lyases clustered together in operons that work together in degrading the alginate into to digestible monomers (Jagtap et al., 2014; Yoon et al., 2000). Most microbes utilising alginate seem to secrete endolytic alginate lyases before transporting them into the interior for ensuing digestion by exolytic alginate lyases. However, a large transport system has been found in *Sphingomonas sp.* A1 that is capable of importing the untreated polymer directly before intracellular digestion (Hashimoto et al., 2010; Hobbs et al., 2016).

After saccharification of alginate, the unsaturated monomer is efficiently converted to linear DEHU by the assistance of KdgF or spontaneously at a slower pace as described above. DEHU is then reduced by a dehydrogenase to 2-keto-3-deoxy-D-gluconate (KDG) which is also an intermediate in the metabolism of D-glucuronic acid and D-galacturonic acid of pectin and is closely related to 2-keto-3-deoxyaldonat analogues from the metabolism of a broader range of compounds including glucose (Preiss & Ashwell, 1962b). The dehydrogenase utilises the reducing power of nicotinamide adenine dinucleotide (NADH) or the phosphorylated version (NADPH) or both, but with different affinity (Enquist-Newman et al., 2014). KDG is further ATP-phosphorylated by a kinase (Cynkin & Ashwell, 1960), and the resulting 2-keto-3-deoxy-6-phosphate-gluconate (KDPG) enters the Entner-Doudoroff pathway. Here, KDPG is broken to pyruvate and glyceraldehyde-3-phosphate by KDPG aldolase (KdgA), which is metabolised into pyruvate via glycolysis.

The net yield for the breakdown of one DEHU through the Entner-Doudoroff pathway is one ATP and two molecules of pyruvate which can be used in anabolic- or catabolic pathways including

fermentation to ethanol (Entner & Doudoroff, 1952). Pyruvate is also used as a raw material in chemical, biochemical and pharmaceutical industries (Akita et al., 2016), and Cesario et al. (2018) suggest that alginate should be used for the future sustainable production of pyruvate (Cesario et al., 2018). Figure 6 shows the catabolism of the monomer form of Δ to pyruvate.

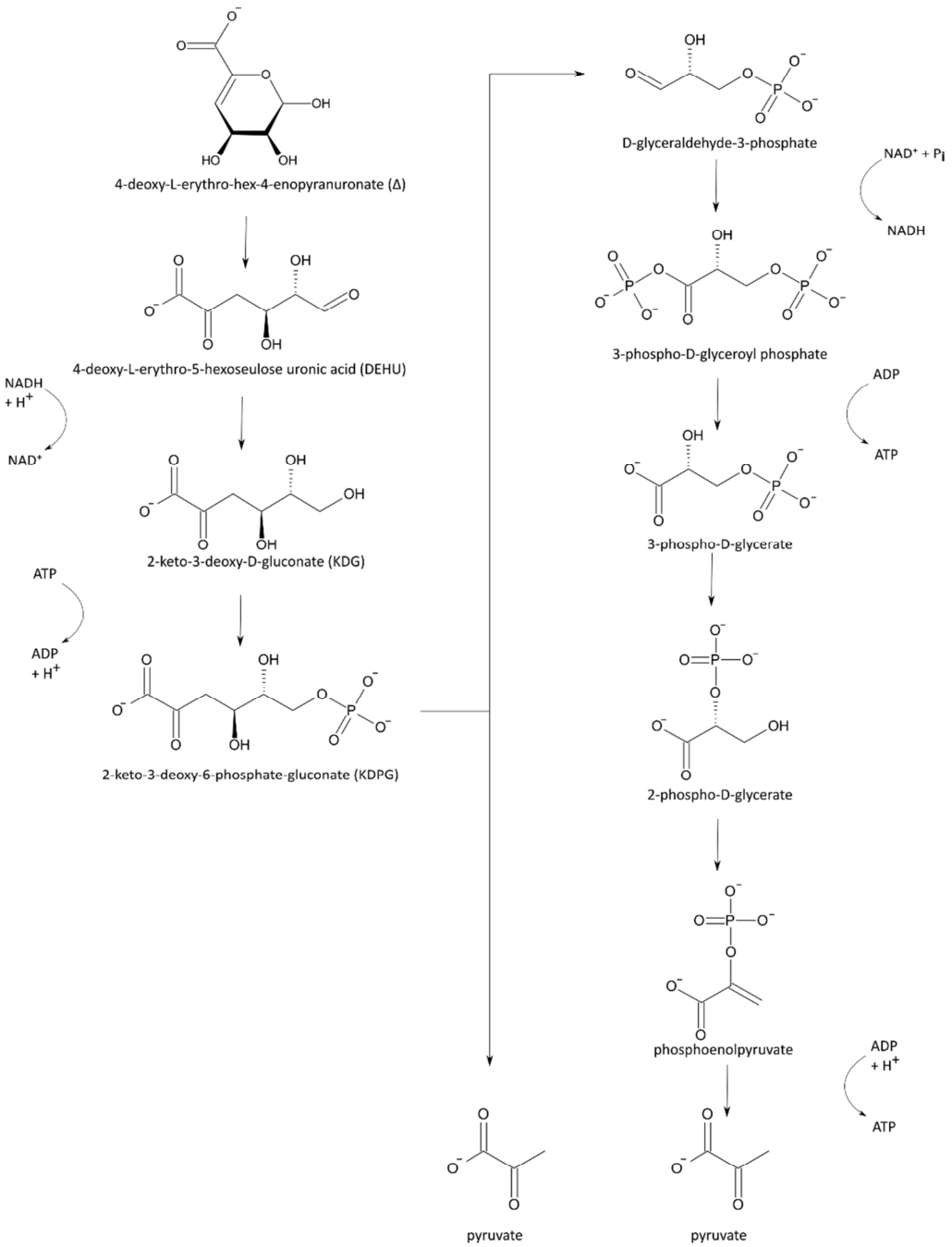

Figure 6: **Catabolism of 4-deoxy-L-*erythro*-hex-4-enopyranuronate (Δ) to pyruvate.** The catabolism of Δ to pyruvate is shown with intermediate structures and ATP/ADP and NADH/NAD^+ conversions.

1.7.1 Fermentation of alginate

Like all polymeric carbohydrates, alginate needs to be saccharified in order to fermented. It has been suggested that mannuronate and guluronate are not well suited for fermentation by industrial microbes (Wang et al., 2016). Thermochemical methods can only yield saturated alginate monomers, which gives yet another reason beyond environmental consideration to use enzymes for alginate saccharification as it yields DEHU as a final product. DEHU is what is metabolised by organisms using alginate as a carbon source (Yoon et al., 2000), so it would seem logical to use alginate lyases in the quest for obtaining readily fermentable sugars from alginate. There are currently few alternatives when it comes to industrial microbes capable of fermenting DEHU, but there have been great advances in the creation of engineered alternatives in recent years. The following paragraphs gives a summary of two quite recent examples.

Wargacki and co-workers engineered an *Escherichia coli* platform for the catabolism of whole alginate and fermentation to ethanol. *E. coli* has no innate ability to metabolise alginate, so a range of components had to be integrated; extra- and intracellular alginate lyases, a secretion system for the extracellular alginate lyase, an oligoalginate transporter and enzymes involved in the digestion of DEHU to pyruvate. The alginate lyase Aly_SM0524 from *Pseudoalteromonas sp*. SM0524 was chosen as the extracellular enzyme to degrade polymers into oligoalginates for transport into the cell. Even though the alginate polymer transport system from *Sphingomonas sp*. A1 was known at the time, it was not chosen because of its complexity, size and the lack of previously successful integration of such large transport systems it into *E. coli*. Genes encoding oligoalginate lyases and other enzymes necessary for metabolising alginate were all obtained from *Vibrio splendidus* 12B01.

The microbe was grown on alginate, mannitol and glucose in a ratio of 5:8:1, which according to Wargacki and co-workers (2012) is representative of a ratio found in brown seaweed. Glucose is the monomer of cellulose and laminarin which are both present in brown seaweed. The strain achieved a titre of 4.7% v/v, converting 80% of the available sugar to ethanol. *E. coli* already has an innate ability to metabolise glucose and mannitol, but mannitol digestion was enhanced in the engineered strain (Wargacki et al., 2012).

Enquist-Newman and collaborators engineered a variant of the industrial microbe *Saccharomyces cerevisiae* (baker's yeast) that was able to co-digest DEHU and mannitol. Mannitol is a simple sugar alcohol found in brown seaweed among other sources. To enable digestion of DEHU, the engineered microbe required a DEHU transporter and genes for digesting DEHU into ethanol. The DEHU transporter was obtained from the alginolytic eukaryote *Asteromyces cruciatus* while DEHU digestion

genes were taken from the same bacterial source utilised by Wargacki and co-workers (2012); *V. splendidus* 12B01. *S. cerevisiae* already has an innate ability to digest mannitol, but the pathway needed reregulation. As mannitol is digested, reducing potential is accumulated in the form of NADH. DEHU catabolism was modulated by selecting a DEHU reductase (DehR) from *Vibrio harveyi* with the ability to use either NADH or NADPH with a preference for NADH, contributing to redox-balance. The microbes went through a 3-month adaptation for growth exclusively on DEHU in aerobic conditions before selecting a strain for adaptation for anaerobic DEHU-fermentation. When growing cells anaerobically with DEHU and mannitol in a 1:2 ratio, ethanol yield of 4.6% v/v or 36.2 g/L was achieved corresponding to 83% conversion of available sugars (Enquist-Newman et al., 2014).

NAD and NADP are carries of reduction- (NADH/NADPH) and oxidation- (NAD^+/$NADP^+$) potential within cells and are formed and used during the metabolism of nutrients. They are vital for cell survival and the ratio of their reduced and oxidised forms largely determine the intracellular redox-balance and affect the drive of metabolic pathways (Xiao et al., 2018; Zhu et al., 2015). For each molecule of mannitol that is fermented to ethanol, three NADH are generated and two are consumed. For each molecule of DEHU fermented to ethanol, one NADH is generated and three are consumed. The net yield of +1 NADH pr. unit mannitol and -2 NADH pr. unit DEHU should be considered when aiming to achieve a redox-balanced environment with overexpressed genes for mannitol- and DEHU digestion, as was done in both the examples of engineered microbial platforms described above.

The function of KdgF which catalyses the transition of 4,5-unsaturated uronic acid monomer to linear DEHU, was still unknown when the *E. coli* and *S. cerevisiae* were designed and was left out from their genomes. The inclusion of KdgF in future design of industrial DEHU-fermenting microbes should provide even greater efficiency of ethanol production (Hobbs et al., 2016). Still, the engineered *E. coli* and *S. cerevisiae* described above achieved titres of 4.7% and 4.6% v/v respectively, which is close to the benchmark ethanol yield from lignocellulosic biomass as of 2009 (Lau & Dale, 2009). In another example, Takagi and co-workers successfully integrated alginate lyases in a *S. ceravisiae* platform, but obtained considerably lower ethanol-yield than the microbes described here (Takagi et al., 2017).

1.8 Aim of study

The preface for this study was the discovery of a gene from a metagenomic sample that coded for an enzyme with high similarity to functionally characterized enzymes of PL17, subfamily 2. The metagenomic sample was obtained from hot vents at Mohn's ridge at 71° north in the Jan Mayen hydrothermal vent field which is part of the arctic mid-ocean ridge (Vuoristo et al., 2019). The goal of this study was to express and investigate the properties of this putative PL17 enzyme. This included screening for active substrates and finding optimal conditions for activity with regards to salinity (NaCl), temperature and pH. The enzyme's mode of action was also to be determined and the enzymatic product identified. The goal was also to obtain a crystal of the enzyme for structure elucidation.

2 Materials

2.1 Cells and plasmids

Table 2: Cells and plasmids.

Name	Supplier
Cells	
One Shot® TOP10 (DE3) Chemically Competent *E. coli* (Cat.nr. C4040)	Invitrogen
One Shot® BL21 (DE3) Chemically Competent *E. coli* (Cat.nr. C6000)	Invitrogen
Plasmids	
pNIC-CH	Opher Gileadi, Structural Genomics Consortium
pNIC-CH_Apl17-2	This study
pUC_Apl17-2	This study
pNIC-CH_Y251A	This study
pNIC-CH_Y446A	This study

2.2 Primers

Table 3: Complete list of used primers.

Name	Sequence [5'→3']
Y251AF	CTACTATATGGAAGGTCCGTACGCTATCCGTTATGCGCTGCGT
Y251AR	AGCGTACGGACCTTCCATATAGTAGCC
Y446AF	GGAGCCGAAGTTTGGTGGCCGTGCCCTGCCGGAAAACACCACCT
Y446AR	GGCACGGCCACCAAACTTCGGC
Apl17-2F	TTAAGAAGGAGATATACTATGCTGCCGGCGGGT
Apl17-2R	AATGGTGGTGATGATGGTGCGCCTTGATTTTCTCCACCTTGTAATT
Apl-17-2seqF	GATGGCTACTATATGGAAGGTCC
Apl-17-2seqR	TGATCCACAACCACGGTGTT
pNIC-CHF	TGTGAGCGGATAACAATTCC
pNIC-CHR	AGCAGCCAACTCAGCTTCC
SeqApl17-2RF-F	GCCAGAACATCGAGATTCC

2.3 Substrates

Table 4: Substrates.

Substrates	Catalouge nr.	Supplier
Sodium Alginate	W201502	Merck
Heparin	H3393	Sigma-Aldrich
Chondroitin	Y0000593	Sigma-Aldrich
Laminarin	L9634	Sigma-Aldrich
poly M (Mw = 275 kDa, F_G = 0.0) from *Pseudomonas fluorescens*		Olav Andreas Aarstad, NTNU*
poly G (DP_n = 20, F_G = 0.95) from *L. hyperborea*		Olav Andreas Aarstad, NTNU*
poly M hydrolysate		Olav Andreas Aarstad, NTNU*
poly G hydrolysate		Olav Andreas Aarstad, NTNU*
poly M + M-lyase		Olav Andreas Aarstad, NTNU*
M24		Olav Andreas Aarstad, NTNU*

*Department of Biotechnology, Norwegian University of Science and Technology (NTNU), Trondheim (Aarstad et al., 2012).

2.4 Chemicals and mixtures

Table 5: Chemicals and mixtures.

Chemical/mixture	purity	Catalogue nr.	Supplier
10x Tris/Glycine/SDS (TGS)		161-0772	Bio-Rad
2,5-dihydroxybenzoic acid		85707	Sigma-Aldrich
3,5-Dinitrosalisylic acid (DNS)		12,884-8	Aldrich
32% HCl		1.00319.2500	Merck
Acetic acid (glacial)	100%	1.00063.2500	Merck
Acetonitrile	100%	20060.320	VWR
Agar powder		20767.298	VWR
Ammonia solution 28%		21190.292	VWR
Antifoam 204		A8311	Sigma-Aldrich
Any kD™ Mini-PROTEAN® TGX Stain-Free™ Protein Gels		#456-8123	Bio-Rad

Any kD™ Mini-PROTEAN® TGX Stain-Free™ Protein Gels		#456-8126	Bio-Rad
BD Bacto™ Tryptone		211705	BD Biosciences
BD Bacto™ Yeast Extract		212750	BD Biosciences
BenchMark™ Protein Ladder		10747012	Invitrogen,
Bis-Tris ultrapure	>99%	97062-266	VWR
Citric acid	99%	C0759	Sigma-Aldrich
D(+)-Glucose		97061-166	VWR
D(+)-Saccharose		27480.294	VWR
DL-Dithiothreitol (DTT)		D0632	Sigma-Aldrich
DNA Gel Loading Dye (6X)		#R0611	Thermo Scientific
EDTA		10424	VWR
Glycerol 85%		1.04094.2500	Merck
Imidazole		10040210	VWR
IPTG		I6758-10G	Sigma-Aldrich
K_2HPO_4	≥99.0%	26931.263	VWR
Kanamycin sulfate		K4000	Sigma-Aldrich
KH_2PO_4	≥99.0%	P5655	Sigma-Aldrich
NaCl	≥99.5%	27810.295	VWR
NaOH pellets	≥99%	1.06469.1000	Merck
NaOH solution 50%		71686	Honeywell
NEBuffer™ 2 (10X)		B7002S	New England Biolabs
NuPAGE™ LDS Sample Buffer (4X)		NP0008	Invitrogen
NuPAGE™ Sample Reducing Agent (10X)		NP0009	Invitrogen
peqGREEN staining dye		37-5010	Peqlab
Potassium sodium tartrate tetrahydrate	≥99%	S2377-5KG	Sigma-Aldrich
Q5® Hot Start High-Fidelity 2X Master Mix		M0493S	New England Biolabs
Quick-Load® Purple 1 kb DNA Ladder		N0552S	New England Biolabs
Red Taq DNA Polymerase 2X Master Mix		733-2131	VWR
S.O.C. Medium		15544-034	Invitrogen
SeaKem® LE Agarose		50004	LONZA
Sodium acetate	≥98%	27650.292	VWR

Sodium acetate for HPLC	≥99%	S8750	Sigma-Aldrich
Sodium Acetate pure	≥99.0%	S8750-5KG	Sigma-Aldrich
T4 DNA polymerase		M421	Promega Corporation
TAE Buffer (Tris-acetate-EDTA) (50X)		#B49	Thermo Scientific
tri-Sodium citrate dihydrate	≥99%	A1351	Applichem
Trizma® base (Tris)	≥99%	T1503	Sigma-Aldrich

2.5 Kits

Table 6: Kits.

Kit	Cat.nr.	Supplier
NucleoSpin® Plasmid	740588.250	Machery-Nagel
Qubit™ dsDNA BR Assay Kit	Q32853	Thermo Scientific
NucleoSpin® Gel and PCR Clean-up	740609.250	Machery-Nagel
JCSG-plus™ (Crystal screening kit)	MD1-37	Molecular Dimensions

2.6 Instruments and hardware

Table 7: Instruments and hardware.

Instrument/Hardware	Supplier
1.5 mL Ultrafree-MC Centrifugal Filter 0.22 µm pore size	Merck
250ml bottle top filter, 0.2µm PES membrane, Sterile	VWR
250ml bottle top filter, 0.45µm PES membrane, Sterile	VWR
3510-DTH Ultrasonic Cleaner	Branson
913 pH meter	Metrohm
Äkta Pure	GE Healthcare
Amicon® Ultra 0.5 mL Centrifugal Filters	Merck
Avanti J-25 centrifuge	Beckman Coulter
Benchtop UV transilluminator	UVP
BioPhotometer D30	Eppendorf
Blue Sample Tray	Bio-Rad
CarboPac PA1	Dionex, Thermo Scientific

Corning® 96-well Clear Flat Bottom UV-Transparent Microplate	CORNING
Dispenser of deionized water	Milli-Q
Filtropur S 0.2	Sarstedt
Filtropur S 0.45	Sarstedt
Gel Doc™ EZ Imager	Bio-Rad
HisTrap HP, 5 mL	GE Healthcare
ICS-5000	Thermo Scientific
IonPac AS4A	Dionex, Thermo Scientific
Labcycler	SensoQuest GmbH
LEX-48 bioreactor	Harbinger Biotech (Epiphyte3)
Mastercycler Gradient	Eppendorf
Mini-PROTEAN Tetra Cell	Bio-Rad
Multifuge X1R centrifuge	Heraeus, Thermo Scientific
Multiskan™ FC Microplate Photometer	Thermo Scientific
Nunc™ MicroWell™ 96-Well Microplates	Nunc, Thermo Scientific
PowerPac™ 300 Power Supply (SDS-PAGE)	Bio-Rad
PowerPac™ Basic Power Supply (DNA-gel)	Bio-Rad
qubit quantitation platform fluorometer	Invitrogen
SI400 pH meter	Sentron
SimpliAmp, Thermal Cycler	Apllied biosystems
Stain-Free Sample Tray	Bio-Rad
Synergy™ H4 Hybrid Multi-Mode Microplate Reader	BioTek
Thermomixer C	Eppendorf
UltiMate™ 3000 Variable Wavelength detector	Dionex
ultrafleXtreme™	Bruker
Vibracell sonicator	SONICS
Vivaspin 20, 10000 MWCO PES	Sartorius

2.7 Culture media

This section lists the details of solutions that are not thoroughly described in the Methods section.

Terrific broth (TB)

TB was made by dissolving tryptone (12 g) and yeast extract (24 g) in distilled water and 85% glycerol (4 mL) to 500 mL. The medium was autoclaved at 121 °C for 20 min.

Lysogeny broth (LB)

LB was made by mixing tryptone (10 g), yeast extract (5 g) and NaCl (10 g) in distilled water and diluting to 1 L. The solution was autoclaved.

LB-plates with sucrose and Kanamycin

A solution of agar (7.5 g), tryptone (5 g), NaCl (5 g), yeast extract (2.5 g) and dH_2O (to 400 mL) was mixed with a 100 mL solution of 25 g sucrose. The solution (500 mL) was autoclaved and 50 mg/mL Kanamycin (0.5 mL) was added when the temperature had decreased to below 50 °C.

Phosphate solution

The phosphate solution contained 0.17 M KH_2PO_4 and 0.72 M K_2HPO_4 in distilled water. The solution was autoclaved.

50 g/L Kanamycin

Powdered Kanamycin (500 mg) was dissolved in distilled, autoclaved water (10 mL) and sterile filtered through a 0.20 µm syringe filter. Prepared solutions were kept at -20 °C.

3 Methods

3.1 Agarose gel electrophoresis

The following procedure for gel electrophoresis was used throughout this study. First, an 1% (w/v) agarose gel was prepared by dissolving agarose (0.5 g) in TAE-buffer (50 mL). A small volume (3 µL) of peqGREEN staining dye was added to the dissolved agarose and gently mixed before the solution was poured into horizontal gel-racks and left to solidify. Samples were mixed with loading dye (6X) before application to the gel and a Quick-Load® Purple 1 kb DNA Ladder was used as a size marker. Gels were run at 90 Volts until clear separation was achieved.

3.2 Sodium dodecyl sulfate–polyacrylamide gel electrophoresis (SDS-PAGE)

SDS-PAGE was used to confirm the presence of desired proteins in samples and also to give an indication of their purity. Sample solutions were mixed with LDS loading buffer (4X) and reducing agent (10X) in ratios that would give correct (1X) final concentrations of loading buffer and reducing agent. Samples were exposed to temperatures over 95 °C for 5 minutes. An Any kD™ Mini-PROTEAN® TGX Stain-Free™ protein gel was placed in a Mini-PROTEAN Tetra Cell container which was then filled with Tris/Glycine/SDS buffer. Samples and a BenchMark™ protein ladder were pipetted into the wells and the gels were subjected to 270 Volts for approximately 20 minutes.

3.3 Production of point mutants Y251A and Y446A

Two individual tyrosine to alanine point mutants of Apl17-2 were made to evaluate the importance of these residues to the function of the enzyme. The mutation sites, Tyr251 and Tyr446, were chosen based on the corresponding residues of the PL17 enzyme Alg17c, Tyr258 and Tyr450 (Appendix A: Multiple sequence alignment. The expressed proteins of two individual tyrosine to alanine point mutants of Alg17c, one at position 258, and another at position 450, were found to be completely inactive, showing that these residues were are essential for the enzyme's activity. In combination with structure examination, the native residues at these positions were determined to act as the catalytic base (Tyr450) and -acid (Tyr258) in a β-elimination mechanism.

Mutant genes were produced by splicing using overlap extension – polymerase chain reaction (SOE-PCR). Genes were PCR-amplified and inserted into plasmid vectors by ligation independent cloning (LIC) followed by transformation of *E. coli* TOP10 (DE3) and subsequently *E. coli* BL21 (DE3). Plasmid encoding mutants were purified from transformed TOP10-cells and sent for sequencing (Eurofins GATC Biotech, 78467 Constance, Germany) to verify the sequence of the mutated gene. The following subsections describe the methods used to obtain transformed cells harbouring plasmids containing either Y251A or Y446A genes.

3.3.1 Purification of plasmid encoding wild type (WT) Apl17-2

A plasmid variant (pNIC-CH) containing the gene encoding WT Apl17-2 was purified to be used in the making of mutant genes. A suspension culture of TOP10-cells with WT Apl17-2 plasmid was prepared by applying cells from a glycerol stock of the respective cells to the tip of a sterile inoculation pick and transferring them to LB-medium (5 mL) with added 5 µL of a 50 mg/mL Kanamycin solution. The cells were left to grow overnight at 37 °C. The plasmid was purified from the cells using a NucleoSpin® Plasmid kit. The presence of purified plasmid was confirmed by agarose gel electrophoresis. The plasmid concentration was determined by using a Qubit™ fluorometer and a Qubit™ dsDNA BR Assay kit. The BR-protocol was used for all measurements where the Qubit™ fluorometer was used. The purified plasmids were stored in the elution buffer (buffer AE) from the NucleoSpin® Plasmid kit at -20 °C.

3.3.2 Primers

Primers- Y251AF, Y251AR, Y446AF and Y446AR for the creation of point mutants were designed and evaluated using Net Primer (Premier Biosoft), and were ordered from Eurofins Genomics. A forward- and a reverse primer for the Apl17-2 gene; Apl17-2F and Apl17-2R had previously been produced. All primers used in this study are listed in Table 3.

3.3.3 Assembling mutant genes

The complete, blunt-ended mutant genes were assembled in two steps: 1) A left- and a right fragment of each mutant gene was PCR-amplified using the gene for WT Apl17-2 as a template and the components listed in Table 8 and Table 10 and the program outlined in Table 12. 2) Because of how the primers were designed, both fragments of each gene share a small fragment of DNA at the intersection between the fragmets that includes the site of mutation. This overlap of identical

sequence allows for the fragments to be spliced by overlap extension. The components used for the SOE-PCR of Y251 and Y446A are listed in Table 10 and Table 11 respectively, and the PCR program is listed in Table 12. All samples for amplification in this section were incubated in a SimpliAmp Thermal Cycler PCR machine.

Table 8: Components used in PCR reactions for producing the fragments needed for generation of mutants.

Components	Volume [µL]
Q5® Master Mix (2X)	25
10 µM Forward primer *	2.5
10 µM Reverse primer *	2.5
0.655 ng/µL pNIC-CH_Apl17-2	1.52
(pUC_Apl17-2) **	1
dH_2O	18.48

* The specific primers used are listed in Table 9.
** This alternative pUC_Apl17-2 plasmid was only used in the making of the right fragment of Y251A.

Table 9: Primers used in the production of mutant gene fragments.

Fragment	Forward primer	Reverse primer
Y251A Left fragment	Apl17-2F	Y251R
Y251A Right fragment	Y251F	Apl17-2R
Y446A Left fragment	Apl17-2F	Y446R
Y446A Right fragment	Y446F	Apl17-2R

Table 10: Components used in SOE-PCR of Y251A

Components	Volume [µL]
Q5® Master Mix (2X)	25
10 µM Apl17-2F primer	2.5
10 µM Apl17-2R primer	2.5
0.031 pmol/µL LF Y251A	2.6
0.042 pmol/µL RF Y251A	1.9
dH_2O	15.5

Table 11: Components used in SOE-PCR of Y446A

Components	Volume [µL]
Q5® Master Mix (2X)	25
10 µM Apl17-2F primer	2.5
10 µM Apl17-2R primer	2.5
0.0717 pmol/µL LF Y446A	10
0.109 pmol/µL RF Y446A	6.7
dH_2O	3.3

Table 12: PCR-program for production of mutant gene fragments and SOE-PCR into complete genes.

Stage	Temperature [°C]	Duration
1 (x1)	98	0:00:30
2 (x25)	98	0:00:08
	62	0:00:20
	72	0:00:25
3 (x1)	72	0:02:00
	4	Hold

The outcome of PCR reactions was assessed by agarose gel electrophoresis. The gel was observed under UV-light using a benchtop UV transilluminator, and pieces containing the PCR-products were excised and stored at -20 °C. The PCR-products were later purified from the agarose gel using a NucleoSpin® Gel and PCR Clean-up kit.

3.3.4 Ligation independent cloning (LIC)

Ligation independent cloning was used to generate a plasmid vector for each mutant containing the respective mutant gene that could later be used to transform competent cells. The blunt-ended mutant genes obtained from SOE-PCR and a designated plasmid (pNIC-CH) were both digested by enzymes to create staggered ends with complementary overhanging sequences. Initially, a restriction enzyme which is contained within NEBuffer™ 2, makes a cut in the double stranded DNA sequence at a specific site within the pNIC-CH plasmid. The ends of the PCR-amplified genes are identical to this area of the plasmid and also contain the cleavage site. The cut made by the restriction enzyme creates short, staggered ends. T4 DNA-polymerase is used to generate longer overhangs by removing

nucleotides starting from the 3'-end and working towards 5'-end. The enzyme stops removing nucleotides as soon as it encounters a deoxy nucleoside triphosphate. The result is two staggered ends in the plasmid and the gene with complementary overhangs that can be annealed together to form a vector with the mutant gene. *In vitro* use of Ligases are not a part of the LIC-protocol, so the newly formed vector is not complete and transcribable until it has been transferred into competent cells and the hosts ligases have generated the missing phosphodiester bonds of the four linkage sites of the gene insert.

To digest the blunt ends of each mutant, the ingredients listed in Table 13 were mixed and incubated in a SimpliAmp Thermal Cycler PCR machine at 22 °C for 1 hour before heat deactivation of T4 DNA polymerase at 75 °C for 21 minutes. Digested plasmid was prepared in the same way, but with the components listed in Table 14. The digested mutant insert (9 µL) was mixed with digested pNIC-CH plasmid (1 µL) and left for 1 hour in 22 °C to facilitate annealing of the staggered ends of the insert with the plasmid, before adding 25 mM EDTA (2 µL) to stabilise the gene insert which had not yet been ligated.

Table 13: Components used in the digestion of amplified blunt-ended DNA fragments.

Components	Volume [µL]
NEBuffer™ 2 (10X)	2
dGTP	2
DTT	1
T4 DNA polymerase	1
0.0213 pmol/µL Y251A *	4.6
0.0178 pmol/µL Y446A *	2.7
dH_2O	To 20 µL

* Only one mutant pr. reaction.

Table 14: Components used in the digestion of plasmid for the generation of transformation vectors.

Components	Volume [µL]
NEBuffer™ 2 (10X)	4
dCTP (25 mM)	4
DTT	2
T4 DNA polymerase	2
dH_2O	12
pNIC-CH	14

3.3.5 Transformation of TOP10- and BL21 *E. coli* with mutant vectors

The mutant vectors made by LIC were transferred into TOP10-cells following the regular transformation protocol provided by Invitrogen (Invitrogen, 2013). The transformation protocol includes transformation, preparation of pre-culture and streaking of LB-agar plates. The TOP10 transformants were used to produce high copy numbers of the mutant plasmids. BL21-cells were transformed at a later time by plasmids isolated from TOP10 transformants that had been verified by sequencing. BL21-cells were transformed according to the Invitrogen protocol (Invitrogen, 2010). LB-plates with sucrose and kanamycin were used in both transformation procedures. The pNIC-CH plasmid provides resistance to kanamycin and contains a SacB-gene that leads to sucrose intolerance. This gene is destroyed when other genes are inserted in the proper way. Thus, the mutants are screened based on both kanamycin resistance and sucrose tolerance.

3.3.6 Verification of transformed cells

To determine if the TOP10 transformants had actually been transformed, a PCR reaction with Taq polymerase was conducted to amplify the inserted genes following the procedure outlined in the supplementary protocol (VWR, 2013), using a Mastecycler Gradient PCR machine, the PCR-program listed in Table 15, and the Apl17-2F and Apl17-2R primers. The amplified genes were analysed by agarose gel electrophoresis.

Verification of the sequences of the mutated genes was achieved through four rounds of sequencing. The primers used in each round are listed in Table 16. The same primers were used for both mutants. Samples were prepared from transformed TOP10-cells by mixing 2.5 µL of a 10µM primer solution, plasmid (4 µL ≈ 500 ng) and dH_2O (5 µL). Samples were sent to (Eurofins GATC Biotech, 78467 Constance, Germany) for sequencing.

Table 15: PCR-program for Taq-PCR.

Stage	Temperature [°C]	Duration
1 (x1)	95	2:00:00
2 (x25)	95	0:00:25
	62	0:00:25
	72	0:00:30
3 (x1)	72	0:05:00
	10	Hold

Table 16: Primers used for sequencing.

Round 1	Round 2	Round 3	Round 4
pNIC-CHF			
pNIC-CHR	pNIC-CHR	pNIC-CHR	
Apl-17-2seqF	Apl-17-2seqF	Apl-17-2seqF	
Apl-17-2seqR	Apl-17-2seqR	Apl-17-2seqR	SeqApl17-2RF-F

3.3.7 Storage of transformed cells

After purified plasmids from each of the two TOP10 transformants had been verified by sequencing, they were utilised to transform competent *E. coli* BL21-cells. Saturated suspension cultures were prepared for each of the four types of transformants: TOP10-cells harbouring plasmid encoding Y251A or Y446A and BL21-cells harbouring plasmid encoding Y251A or Y446A. Each culture was prepared by transferring cells from the respective verified colony on the agar plates to LB-medium (5 mL) with added 50 mg/mL Kanamycin solution (5 µL) by a sterile inoculation pick using sterile technique. The cells were incubated over night at 37 °C. Glycerol stocks were made by gently mixing saturated cell culture (1 mL) and 85% glycerol (0.3 mL) in cryotubes. The glycerol stocks were stored at -80 °C.

3.4 Enzyme production

The proteins WT Apl17-2, Y251A and Y446A were all produced using the same heterologous expression system. This system is based on the inducible transcription of the gene insert encoding for the respective protein in the pNICH-CH plasmid. A saturated suspension culture was prepared from BL21-cells containing the gene of the protein to be expressed. This was done in the same way as described in section 3.3.7. The pre-culture (1.5 mL) was mixed with TB medium (450 mL), phosphate solution containing 0.17 M KH_2PO_4 and 0.72 M K_2HPO_4 (50 mL), 50 mg/mL Kanamycin (0.5 mL) and Antifoam 240 (150 µL) in a 1 L bottle which was then placed in a LEX-48 bioreactor for incubation at 22 °C, with aeration overnight. On the following day, gene expression was induced to produce protein by adding 1M IPTG (100 µL) followed by incubation for another ~18 hours in the same bioreactor, using the same conditions.

Approximately 18 hours after induction, the culture was ready for harvest. The cell suspension was transferred to centrifugation bottles, and centrifuged at 5000 *x g* and 4 °C for 15 min in an Avanti J-25 centrifuge. The obtained pellet was frozen at -80 °C for minimum 1 hour.

3.5 Enzyme purification

The wild type and mutants of Apl17-2 were purified in the same way. The following preliminary steps were executed before affinity chromatography on an Äkta Pure protein purification system. The frozen (-80 °C) pellet obtained from the centrifugation of induced cells was thawed and resuspended in 25 mL buffer A which contained 50 mM Tris, 500 mM NaCl and 5 mM Imidazole followed by sonication at 30% amplitude for 3 min with 5 second intervals and 5 second intermissions using a Vibracell sonicator. The sonicated solution was centrifuged at 15000 *x g* and 4 °C for 15 min in an Avanti J-25 centrifuge. The protein-rich supernatant was filtered (0.45 µm) into 50 mL tubes that would be used directly in the purification process.

3.5.1 Äkta Pure protein purification system

His-tagged wild type and mutants were purified by Ni-Sepharose affinity chromatography. An Äkta Pure protein purification system was used in combination with 5 mL HisTrap columns to extract the His-tagged enzymes from the sonicated mixture. Separate, but similar columns were used for the wild type and for the mutants, one column for successive purifications of wild type and one column for both mutants. The software UNICORN™ (GE Healthcare) was used to interface with the Äkta Pure purification system. The following buffers were used in the purification procedure: 1) Buffer A, which

contained 50 mM Tris, 500 mM NaCl and 5 mM Imidazole. 2) Buffer B, which contained 50 mM Tris, 500 mM NaCl and 500 mM Imidazole. Both solutions had pH 8.0 and were sterile filtered through 0.22 µm bottle-top filters.

The same purification procedure was used for all proteins. The following preliminary steps were executed in advance of running a designed and automated purification program (Table 17). All four inlet tubes were placed in 20% ethanol and a pump wash was executed for all pumps. The system was then washed for 10 min with 20% ethanol at 2.5 mL/min. After the system wash, the inlet tubes were placed in deionized water (Milli-Q) and the same pump- and system wash were executed. The flow was then reduced to 0.5 mL/min and the column was mounted into the system while the flow was on to avoid air contamination of the column and the system. Then five column volumes (2.5 mL/min for 10 min) was run through the system to remove the ethanol present in the column. Tubes labelled "A1", "buffer" and "S2" were placed in buffer A, and tube "B1" in buffer B. Pump wash was initiated, and then system wash with buffer A through tube A1 to equilibrate the column.

After preparing the system in this manner, tube S2 was placed in the protein-rich supernatant obtained earlier from lysed, expression-induced cells, and the program (Table 17) for purification was executed. The supernatant was run through the column and the system, and the material that did not attach to the column was collected as flow-through from the outlet tube. The His-tagged protein would be retained due to the His-tag's affinity towards the Ni-Sepharose stationary phase of the column. The program would then start to wash the column with buffer A to facilitate proper elution of un-tagged protein, before initiating a linear gradient towards 100% buffer B, which contained a higher concentration of imidazole. The linear increase of imidazole decreased the affinity of poly-histidine towards the stationary phase, and thereby promoted the elution of the His-tagged protein. During this gradient, the eluate was divided into fractions and collected in assay tubes. At the end of the gradient, the program proceeded to wash the system with five column volumes of 100% buffer B rinse the column of any attached proteins.

After all the steps of the program had been executed, all inlet tubes were placed in deionized water. Pump- and system wash were initiated as in the preliminary steps. Finally, all tubes were placed in 20% ethanol and a last round of pump- and system wash was executed to prepare the system and column for storage.

Flow-through and eluted fractions had been collected, and the fractions potentially containing the purified His-tagged protein were analysed by SDS-PAGE. The content of the tubes that contained the pure protein were then pooled and concentrated using a Vivaspin 20, 10000 MWCO filter tube with continuous buffer exchange to 20 mM NaOAc and 300 mM NaCl until the concentration of imidazole was below 1 mM. The purified and concentrated protein was then stored in 1.5 mL Eppendorf tubes at 4 °C.

Table 17: Protein purification program for Ni-Sepharose affinity chromatography on a Äkta Pure system. *The first equilibration step is virtually non-existent because it is done manually before the initiation of the program. The standard flow rate was 2.5 mL/min except for during the sample application where it was 2.0 mL/min.*

Stage	Comment
Equilibration	100% buffer A for 0.1 column volumes.
Sample application	Injection using air sensor and 40 mL max volume. Flowrate: 2.0 mL/min
Column wash	100% buffer A until UV_{280} < 60 mAU. Maximum wash volume: 10.0 column volumes. Outlet for collection of flow-through.
Elution	Linear gradient from 0-100% buffer B over 16 column volumes. Fractionationated into 4 mL fractions.
Equilibration	100% buffer B for 5 column volumes.

3.5.2 Protein concentration

The protein concentration of stock solutions was determined by measuring the absorbance of diluted samples at 280 nm using a BioPhotometer D30 instrument. Samples were diluted such that the absorption value was between 0.1 and 1, to stay within the standard curve of the instrument. Beer's law was used to calculate the enzyme concentration based on the theoretical extinction coefficients of the respective proteins. Protein stock solutions contained 20 mM NaOAc and 300 mM NaCl, and were stored at 4 °C and pH 5.6.

3.6 Enzyme activity assays

A series of tests were conducted to determine the optimal working conditions for wild type Apl17-2. Here, optimal conditions are defined as the conditions at which the enzyme performs most efficiently during the reaction, i.e. produces the highest amount of product per time unit. The goal was to find conditions that were effective for incubation periods of about 24 hours. The conditions tested were salinity (NaCl), pH and temperature. Progress curves and enzyme stability were also examined.

3.6.1 Setup

The effect of varying conditions on enzyme activity was evaluated by measuring the amount of product generated after equal durations of time. The quantity of formed product was estimated using the DNS-method (Sumner & Graham, 1921), which measures formation of reducing ends. The DNS stock solution was made by dissolving NaOH pellets (8 g) in distilled water at 60 °C. potassium sodium tartrate tetrahydrate (150 g) was added to the solution before 3,5-Dinitrosalisylic acid (5 g) and dilution to 500 mL.

All reactions were carried out in Thermomixer C thermomixers at 600 rpm. The reaction volume was 100 µL where not stated otherwise. Except for in the thermal stability test, the reactions were initiated by adding enzyme to a preheated mixture of substrate and buffer. With one exception, all activity assay reactions were terminated by transferring half of the volume of the respective reaction mixture to DNS-filled wells in 96-well plates to a final ratio of 1:3 (reaction solution : DNS solution). Substrate blanks were included in all DNS-assays. In this study, substrate blanks refer to samples containing all the components present in the other samples of the respective experiment, but which does not contain enzyme. In cases with large variation in reaction conditions, such as high and low temperature, -NaCl concentration or -pH, the average absorption value of multiple substrate blanks was used. It was found that none of these variables affected the absorbance of substrate blanks significantly.

Glucose standards were prepared by dissolving glucose in distilled water and were included on all plates unless indicated otherwise. The standards had concentrations of 1.5, 0.75, 0.375, 0.15, 0.075 and 0 mg/mL before addition to the DNS reagent. Standards had the same volume ratio to DNS as reaction samples; 50 µL glucose was always transferred to 100 µL DNS. All samples, blanks and standards were triplicates. The 96-well plates with reaction solutions mixed with DNS, were sealed with plastic film and left in thermomixers at 100 °C for 15 min. A Multiskan™ FC microplate photometer was used to measure the absorption of samples and standards at 540 nm.

3.6.2 Progress curves

Initially, enzyme activity was monitored over time to find a reaction time that would be well suited to evaluate the enzyme's response to changing reaction variables later on. At each point of sampling, samples were taken from three separate, parallel reactions mixtures (triplicates). All individual samples were taken from standalone reactions, i.e. no reaction solution was sampled more than once. Reaction solutions of time-variable activity experiments for the generation of progress curves contained 1 µM Apl17-2, 0.5% (w/v) sodium alginate, 25 mM NaOAc and 300- or 500 mM NaCl with a pH of 5.6 and

were incubated at 50 °C. Samples (50 µL) were taken at different time-points and directly mixed with DNS reagent (100 µL) at the time of sampling. Because of results indicating product instability, and preliminary indications of NaOH being able to accommodate this issue, some reactions (100 µL) were stopped by adding 1 M NaOH (10 µL).

3.6.3 NaCl screening

In the NaCl screening experiment, the concentration of NaCl was the only variable. The reactions were carried out at pH 5.6 and 50 °C and incubated for 5 minutes. The reaction solutions contained 1 µM Apl17-2, 0.5% (w/v) sodium alginate, 25 mM NaOAc and NaCl ranging from 0 to 2 M. Substrate blanks for 0.1 M and 2 M were included, but there was no significant difference in absorption at 540 nm between them. Based on the results, reported below, 300 mM was chosen as the standard salt concentration for future experiments.

3.6.4 Temperature screening

Enzyme activity was tested at 40 °C to 90 °C with 10-degree intervals to find out how temperature would affect the efficiency of the enzyme. The conditions were 1 µM Apl17-2, 0.5% [w/v] sodium alginate, 25 mM NaOAc and 300 mM NaCl at pH 5.6. Substrate blanks at 40-, 80- and 90-degrees Celsius were included. The reaction mixtures were incubated for 5 minutes.

3.6.5 pH screening

The activity of the enzyme was tested at different pH to get an overview of the working pH range. Three different buffers were used to manage this: citric acid/citrate (pH 3.3-6.1), Bis-Tris/HCl (pH 5.8-7.0) and Tris/HCl (pH 7.0-8.8). The concentrations of the buffers in the reaction solutions were about 40 mM, 45 mM and 30 mM and respectively. The buffer concentrations are not exact because of pH adjustments. The reactions contained 1 µM Apl17-2, 0.5% sodium alginate and 150 mM NaCl. The pH of each sample was measured at 50 °C before the reactions were initiated. Reactions proceeded for 5 minutes. Based on this experiment, subsequent experiments were done using a standard pH of 5.6.

3.6.6 Thermal stability

To examine the thermal stability of Apl17-2, a 2 µM enzyme solution in 50 mM NaOAc with 600 mM NaCl was pre-incubated at 60 °C and 65 °C. The pre-incubation times were 0, 1, 2, 4, 6, and 24 hours. To assess remaining activity, reactions were initiated by adding preheated (50 °C) 1% (w/v) sodium

alginate in a 1:1 volume ratio to achieve the standard reaction conditions 1 µM Apl17-2, 0.5% sodium alginate, 25 mM NaOAc and 300 mM NaCl at pH 5.6 and 50 °C. The reaction mixtures were incubated for 5 minutes. Pre-incubated samples were stored at 4 °C before initiating all reactions at approximately the same time. Even though the results indicated that the enzyme was stable at 60 °C for at least 24 hours, 50 °C was chosen as the standard temperature in most of the successive experiments.

3.6.7 Assessing activity on different substrates

The enzyme was tested for activity on the following substrates: poly G (DP_n = 20, F_G = 0.95), poly M (M_w = 275 kDa, F_G = 0.0), heparin, chondroitin, laminarin and alginate as a control. Substrates are listed in Table 4. The wild type Apl17-2 and both mutants, Y251A and Y446A, were tested on all the substrates. The reaction solutions contained 1 µM enzyme 0.1% (w/v) substrate, 25 mM NaOAc, 300 mM NaCl and were incubated at pH 5.6 and 60 °C for 20 hours.

3.7 Product analysis by anion exchange chromatography

A series of experiments were conducted using high performance anion exchange chromatography with pulsed amperometric detection (HPAEC-PAD). The purpose was to look for products from the enzymatic reactions of Apl17-2 on different substrates. The reaction solutions were examined for both oligomers and monomers. Anion exchange chromatography uses columns with positively charged inner linings (stationary phase) that consequently have an affinity for negatively charged ions. As increasingly stronger eluent (mobile phase) passes through the system, molecules will detach and reach the detector at different times depending on their affinity for the stationary phase. Anion exchange chromatography is well suited to study uronic acids like the alginate mono- and oligomers which are deprotonated in the basic environment.

3.7.1 Setup and procedure

An ICS-5000 ion chromatography system was used in the analysis of both oligomers and monomers. The Chromeleon v7.2 software was used to control the instrument and analyse the results. All eluents were filtered through 0.45 µm PES membrane bottle-top filters and degassed in a 3510-DTH Ultrasonic Cleaner. In two experiments, an UltiMate™ 3000 Variable Wavelength detector was placed between the column and the amperometric detector to measure the UV-absorption of compounds at 235 nm.

3.7.2 Oligomers

Oligomers were analysed by an IonPac AS4A column. The following eluents were used: A: 0.1 M NaOH, B: 1 M NaOAc + 0.1 M NaOH and C: deionized water (Milli-Q). The column was primed by running 70% B for 20 min, 100% B for 10 min and 0% B for 30 min at 1 mL/min. Eluent A made up the remaining fraction in each of these steps. A blank injection not containing any sample was always executed at the start of a sequence before any reaction samples. Four different methods were used to elute the contents of the samples. All of them started at 0% B with a gradient of increasing concentration. The runtime of the gradient varied from 50- to 100 minutes and was the only difference between the methods. The increment was always 8.75 mM NaOAc/min (Aarstad et al., 2012). After the gradient, there was 15 min of equilibration with 100% A.

3.7.3 Monomers

Monomers were analysed by a CarboPac PA1 column. The eluents were A: 600 mM NaOAc + 60 mM NaOH and B: deionized water. The column was primed by running 25% eluent A for 20 minutes at 0.25 mL/min. A blank injection was run before any samples. The same method was used in all experiments, and it started at 25% A for 6 minutes before proceeding with a curved gradient of increasing A to 100% at which it stayed for 1 min before equilibrating at 25% A for 10 min.

3.8 UV-analysis

In this study, UV-absorption at 235 nm was used to examine if UV-active product was formed after reaction of Apl17-2 with alginate, and also to monitor the spontaneous rearrangement of the putative immediate monomer product 4-deoxy-L-*erythro*-hex-4-enopyranuronate (Δ) to 4-deoxy-L-*erythro*-5-hexoseulose uronic acid (DEHU). Δ absorbs UV at 235 nm (Shevchik et al., 1999), while DEHU does not (Preiss & Ashwell, 1962a).

The UV-absorption of stopped reactions were analysed over the course of 24 hours with sample absorption readings at 235 nm every hour in a Synergy™ H4 microplate reader. The reaction ingredients were 1 µM enzyme, 0.5% sodium alginate, 25 mM NaOAc, 300 mM NaCl and samples were incubated at pH 5.6 and 50 °C. Parallel reactions (200 µL) were incubated for 2 hours and terminated either by heat (100 °C, 10 min), addition of 1 M HCl (20 µL) or addition of 1 M NaOH (20 µL). Half the reaction solution (100 µL) was transferred to wells in a UV-transparent microplate to measure the absorption at 235 nm of the undiluted solution. Triplicates were used.

3.9 MALDI-TOF

Products were also analysed by mass spectrometry (MS), using matrix assisted laser desorption ionization (MALDI) with time of flight (TOF) based separation. An ultrafleXtreme™ mass spectrometer was used. A single reaction mixture containing 1 µM Apl17-2, 0.05% (w/v) poly M, 25 mM NaOAc and 300 mM NaCl were incubated for 24 hours at pH 5.6 and 50 °C. The solution was separated into two parts before termination. The reactions were stopped either by boiling for 10 minutes or by adding 1 M NaOH in a ratio of 1:10 (NaOH solution : reaction solution). The terminated reactions mixtures were left at room temperature (~22 °C) and samples were taken after 4-, 24-, 48-, and 72 hours of standstill. Each sample (1 µL) for MS analysis was mixed with a solution (2 µL) of 30% acetonitrile and 60 mM of 2,5-dihydroxybenzoic acid, applied to a MALDI target plate and solidified by liquid evaporation using hot air. Reference cellulose oligomers were also added to the matrix to be used for calibration.

3.10 Crystallography

Efforts were made to obtain protein crystals of Apl17-2 and to determine its structure by X-ray crystallography. A JCSG-plus™ crystal screening kit was used to screen for different crystallization conditions by the hanging drop method. Plate wells were filled with crystallisation conditions (150 µL) and glass slides containing protein (1 µL) and the respective condition (1 µL) were placed upside down on top of the wells, which had silica grease on the edge to provide an airtight seal. The protein stock solution, in 20 mM NaOAc and 300 mM NaCl, had a concentration of 212 µM or 17.4 g/L.

4 Results

4.1 Bioinformatics

The protein sequence of the non-recombinant WT Apl17-2 was used to search the Pfam database (Bateman et al., 2018). The database predicted the presence of an alginate lyase domain (PF05426) and a heparinase II/III domain (PF07940). A search in the SignalP database with the same protein sequence indicated that the probability that Apl17-2 has a signal peptide is 0.62, and that the predicted cleavage site is between residues 21 and 22. These results were combined to make a graphic representation (Figure 7) of predicted domains using the MyDomains image creator (Hulo et al., 2008).

Figure 7: **Predicted domain structures of non-recombinant WT Apl17-2.** The figure shows the untruncated, non-recombinant wild type protein sequence without the C-terminal polyhistidine tail of the enzyme that was appended to the protein used in this study.

A multiple sequence alignment of the amino acid sequence of Apl17-2 and all the characterized PL17 enzymes listed in the CAZY database (seven, as of March 31, 2019) was obtained by using Clustal Omega (Chojnacki et al., 2017) and ESPript (Gouet & Robert, 2014). The complete alignment (Appendix A: Multiple sequence alignment) shows that several residues are conserved, as would be expected from comparison of proteins within the same family. A phylogenetic tree (Figure 8) was constructed based on the output from the Clustal Omega alignment file, using IQ-Tree (Trifinopoulos et al., 2016) to generate a consensus tree, and Tree viewer from ETE toolkit (Huerta-Cepas et al., 2016) to draw a visual representation of it.

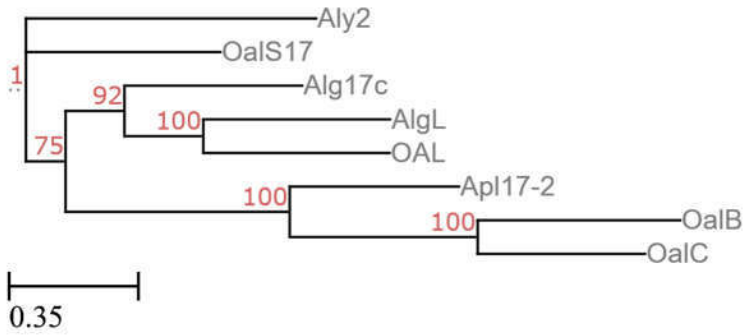

Figure 8: **Phylogenetic tree of functionally characterized PL17, subfamily 2 alginate lyases and Apl17-2.** The phylogenetic tree illustrates how the characterized proteins of PL17 subfamily 2 are related based on their amino acid sequences. The difference in protein sequence is indicated by the distance of the horizontal lines, and the numbers at the nodes indicate the support for the placement of the node, i.e. where the sequences diverged into separate forms from a common ancestor. The tree was generated from the alignment file obtained from multiple sequence alignment of the respective proteins in Clustal Omega, by using IQ-Tree.

The phylogenetic tree in Figure 8 is a graphical representation of the ancestral relationship between the proteins of PL17 subfamily 2 based on computational analysis of their amino acid sequences. The horizontal lines are not only an indication of how dissimilar the sequences are, but also represents a relative timeline for the when the proteins diverged at the branch nodes. The tree indicate that Apl17-2 is ancestral to OalB and OalC, and is strictly comparatively speaking, not very closely related to the other proteins. The tree is unrooted, meaning that there is no common ancestor is inferred.

4.2 Production of point mutants Y251A and Y446A

The two point-mutants Y251A and Y446A were generated by SOE-PCR. The left and right fragments of each mutant were PCR-amplified before splicing them by overlap extension in subsequent rounds of PCR. Agarose gel electrophoresis was used to evaluate the success of the gene production steps. Figure 9 shows agarose gels with various DNA fragments generated for mutant construction.

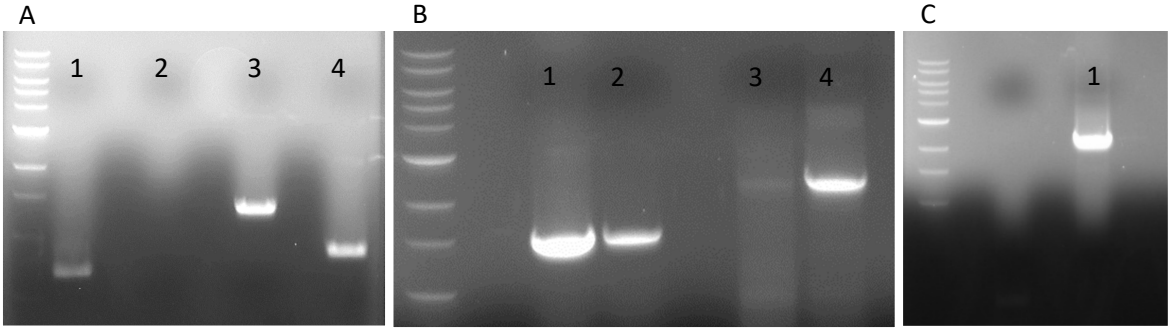

Figure 9: **Gel electrophoresis of PCR products generated for mutant construction.** Panel (A) shows left and right fragments generated during the first PCR step. If the procedure was successful, well 1 and 2 would contain the left and right fragments of Y251A and well 3 and 4 would contain the left and right fragments of Y446A. The fragments had theoretical lengths of 720 bp, 1481 bp, 1350bp and 896 bp, respectively. As in all cases of DNA-gel-electrophoresis in this study, a Quick-Load® Purple 1 kb DNA Ladder was used. Panel (B): Well 1 and 2 both contain amplified right fragment of Y251A (1481 bp). Well 3 and 4 were both expected to contain the complete Y446A mutant gene (2176 bp). Panel (C): Lane 1 shows the result of the SOE-PCR for Y251A (2176 bp).

Lane 4 in Figure 9B and lane 1 in Figure 7C show that seemingly correct DNA fragments were obtained for both mutants. The DNA fragments were purified from the gels and used in subsequent ligation independent cloning to generate plasmid expression vectors.

The blunt-ended, PCR-amplified DNA fragments were digested and inserted into plasmids following the LIC-protocol. The mutant vectors were used to transform TOP10-cells. Three colonies of transformed TOP10-cells were selected for each mutant and were used in Taq-PCR to assess if transformation had occurred. Figure 10 shows the results from the analysed PCR-samples.

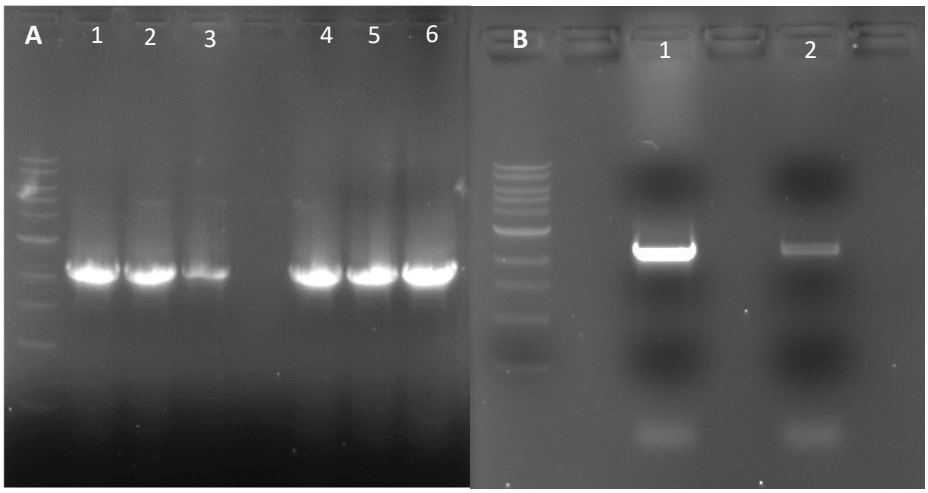

Figure 10: **Control of transformed mutants.** Panel (A) shows the results of agarose gel electrophoresis of PCR fragments amplified from plasmids purified from transformed TOP10-cells. Lanes 1-3 were expected to contain Y446A, and lanes 4-6 were expected to contain Y251A. Panel (B): PCR fragments amplified from plasmids purified from transformed BL21-cells. Lane 1 was expected to contain Y251A and lane 2 was expected to contain Y446A.

On the basis of agarose gel electrophoresis, all selected cell colonies of TOP10 transformants were considered successfully transformed for both mutants (Figure 10A). Plasmid from one colony from each TOP10-mutant was selected for sequencing and used to transform BL21-cells (Figure 10B). DNA sequencing verified that Y251A and Y446A had been constructed as intended.

4.3 Enzyme activity assays and optimization

This section will display results from several enzyme activity DNS assays that were conducted as described in the Methods section. Triplicates were used, and standard deviations are represented by vertical bars. The activity was assessed by how much product was formed. Newly formed products would generate new reducing ends that could react with the DNS reagent regardless of whether the enzyme is endo- or exoactive and regardless if it produces oligomers or monomers as the final end product. The more reducing ends, the higher absorption the sample would have after boiling with the DNS reagent. Glucose was used as standard, and the initial absorption was therefore converted to glucose equivalents via the standard curve. The product yields were calculated based on the measured amount of product compared to the theoretical conversion of all the available substrate to monomers (Appendix C). Unless otherwise stated, the enzyme and substrate concentrations were 1 µM and 5 mg/mL (0.5% w/v).

4.3.1 Progress curves

In all activity progression experiments, samples were taken from parallel reactions and never from the same solutions. In an initial activity progression experiment (Figure 11) and in three subsequent 24-hour progression experiments (Figure 12), the conditions were 1 µM Apl17-2, 0.5% w/v alginate, 25 mM NaOAc, 500 mM NaCl, 50 °C and pH 5.6. Initially, the goal was to determine what reaction time would be suitable for subsequent experiments with fixed incubation times.

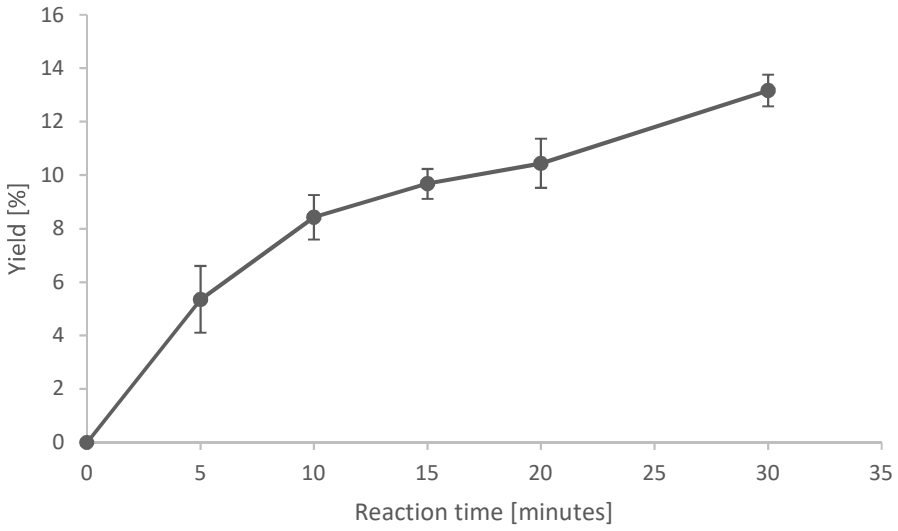

Figure 11: **Initial activity progression assay of Apl17-2.** The progression curve was used to determine a standard reaction time that would be appropriate for other subsequent experiments with fixed reaction times and similar enzyme and substrate concentrations. The reaction conditions were 1 µM Apl17-2, 0.5% w/v alginate, 25 mM NaOAc, 500 mM NaCl, 50 °C and pH 5.6.

The initial progress curve (Figure 11) has an almost linear incline towards 10 minutes, before it shifts to a trend of slower increase in yield. An appropriate duration for time-fixed experiments would be within the initial, linear area of the progress curve, as it would give the most accurate information about the enzyme's response to changes in conditions in subsequent optimisation experiments. An incubation time beyond the initial linear area, would be more prone to give inaccurate information about the enzyme's true response, as the same yield may be achieved at an earlier stage, like e.g. 15- versus 20 minutes in Figure 11 giving almost equal yields. Based on this result, 5 minutes was chosen as the standard reaction time for subsequent fixed-time activity assays.

Three activity progression experiments that all lasted for 24 hours were conducted to obtain progress curves that would show how reactions of Apl17-2 proceeded with regards to product formation. The results from these experiments are shown in Figure 12. They were all conducted under similar conditions, but with different timing of reaction initiation and termination, and sample storage times. The reason why three such experiments were conducted and not only one, was because of other results indicating that inaccuracies of measured product could arise because of product instability (data not shown).

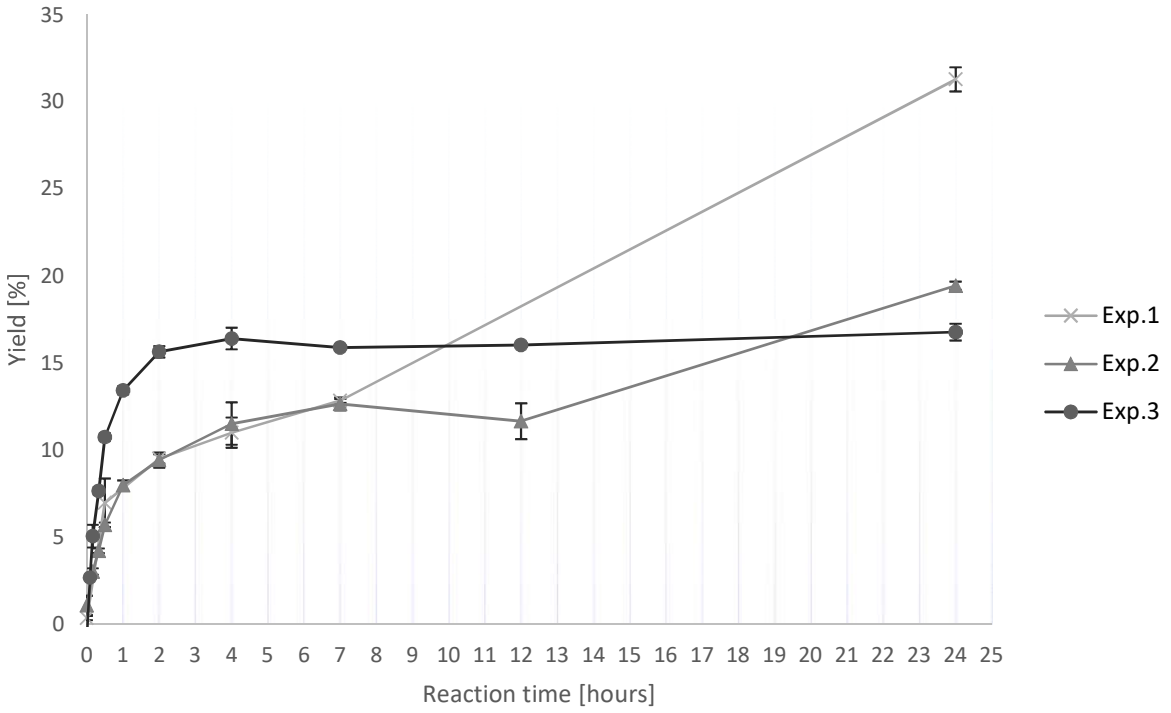

Figure 12: **24-hour progress curves of Apl17-2 activity.** The reaction conditions were1 µM Apl17-2, 0.5% w/v alginate, 25 mM NaOAc, 500 mM NaCl, 50 °C and pH 5.6. Each point represents a separate reaction. Exp.1: All reactions were started at approximately the same time and stopped after different periods of time by mixing with the DNS reagent. Exp.2: The reactions were started at approximately the same time, but were stopped by addition of 1M NaOH in a 1:10 ratio (NaOH : reaction mixture) at the sampling times. Exp.3: Reactions were started at different points in time in such a way that they were all terminated at approximately the same time and that handling times after addition of the DNS reagent were very similar.

The three 24-hour progress curves indicate that storage of reaction solutions reduce the amount of product that is measured. This product instability is shown for reactions that are terminated by addition of the DNS reagent or by addition of NaOH, and explains the low yield of the initial reactions of Exp.1 and -2 and their continuously rising progress curves. Here, the term product instability refers to the fact that the amount of measured product decrease when the solutions of terminated reactions are stored before measurement, and does not infer explanations as to what actually happens on a chemical level.

Figure 13 shows progress curves for reactions carried out at different temperatures. Sampling times and temperature is the only deliberate difference between the experiments. In all cases, due to earlier indications of product instability, precautions were taken to minimize the time between the termination of the first and last sample by using non-chronological initiation times.

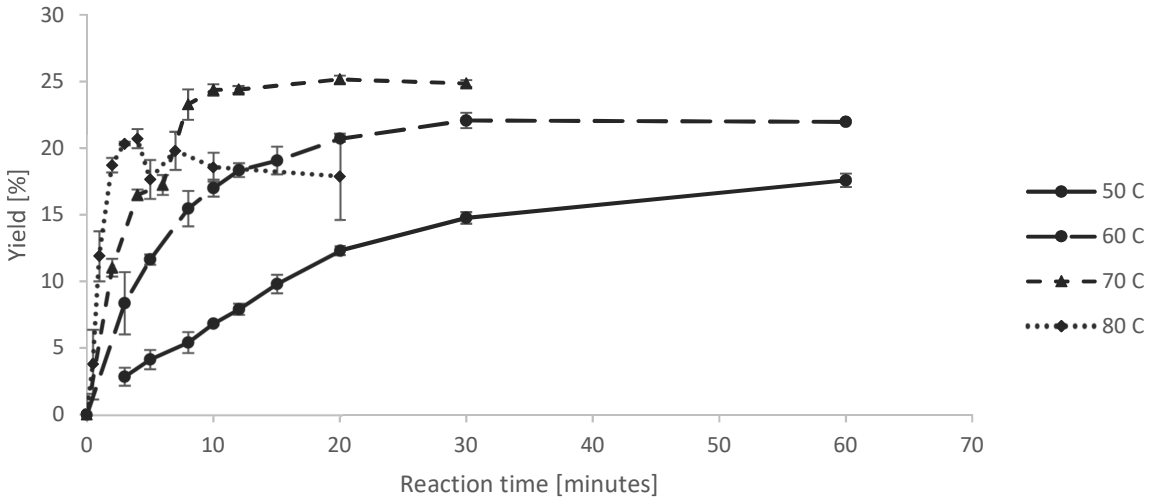

Figure 13: **Progress curves for Apl17-2 with alginate at different temperatures.** The figure illustrates how reactions with Apl17-2 progress at different temperatures from 50 °C to 80 °C. The reaction conditions were 1 µM Apl17-2, 0.5% (w/v) alginate, 25 mM NaOAc, 300 mM NaCl and pH 5.6.

Figure 13 shows that the enzyme's activity increases drastically with temperature and shows signs of enzyme inactivation at the highest used temperature, 80 °C. After 3 minutes reaction time of Apl17-2 and alginate at 80 °C, the amount of reducing ends is equivalent of 20% yield with regards to available substrate. The highest measured yield in this experiment was 25%, achieved after 30 minutes at 70 °C. The curves representing reactions at 60 °C and 70 °C flatten out within 30 minutes, while the 50 °C-curve is rising slightly from 30- to 60 minutes. Based on the results shown in Figures 9 and 11, to avoid stability issues, an incubation temperature of 50 °C was used in the subsequent screening assays, while incubation times were limited to 5 minutes.

4.3.2 Screening of conditions for optimal activity

The activity of Apl17-2 was tested in different ranges of salinity (NaCl), temperature and pH to determine the enzyme's optimal conditions. The reaction mixtures were incubated for 5 minutes, and concentrations of enzyme and substrate were 1 µM and 0.5% (w/v). The results are presented in Figure 14.

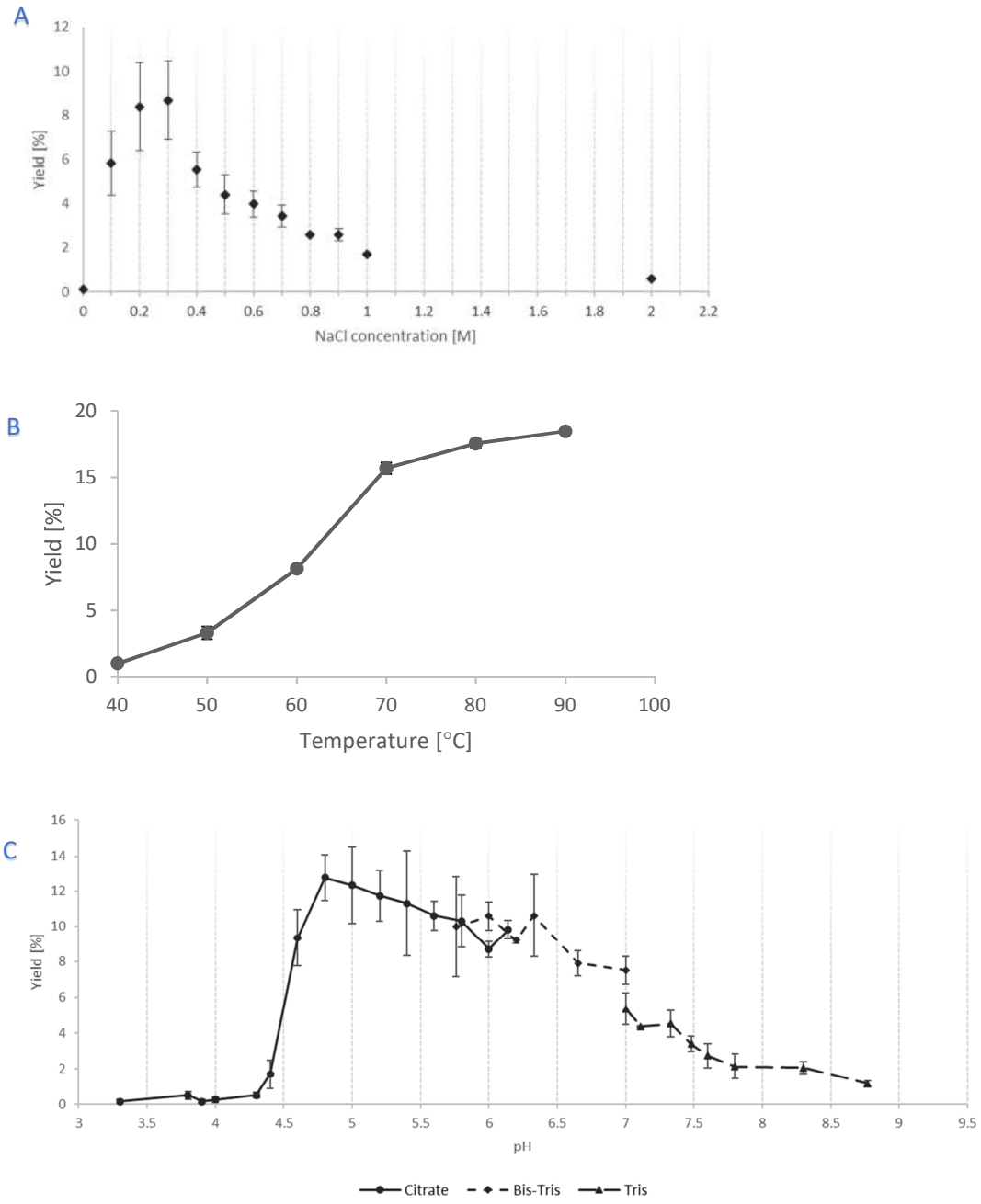

Figure 14: **Salinity-, temperature- and pH screening of Apl17-2.** (A) Salinity screening. The enzyme was exposed to different grades of salinity (NaCl) to determine how it would perform across the range from 0 to 2 M NaCl. . (B) Temperature screening. The enzyme was tested at temperatures from 40 °C to 90 °C, with 10 °C-intervals in 25 mM NaOAc and 300 mM NaCl at pH 5.6. (C) Enzyme activity response to pH variation at 50 °C. The activity of Apl17-2 was examined in the range of pH 3.3-8.8. The full names of the three buffers that were used are Citrate-/citric acid, Bis-Tris/HCl and Tris/HCl.

The salinity screening indicates that Apl17-2 works most efficiently in about 300 mM NaCl. However, there is no significant difference in activity at 200 mM versus 300 mM NaCl. The enzyme is either close to- or totally inactive in the absence of NaCl. There is a steep rise in efficiency from 0 to 0.2 M NaCl. The effect of temperature on Apl17-2 activity was tested for 5-minute reactions at 40 °C, 50 °C, 60 °C, 70 °C, 80 °C and 90 °C. The data shows that temperature has a dramatic effect on enzyme activity,

with product yields being more than 18-fold higher at 90 °C versus 40 °C for 5-minute reaction times under the given conditions. These results do not account for thermal stability and cannot be used to make assumptions about the enzyme's response to these temperatures for longer incubation times. The results from the pH-screening suggest that the enzyme has a broad pH optimum in the 5.0 – 6.0 region. There is a dramatic shift from no significant activity until and including pH 4.3, to almost maximal activity at pH 4.8. The data (Figure 14C) indicate a buffer-dependent difference in activity between Bis-Tris/HCl and Tris/HCl at pH 7.0.

Thermal stability was assessed by pre-incubating Apl17-2 in 50 mM NaOAc with 600 mM NaCl at 60 °C and 65 °C for different durations up to 24 hours. The pre-incubated enzyme was mixed with pre-heated substrate to achieve the standard reaction conditions: 1 µM Apl17-2, 0.5% (w/v) sodium alginate, 25 mM NaOAc and 300 mM NaCl at pH 5.6 and 50 °C.

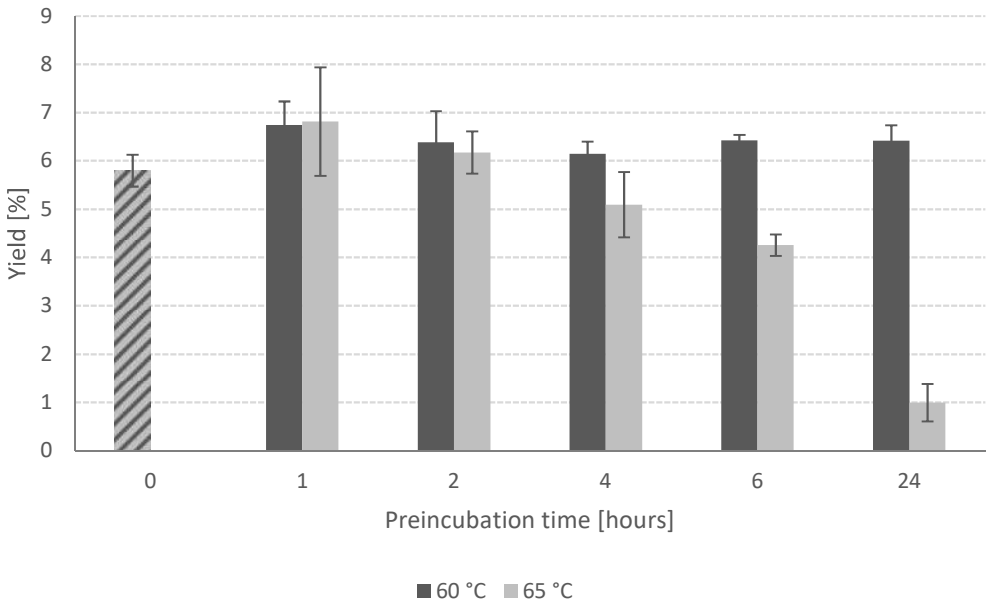

Figure 15: **Thermal stability of Apl17-2.** The figure shows the product yields after 5-minute reactions of 1 µM enzyme and 0.5% (w/v) alginate in 25 mM NaOAc and 300 mM NaCl at 50 °C after pre-incubation at 60 °C or 65 °C for the durations listed along the x-axis. The reaction of unincubated enzyme is represented by only one column since it only represents one situation.

The results from the thermal stability experiment (Figure 15) show that the enzyme is stable for at least 24 hours at 60 °C. On the other hand, pre-incubation at 65 °C led to a gradual decrease in activity, indicating that the enzyme is not stable at this temperature.

4.3.3 Substrate specificity

WT Apl17-2, Y251A and Y446A were all tested on a selection of substrates (Figure 16). Glucose equivalents were used instead of yield because of the different masses of the substrates. Both WT and Y446A showed very similar activity on alginate, poly M and poly G in decreasing order. The relative activity on alginate, poly G and poly M may actually be very different to what is indicated in Figure 16, since the measured value of the samples would be likely to be located beyond the initial linear area if progress curves were made. Neither WT or any of the two mutants showed detectable activity on heparin, chondroitin or laminarin. Even though mutant Y251A seems to have marginal activity on all substrates except for poly G, the amount of generated product is so low that it is hard to determine if it is significant.

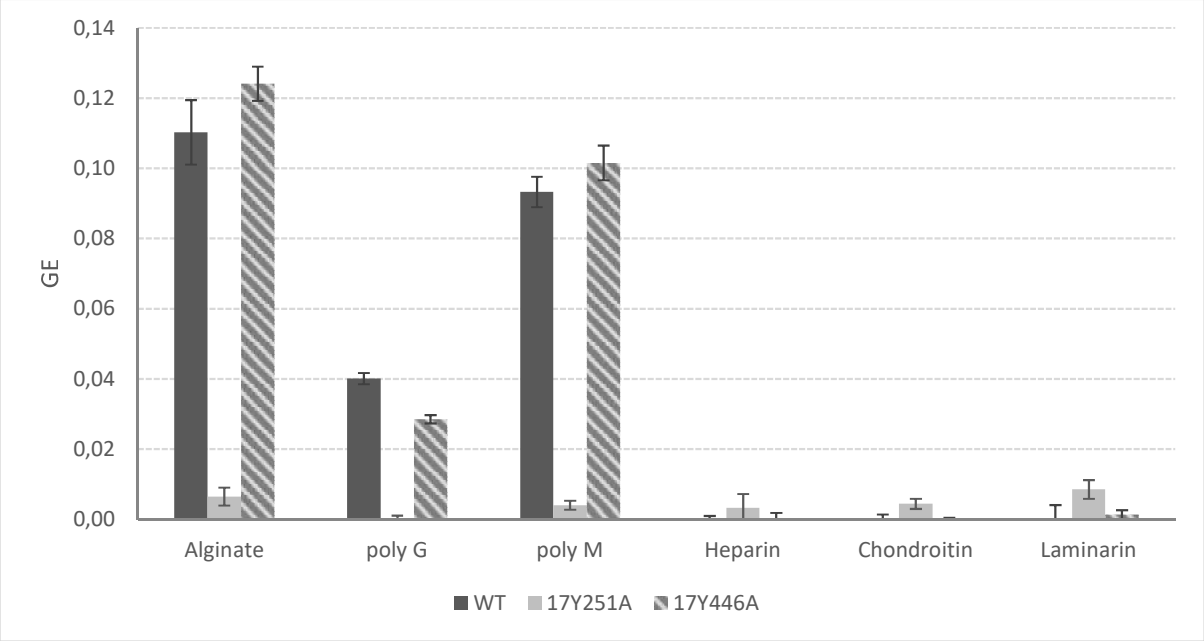

Figure 16: **Activity of WT Apl17-2, Y251A and Y446A on different substrates.** GE was used instead of yield (%) because of the variation in monomer mass between the substrates. The reaction conditions were 1 µM enzyme, 0.1% (w/v) substrate, 25 mM NaOAc and 300 mM NaCl. The reaction mixtures were incubated for 20 hours at 60 °C and pH 5.6.

4.4 Characterization of products

Anion exchange chromatography was conducted to examine the final enzymatic products, and also to reveal more about the enzyme's mode of action by studying intermediate and final products. In analysis by anion exchange chromatography, all samples were obtained from reaction solutions where the following variables were the same: 25 mM NaOAc, 300 mM NaCl, pH 5.6 and 50 °C. The enzyme- and substrate concentrations, reaction times and stopping methods varied and this information is provided in the respective figure legends.

4.4.1 Oligomers

The IonPac AS4A column was used for analysis of alginate oligomers. This included samples from reactions of Apl17-2 with various substrates, oligomer standards, acid hydrolysate of poly M and -poly G, and poly M digested by an endotype M-specific alginate lyase. The acid hydrolysates were, as the name suggests, produced by acid hydrolysis of either poly M or -G under harsh conditions and yields saturated oligomers. Endolytic digestion of poly M yields oligomers with unsaturated non-reducing ends (4-deoxy-alpha-L-erythro-hex-4-enuronosyl) as described in the Introduction. These oligomers are often denoted ΔM#, where Δ is the unsaturated residue and # is the degree of polymerisation (DP) or total number of residues in the oligomer (including Δ). These degradative reactions can be controlled to avoid maximal degradation, generating a wide spectrum of oligomers of different chain lengths, as was done for the oligomeric substrates used in this study. The saturated M- and G-oligomers have different retention times compared to each other and to their counterparts with an unsaturated non-reducing end.

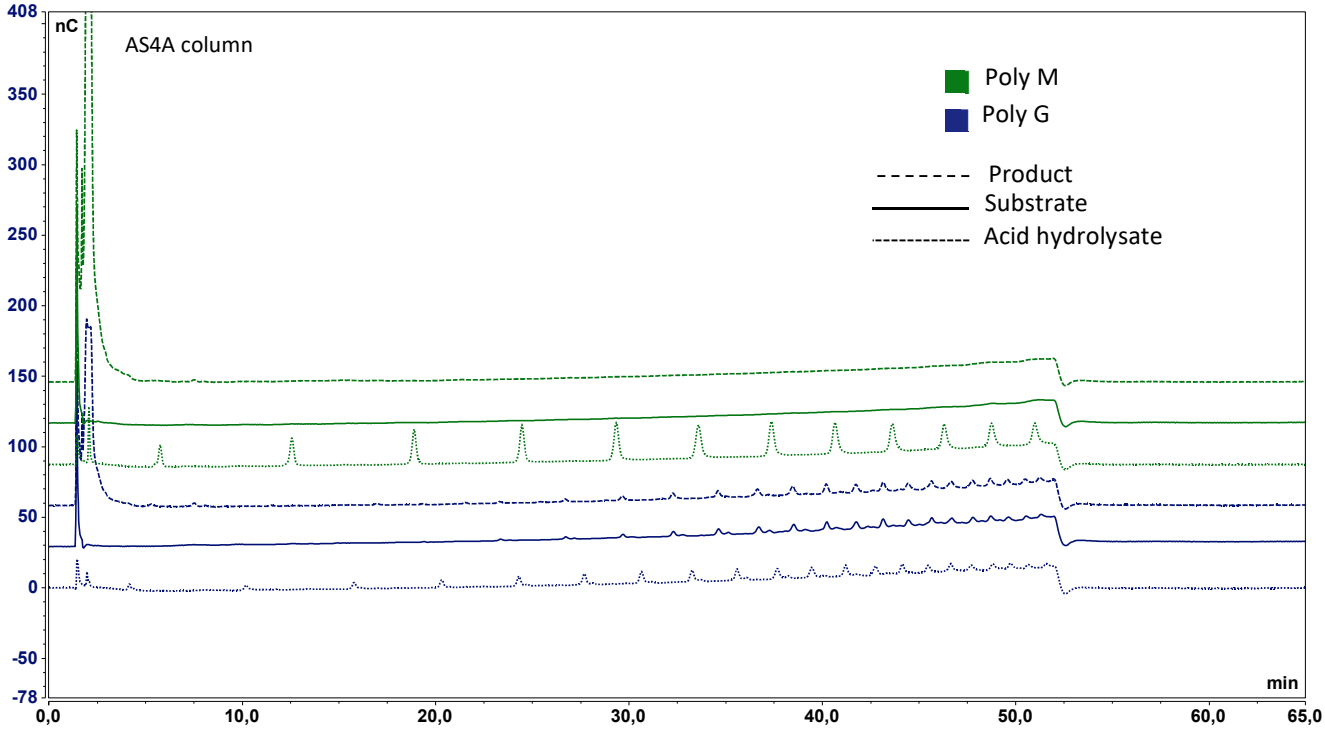

Figure 17: **Chromatograms showing product generated after incubation of Apl17-2 with poly M and poly G.** The figure shows chromatograms from substrate blanks of poly M and poly G, reaction solutions of Apl17-2 with these substrates, and also chromatograms of acid hydrolysates of poly M and poly G. The substrate concentration was 0.1% (w/v) and the enzyme concentration was 1 µM. The reaction went on for 1 hour and was stopped by boiling for 10 minutes.

Apl17-2 converts polymeric substrates to monomers

Figure 17 shows chromatograms from reactions of Apl17-2 with poly M and poly G. Poly M and -G are large, saturated polymers reminiscent to the poly M and -G blocks found in natural alginate. Acid hydrolysates of both poly M and poly G were included as standards to compare with potential oligomers generated by the enzyme. The chromatograms show that large peaks are detected right after the injection tops (ca. 2 minutes) when samples from reactions with Apl17-2 on both poly M and poly G are analysed. These peaks do not appear in the substrate blanks or the acid hydrolysates. This strongly suggests that Apl17-2 is able to convert large, saturated polymers of M and G to one or more monomer products.

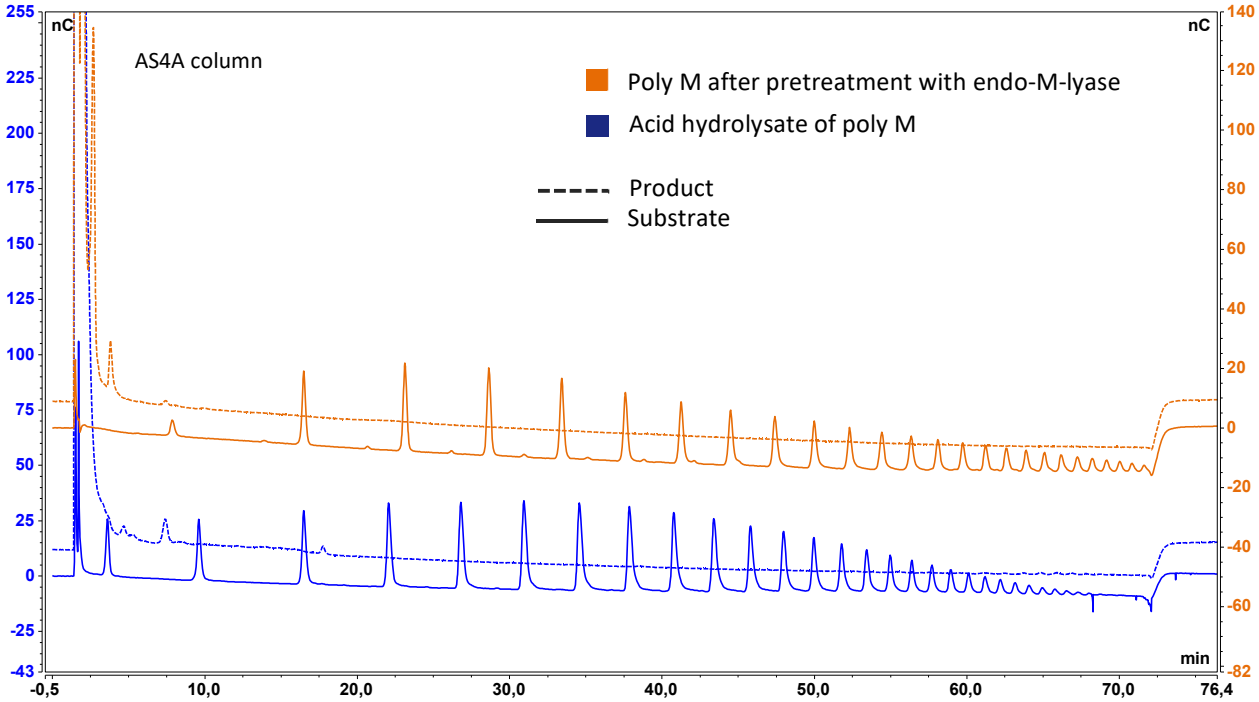

Figure 18: **Chromatograms showing products from reactions of Apl17-2 with oligomers of saturated and unsaturated mannuronate.** Poly M digested by an endotype M-lyase and acid hydrolysate of poly M were used as substrates. The enzymatically pre-treated substrate has unsaturated non-reducing ends that affect the retention of the substrate, and explains why the oligomers elute at different times compared to the purely saturated oligomers obtained from acid hydrolysis. The chromatogram shows that all the oligomeric peaks of both substrates are absent in samples treated with Apl17-2. There are also large peaks present after the injection tops, like what was seen in Figure 17. Enzyme and substrate concentrations were 5 µM and 0.25% w/v. Reactions were stopped after 24 hours by adding 1 M NaOH in a ratio of 1:10.

Apl17-2 depolymerises saturated and unsaturated substrates

Figure 18 shows that the oligomeric peaks of both poly M acid hydrolysate and poly M pre-treated by endotype M-lyase are absent from samples after treatment with Apl17-2. Again, there are large peaks at the start of the product-chromatograms that partly overlap with the injection peaks. The results clearly point towards the enzyme being able to degrade both saturated and unsaturated mannuronate oligomers.

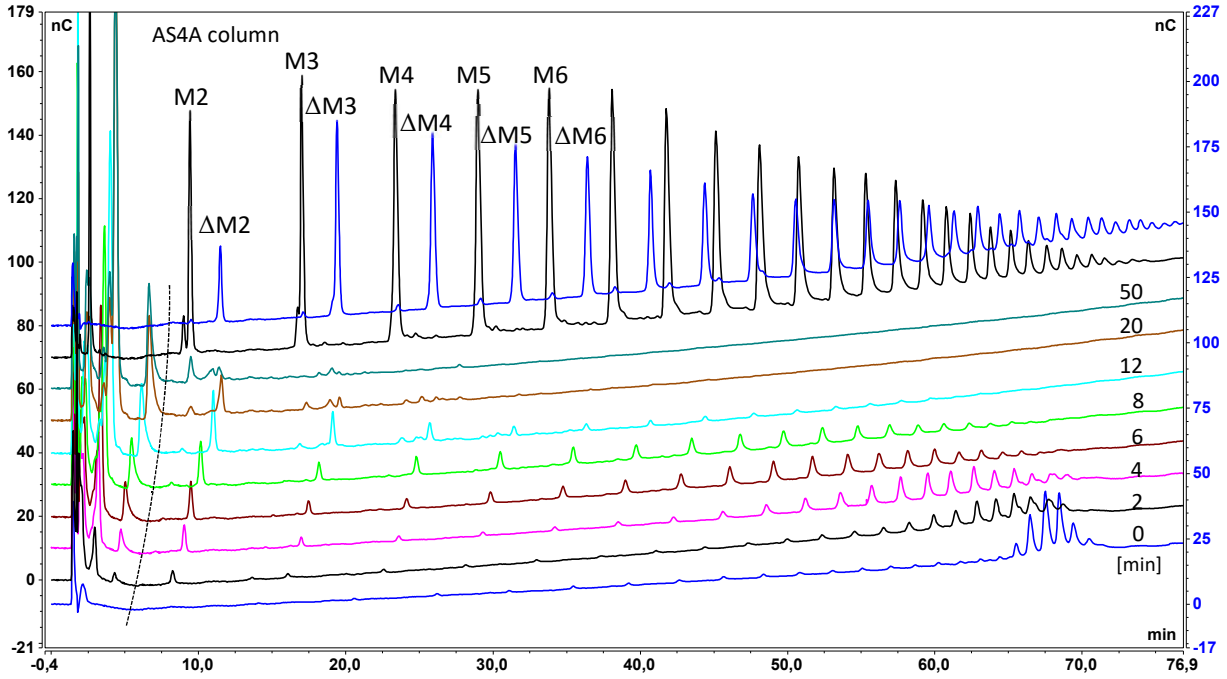

Figure 19: **Time-resolved analysis of products after treatment of M24-substrate with Apl17-2.** The chromatogram shows the progress of reactions with Apl17-2 and oligomeric M substrate with 24 degrees of polymerisation (DP) shortened to M24. The progress is resolved from the bottom up, and reaction times are shown on the right side of the chromatograms. The two uppermost lines are standards: acid hydrolysate of poly M (second from the top) and poly M pre-treated with endotype M-lyase at the top, with expected identities assigned. Each line represents an individual reaction. There is a trend of increasing number of peaks up to 8 minutes reaction time, followed by a decrease. The average elution time of the peaks of each chromatogram decrease gradually as the reactions proceed. There is also an increase in peaks that elute within ~12 minutes, but then a decrease again from 12-50 minutes for the most prominent peak closest on the right side of the dotted line. There is an analytical, non-linear retention time shift between runs as seen along the dotted line, indicating a drift in the system. The enzyme concentration was 0.1 µM, but the substrate concentration is unknown (estimate: ~0.5% w/v). Reactions were stopped by adding 1M NaOH in a ratio of 1:10.

Apl17-2 has exolytic activity

The results from a time-resolved analysis of M24-degradation by Apl17-2 are displayed in Figure 19. Samples were taken from reactions of Apl17-2 with M-oligomer of DP24 at the times indicated in the figure. There is an increasing number of peaks toward 8 minutes reaction time, followed by a decrease. There is also a trend of shorter elution times of product-peaks for reactions with longer incubation times, i.e. smaller and smaller oligomers as the reactions proceed. Both endo- and exolytic activity, would yield progressively shorter chain lengths. However, endolytic catalysis would yield a large variation of chain lengths in the initial samples as the M24 chains would be cleaved at random sites presumably resulting in an even distribution of shortened oligomers. Assuming the enzyme uses β-elimination, an endolytic enzyme would yield both saturated and unsaturated fragments, causing a larger number of peaks to appear. An exolytic lyase would only yield monomeric products and unsaturated polymer/oligomer intermediates. In this case, there is a shift from a majority of long oligomers to even spreading, to only putative monomers and a small proportion of dimers.

Additionally, there is a build-up of monomer peaks right from the start that elute within ~7 minutes. These findings strengthen the hypothesis that Apl17-2 is an exotype alginate lyase.

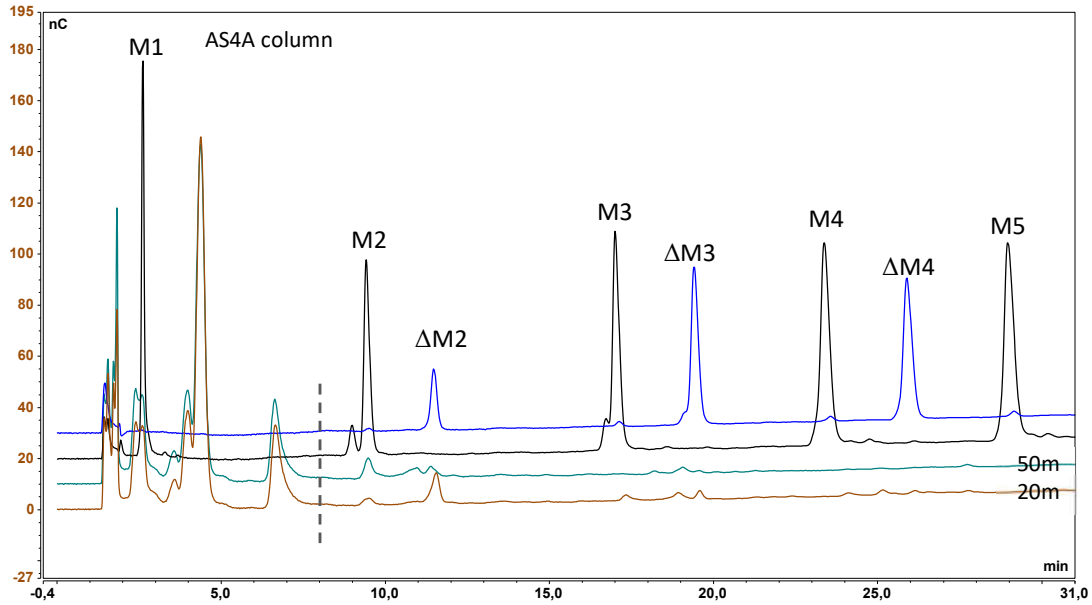

Figure 20: **Close-up of the upper left section of Figure 19.** The zoomed in section reveals more detail from the results in Figure 19. From the bottom up, the lines represent samples from a reaction of 20 min, a reaction of 50 min, the poly M acid hydrolysate and the poly M pre-treated with endotype M-lyase at the top. The peaks on the left side of the dotted line are thought to be monomers.

Apl17-2 works from the non-reducing end

The close-up view of the initial elution peaks of 20- and 50-minute incubations of M24 with Apl17-2 (Figure 20) reveals some interesting details. The putative monomer segment on the left side of the dotted line, seems to contain two more peaks than what is observed in the t = 0 sample of Figure 19. The non-linear retention time shift observed in Figure 19 is less pronounced for the four chromatograms in Figure 20. The brown peak which elutes at ca. 11.5 minutes is strongly suspected of being a dimer because of the proximity to M2 and ΔM2. The peak elutes at the same time as ΔM and there doesn't seem to be an analytical retention time shift in the system for these injections. Although different compounds can have similar retention times, the chromatograms points toward that the brown peak at ~11.5 minutes actually represent the ΔM2 dimer. If the assumption is true, it is almost guaranteed that the other peaks that appear below this peak in Figure 19 are ΔM2 as well. This again strongly implies that all the other intermediate oligomeric peaks generated from activity of Apl17-2 on M24 have unsaturated non-reducing ends. Thus, Figure 20 together with Figure 19, indicates that Apl17-2 generates intermediate oligomers with unsaturated non-reducing ends which are

continuously cleaved off to monomers by the enzyme's exolytic activity, i.e. the enzyme operates from the non-reducing end towards the reducing end.

4.4.2 Monomers

The results displayed in Figure 17 -Figure 19 indicate that Apl17-2 continuously generates monomers in an exolytic manner. HPAEC-PAD, UV-analysis, MS, and NMR were used to obtain more knowledge about the properties of monomers produced form the activity of Apl17-2. In the anion exchange analysis of monomers, an UV module was placed between the column and the amperometric detector. UV absorption was monitored at 235 nm to examine if UV-active products were formed.

As part of an experiment that was conducted for examining oligomers, four electrochemical peaks were detected from the product sample that eluted within 6 minutes (Figure 21). These peaks elute too fast to represent oligomers (elaboration below) and are therefore included in the monomer section.

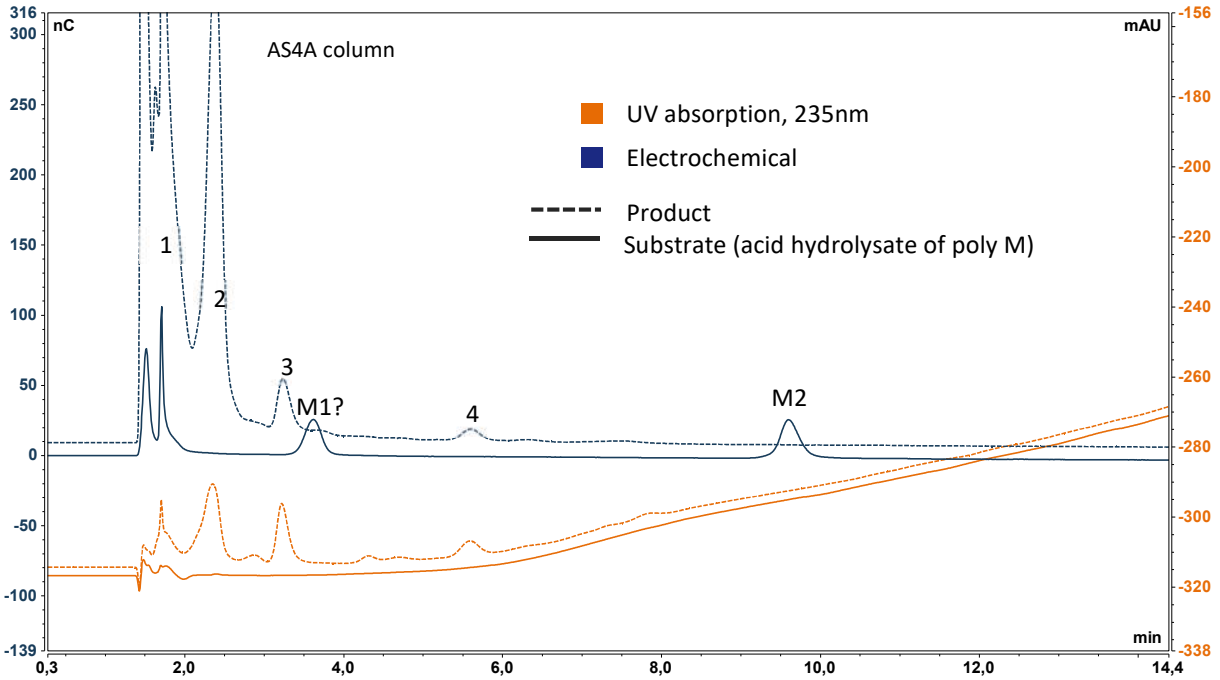

Figure 21: **Chromatographic analysis of samples from Apl17-2 incubated with acid hydrolysate of poly M.** The figure shows both UV-absorption and amperometric detection of a sample from a reaction solution of acid hydrolysate of poly M treated with Apl17-2. The reaction contained 5 µM enzyme and 0.25% (w/v) substrate and was terminated by adding 1 M NaOH in a 1:10 ratio after 1 hour. Peaks numbered 2, 3 and 4 seem to represent UV-active compounds, while the two peaks visible in the electrochemical chromatogram of the substrate (blue solid line), M1 and M2 do not show signs of UV-absorption.

Figure 21 shows that there are four distinguishable peaks that are only present in the reaction samples. The electrochemical peaks numbered 2, 3 and 4 clearly absorb UV at 235 nm. As expected for saturated uronic acids such as mannuronate, there is no UV-absorption corresponding to the two electrochemical peaks of the substrate. However, the appearance of 4, UV-active product-peaks was surprising. These peaks elute close to the substrate monomer and well before the dimer. The results from the M24-analysis indicated that the enzyme produces oligomers with unsaturated non-reducing ends, and Figure 19 and Figure 20show that ΔM2 elutes after M2 which is in accordance with what others have found on the same column (Aarstad et al., 2012) or using a SB Nucleosil column (Heyraud et al., 1996). Thus, it seems reasonable to assume that all the numbered product-peaks are monomer variants. Only the putatively formed Δ was expected to be UV-active. It is therefore surprising to see 4 UV-active peaks.

The AS4A column which was used in the analysis of oligomers, may also, to some extent resolve peaks arising from rapidly eluted compounds such as monomers, as seen in Figure 20 and Figure 21. However, a CarboPac PA1 column was used to provide better resolution of the putative monomer peaks observed in Figure 20 and -21, and to determine if Apl17-2 produces saturated or unsaturated monomers. Mannuronate and guluronate monomers have different retention times and were included as standards in all the experiments where the PA1 column was used.

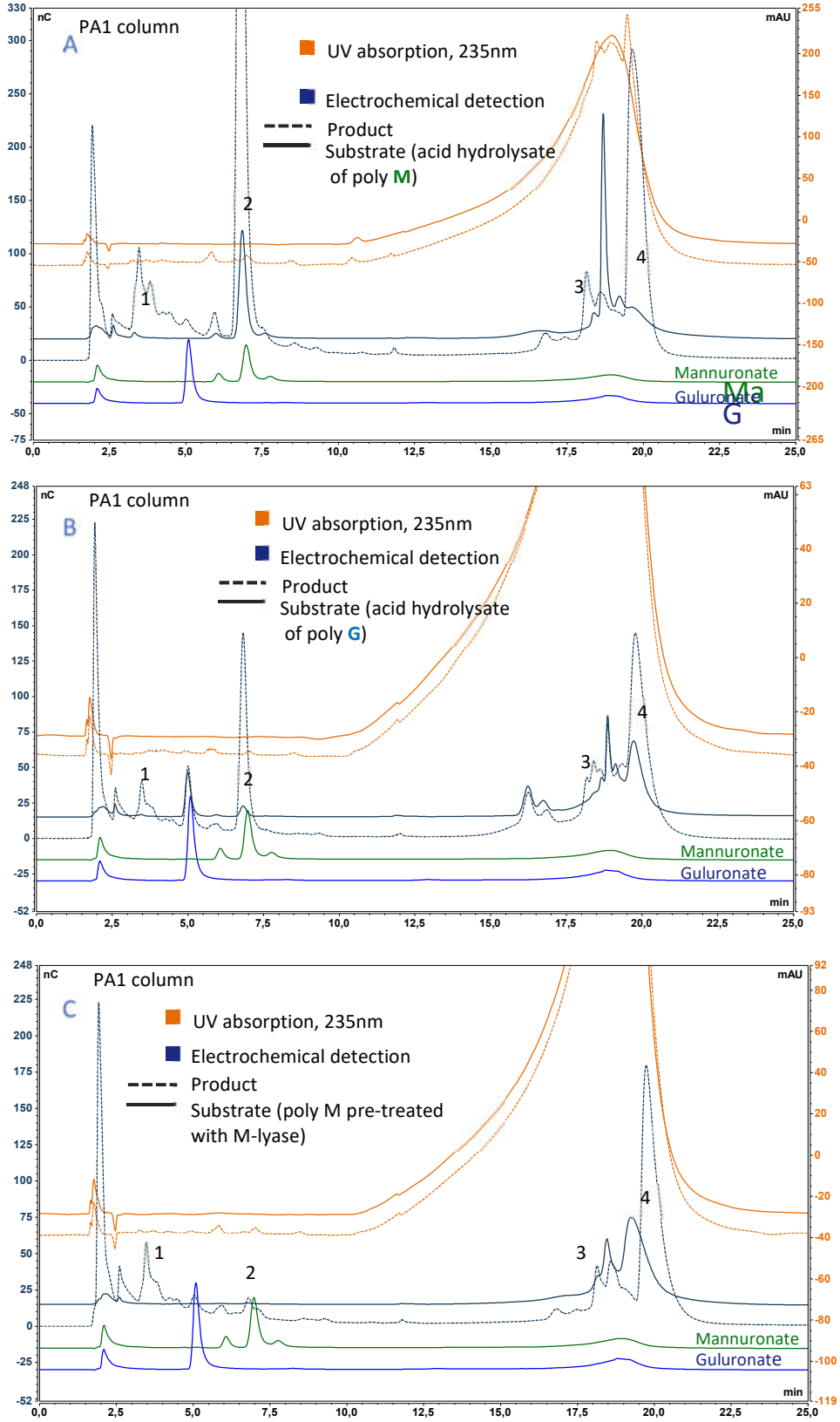

Figure 22: **Chromatograms of monomer analysis of samples from Apl17-2 and acid hydrolysate of poly M.** The chromatograms in all three panels of the figure are as follows in rising order from the bottom up: guluronate and mannuronate standards, substrate treated with Apl17-2, substrate blank, UV-absorption at 235 nm for the Apl17-2 reaction and for the substrate blank at the top. The enzyme and substrate concentrations in the reactions were 1 µM and 0.5% (w/v).

Reaction mixtures were incubated for 1 hour and stopped by adding 1 M NaOH in a ratio of 1:10. Similar reaction conditions were used in all three situations, but different substrates. (A) There are four distinct electrochemical peaks in the sample from the reaction solution that are not present in the substrate. There are several small peaks in the UV-absorbtion lines for the reaction sample. (B) The only difference between A and B is that in B, Apl17-2 reacted with acid hydrolysate of poly G instead of poly M. (C) The situation is similar to the ones in A and B except for that the substrate in this case is poly M pretreated with an endotype M-lyase. The substrate has unsaturated non-reducing ends.

In segment A and B of Figure 22, there are four distinct peaks in the electrochemical chromatograms of samples from the reaction solutions that elute at similar times and that are not present in the substrate, analogous to what was seen in Figure 21. The four numbered peaks (1-4) may or may not represent the same compounds in the two figures. The order might also be different since a different column and eluents are used. Product-peak 2 elutes at the same time as the mannuronate monomer. However, corresponding peaks are also present in reaction samples of acid hydrolysate of poly M and acid hydrolysate of poly G, indicating that peak 2 is not the monomer of mannuronate. Additionally, peak 2 seems to be UV-active, which points away from saturated M and towards Δ or some other variant. Surprisingly, peak 2 is virtually absent in part C, while peaks 1, 3 and 4 still appear in very similar forms in all three panels of the figure. This strongly indicates that product-peak 2 is the result of enzyme activity, but this does not mean that the other peaks are not products of enzyme activity. Perhaps product-peak four could be Δ or DEHU since it elutes after the M- and G standards, analogous to oligomers of ΔM# eluting after M# of similar DP. It is not likely that any of the peaks are dimers since there is little to no difference in the elution time of the corresponding peaks in the three panels of Figure 22. Overall, it is inconclusive what the product-peaks represent. Unfortunately, a Δ/DEHU standard was not available. It was attempted to construct a Δ/DEHU standard by hydrolysing ΔM3 by HCl at pH 3.6 and 90 °C for 2 hours, but this was not successful (data not shown).

4.5 UV/Vis spectral analysis

Both endolytic and exolytic enzymes that follow the canonical β-elimination mechanism of polysaccharide lyases (PL), generate product that absorbs UV at λ_{max} = 235 nm. Endolytic and exolytic enzymes of this type form 4-deoxy-α-L-*erythro*-hex-4-enopyranuronosyl at the new non-reducing end, while the exolytic enzymes also generate a free monomeric version of this product: 4-deoxy-L-*erythro*-hex-4-enopyranuronate. The only difference between the compounds being that 4-deoxy-α-L-*erythro*-hex-4-enopyranuronosyl stays linked to one or more successive G- or M residues on its reducing end, while the monomer 4-deoxy-L-*erythro*-hex-4-enopyranuronate obtains a hydrogen at the oxygen of the newly broken glycosidic linkage upon separation from the chain. Both of these compounds are

referred to as Δ in this study, but the linked Δ residue is mostly mentioned in association with its neighbouring residue, ΔM or ΔG.

Previous studies have shown that the enzymatically produced Δ absorbs radiation at 235 nm both when attached to the non-reducing end of an oligomer/polymer (Preiss & Ashwell, 1962a) and in its free monomeric form (Shevchik et al., 1999). It has also been shown that DEHU does not absorb UV at 235 nm (Preiss & Ashwell, 1962a). After Hobbs and co-workers discovered the function of the enzyme KdgF, the consensus is that the conversion of the 4,5-unsaturated monomer to DEHU is catalysed by KdgF, but that it also happens spontaneously at a much slower rate (Hobbs et al., 2016). Since the results from the experiments investigating the enzyme's mode of action showed that UV-active product was generated from exolytic activity, it was natural to examine if a decrease in UV-absorption could be measured over time, which would coincide with the transition from the putatively formed UV-active Δ monomer to UV-inactive DEHU. In addition, reactions were terminated either by heat, addition of HCl or addition of NaOH to assess possible effects on the transition between the two compounds.

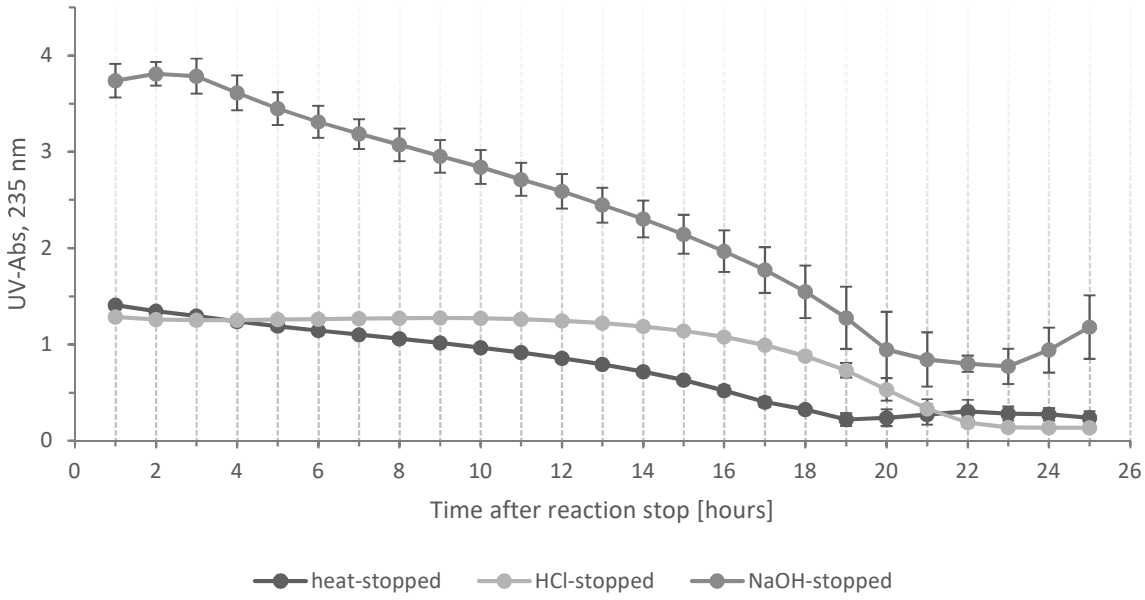

Figure 23: **UV-absorption of product mixtures resulting from reactions of Apl17-2 with sodium alginate.** The figure shows the absorbance at 235 nm of a reaction mixtures from Apl17-2 with sodium alginate. The reaction conditions were 1 µM enzyme, 0.5% (w/v) sodium alginate, 25 mM NaOAc, 300 mM NaCl and were incubated at pH 5.6 and 50 °C. Parallel reactions (200 µL) were incubated for 2 hours and were stopped either by boiling for 10 minutes, adding 1 M HCl (20 µL) or adding 1 M NaOH (20 µL).

Figure 23 shows a dramatic difference (2.6 times) in UV-absorption of the samples containing NaOH compared to samples that had been boiled or contained HCl, which have similar absorbance after one hour. The NaOH-containing samples showed stable absorption values for 3 hours, after which the signal starts an almost linear decline. The HCl-containing samples showed relatively stable absorption, with a decline only becoming noticeable after about 12 hours. The heat-treated (100 °C, 10 min) samples, showed an almost linear trend of decreasing absorption towards 13 hours. Although the data in Figure 23 are not easy to explain, it is clear that the products formed are unstable and that several chemical conversions may occur that either increase or decrease UV absorbance. Thus, it would seem that multiple products may be generated, chemically, which may explain the complexity of the results from Figure 21 and Figure 22.

When NaOH was added to reaction mixtures, there was an immediate colour change from a colourless solution to a bright yellow-green colour, while the solution remained clear (transparent). This effect was confirmed to be solely associated with the enzymatic products, as the colour change was seen after addition of NaOH to product-solutions where the enzyme had been removed, and was not observed after addition of NaOH to substrate blanks or substrate incubated with the inactive mutant Y251A.

An experiment was conducted where different bases were added to reaction mixtures in the same 1:10 volume ratio (base : reaction solution); these bases were (pH after addition is displayed in parenthesis): 1 M NaOH (pH = 13.5), 1 M KOH (pH = 13.5), 1 M Na_2CO_3 (pH = 11.5), 1 M NH_3 (pH = 10) and 15 M NH_3 (pH = 11.5). The solutions with added NaOH or KOH immediately obtained the same bright yellow/green colour (Appendix F). There was a gradual development of colour in most of the other samples as well, but it took several days and was not as pronounced. Interestingly, after 15 days of standstill, all solutions except for the one with added 15 M NH_3 had quite similar colours. The bright colour after addition NaOH or KOH was shown to be moderately unstable, but was still clearly visible after more than two weeks and was never observed to diminish completely. Please note that these colorimetric results are purely based on eyesight observation. Again, these observations indicate product instability and possible chemical formation of multiple products.

4.6 Product analysis by MALDI-TOF MS

Enzymatic products of the degradation of poly M by Apl17-2 were also analysed using negative mode MALDI-TOF mass spectrometry. The samples originated from reactions stopped by heat (100 °C, 10

min) or by addition of NaOH in a 1:10 ratio. The stopped reactions were left standing still before samples were applied to the target plate after 30 minutes, 24 hours, 48 hours and 72 hours.

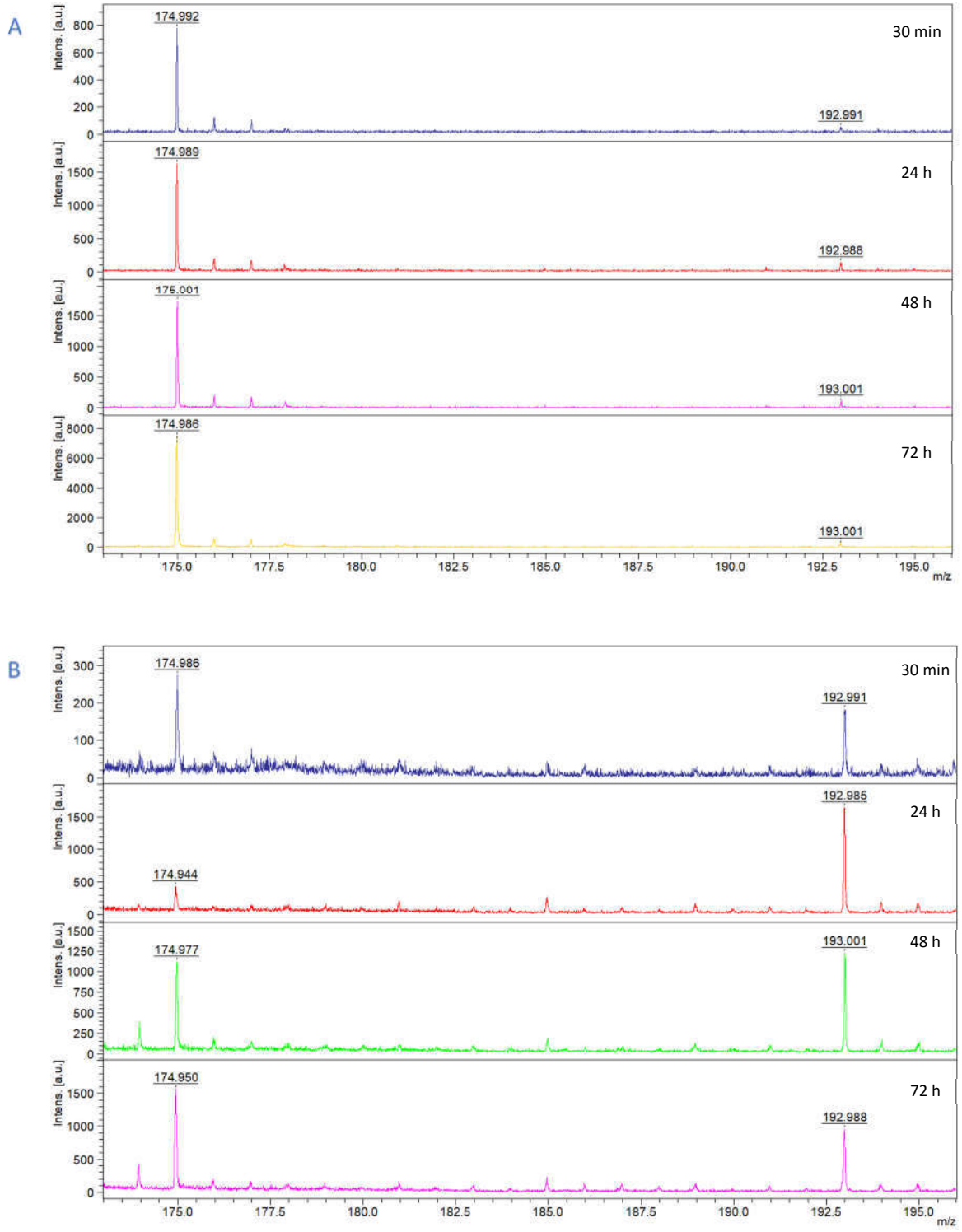

Figure 24: **MALDI-TOF analysis of samples obtained from reaction mixtures of Apl17-2 with poly M.** The figure shows MS-analysis of poly M substrate treated with Apl17-2 that was either stopped by boiling (A) or by addition of NaOH (B). A single reaction mixture was separated into two parts where one was subjected to heat (100 °C for 10 min) and one was treated

with 1 M NaOH in a 1:10 volume ratio, at the time of termination. The terminated reaction mixtures were sampled at 30 min, 24 h, 48 h and 72 h of standstill at 22 °C. The reaction conditions were: 3.3 µM Apl17-2, 0.25% (w/v) poly M, 25 mM NaOAc, 300 mM NaCl, 50 °C and pH 5.6. The reactions were stopped after one hour of incubation.

The MALDI-analysis revealed a key difference in observed peaks within the range of $[M-H]^-$ = 174-195 m/z. The samples from reaction mixture that was stopped by boiling mainly gave rise to one prominent peak at m/z = 175, while samples containing NaOH showed peaks at m/z = 175 and m/z = 193. With the exception of the 24-hour sample of the NaOH-stopped reaction, the peaks in both situations are stable over time. In negative mode MS, $[M-H]^-$ = 175 m/z corresponds to DEHU (Inoue et al., 2015) and m/z = 193 equates to both mannuronate and hydrated DEHU. It is believed that 193 m/z represents hydrated DEHU in these conditions, since basic hydrolysis of alginate have not seemed to occur at identical NaOH concentrations in previous experiments of this study; e.g. no measured increase of reducing ends in samples containing NaOH versus those that do not in DNS assays. The MALDI-analysis indicate that NaOH (pH > 13.0) promotes hydration of DEHU.

4.7 Crystallography

Attempts were made to obtain crystals of Apl17-2 for structure elucidation by X-ray crystallography. A JCSG-plus™ crystal screening kit was used, and a small crystal was observed in a drop prepared by condition 2-8, which has not yet been subjected to X-ray crystallography.

5 Discussion

This study aimed at investigating the properties of an alginate lyase from hot vents in the arctic mid-ocean ridge. WT Apl17-2 and two point-mutants were expressed, purified and tested for activity on different substrates. Optimal conditions for WT Apl17-2 were determined and in-depth studies of its mode of action were conducted. Properties of the enzymatic product were also explored.

The initial step of this study was the design of two point-mutants for Apl17-2. The sites of mutation were based on two previously published tyrosine to alanine mutations in the PL17 alginate lyase Alg17c: Y258A and Y450A, which were concluded to be the catalytic base (Tyr258) and acid (Tyr450) based on structural studies and the observation that the two mutant enzymes were inactive (Park et al., 2014). The corresponding mutation sites were determined by sequence alignment of Apl17-2 and Alg17c. As expected, the respective residues were conserved in Apl17-2 and were located at positions 251 and 446 in the WT sequence. Similar tyrosine to alanine mutations were produced, Y251A and Y446A.

The enzyme referred to as WT Apl17-2 in the experiments of this study, was not strictly a wild-type, as the putative N-terminal signal peptide was excluded, and a His-tag (-AHHHHHH) was added to the C-terminal of the original sequence. Signal peptides are important for protein location and secretion in the native organism (von Heijne, 1990), but they may affect the heterologous expression of the protein (Blocker et al., 2015), i.e. the expression of a protein in another organism. The His-tag was necessary for protein purification by Ni-Sepharose affinity chromatography.

5.1 Mode of action

The data obtained from analysis using HPAEC-PAD, showed that Apl17-2 converts all chain lengths of substrates with saturated- or unsaturated non-reducing ends to monomer products in an exolytic manner working from the non-reducing end. Additionally, it produces UV-active products. All these findings are in accordance with the canonical β-elimination mechanism of PL enzymes and the mode of action utilised by oligo-alginate lyases (EC 4.2.2.26). In combination with sequence similarities to other PL17 enzymes, these findings strongly indicate that Apl17-2 is a PL17 oligo-alginate lyase continuously generating monomers by the conventional mechanism and mode of action. So far, there seems to be only one enzyme, HdAlex, classified as an oligo-alginate lyase, which has a deviant mode of action compared to other enzymes of this class. This strange enzyme was reported to operate from

the reducing end of the substrate and cleave off dimers in an exolytic manner (Suzuki et al., 2006). Even though no alginate lyase operating by a hydrolytic mechanism seems to have been discovered, several enzymes have been characterized which hydrolytically degrade pectin (EC 3.2.1.15), which like alginate, consists of uronic acids. Given that other pectin lyases utilise β-elimination, this implicates that there might be hydrolytic alginate lyases to be discovered.

5.2 Activity measurements and product stability

Different methods have been used for product quantification in the characterisation of both endotype- and exotype alginate lyases, in particular the thiobarbituric assay (TBA) (Ochiai et al., 2010; Park et al., 2014), UV absorption at 235 nm (He et al., 2018; Vuoristo et al., 2019) and the DNS assay (Wang et al., 2018; Wang et al., 2015). DNS was used in the enzyme activity assays of this study with glucose as standards. Ideally, alginate monomers would have been used, even though they are similar to glucose with regards to having a reducing end that can interact with the DNS-reagent, and have been used as standards in alginate lyase assays before (Zhu et al., 2016). Still, the alginate monomers themselves, nor glucose, are similar to Δ or DEHU, which are the suspected enzymatic products of PL enzymes. UV-absorption was not used for quantification because of the effect of the spontaneous loss of UV-activity when the unsaturated monomer product rearranges to DEHU which will affect product quantification of reactions that are incubated several hours (Shevchik et al., 1999).

The results shown in Figure 12 and results from several other experiments (data not shown), showed that the amount of measured product decreased in samples from terminated reaction mixtures that were stored for several hours. This time-sensitive decrease of detectable product is what would be expected to be observed for enzymes that operate by the conventional β-elimination mechanism if UV-apsorption was used for quantification, in accordance with what was discovered by Shevchik and co-workers (Shevchik et al., 1999). Reports of a similar phenomenon for quantification by the DNS method were not found. Experiments with 5-minute incubations of Apl17-2 with alginate, indicated that the addition of NaOH to terminate reactions stabilised yield readings of samples from these solutions, compared with samples that were terminated by addition of the DNS reagent and stored for the same amount of time (data not shown). This was why addition of NaOH was used to terminate so many of the reactions in this study. However, similar experiments with equal conditions and incubation times of 1 hour, indicated that NaOH had no effect on product stability, as samples from reactions that were stopped by mixing with the DNS reagent or by addition of NaOH, gave similar yields after 24 hours of storage at 4 °C. The yields from these samples were roughly half of what was obtained from samples

from solutions of similar reactions that were not stored but measured immediately after boiling with the DNS reagent. In conclusion, the best strategy for accommodating the issue of product instability in DNS assays, was to minimise the storage time of solutions of terminated reactions before measurement as indicated by the data shown in Figure 12.

Perhaps the product instability is an effect of the Δ to DEHU transition. It seems reasonable to assume that Δ and DEHU may have different abilities of interacting with the DNS reagent. Reducing sugars are able to interact with the DNS reagent because of their ability to convert to an open (non-circular) form giving rise to an aldehyde or ketone group depending on the sugar, however, the ketone may also tautomerize to an aldehyde. The aldehyde can reduce the DNS reagent during boiling to give a compound with an absorption maximum at 540 nm. However, this logic could be used to argue that DEHU should be better able to reduce the DNS molecules and give higher absorption values since DEHU contains an aldehyde functional group while Δ does not. The issue of product stability should be considered when investigating the kinetics of alginate lyases.

Conditions were screened for optimal activity of Apl17-2, with regards to salinity (NaCl), pH and temperature (Figure 14). It is generally desirable to use a minimal number of additives in enzyme applications. In hindsight, it would therefore be most ideal to use 0.2 M NaCl given the results from the salinity-screening. Based on the results of the temperature screening and thermal stability assessment (Figure 15), the ideal temperature for efficient enzyme activity and stability would be 60 °C. Still, 50 °C was chosen with potential industrial applications in mind, since heating a large-scale solution is energy demanding. Based on the pH-screening the optimal value was 4.8. To the authors knowledge, this is the lowest pH-optimum of any exolytic alginate lyase discovered to date (He et al., 2018; Hreggvidsson et al., 2015; Jagtap et al., 2014; Kim et al., 2012; Miyake et al., 2003; Ochiai et al., 2006; Park et al., 2012; Shin et al., 2015; Thomas et al., 2013; Wang et al., 2018; Wang et al., 2015). The standard pH-value was kept at 5.6. The main reason was to avoid pH-drift induced by temperature or unforeseen factors in experiments to follow. Perhaps this was a too safe choice and pH 5.0 could have been more appropriate. Still, the difference in yield between 5.0 and 5.6 is not very large.

Apl17-2 was shown to retain 100% relative activity after pre-incubation at 60 °C for 24 hours (Figure 15). This means that Apl17-2 is among the most thermostable exolytic alginate lyases that have been discovered and characterized to date (He et al., 2018; Hreggvidsson et al., 2015; Jagtap et al., 2014; Kim et al., 2012; Miyake et al., 2003; Ochiai et al., 2006; Park et al., 2012; Shin et al., 2015; Thomas et al., 2013; Wang et al., 2018; Wang et al., 2015). One example was found of another thermostable

exolytic alginate lyase, AlyRm4 from *Rhodothermus marinus* str.378. AlyRm4 has been assigned to the PL17 family and is part of a patent of thermostable alginate lyases (Hreggvidsson et al., 2015).

WT Apl17-2, Y251A and Y446A were all tested on alginate, poly G, poly M, heparin, chondroitin and laminarin. The reactions were analysed both by the DNS method and by anion exchange chromatography in case the enzyme activity generated products that could not be detected by the DNS method. Activity was found on alginate, poly G and poly M. Additionally, experiments conducted using HPAEC-PAD, revealed that the enzyme is also active on substrate with unsaturated non-reducing ends. Both WT and Y446A were active on alginate, poly M and poly G. This was unexpected, since both mutation sites correspond sequentially to the catalytic base and acid of Alg17c and the same residues were conserved in all characterized PL17 enzymes (Appendix A). Even if Tyr446 did not correspond to the catalytic base or acid, a tyrosine to alanine mutation in the active site would be expected to negatively affect the enzyme's activity. Because Y446A was shown to be active, residue Tyr446 cannot be detrimental for activity. Due to very different reaction conditions in the substrate screening compared to the experiment conducted to find an appropriate incubation time for fixed time experiments (Figure 11), the results obtained from the substrate screening are unlikely to give accurate indications about the relative activity of Y446A to the wild type. Further studies may therefore reveal that Y446A is actually less active than the wild type. However, there are clear differences between the activity of the enzymes on the different substrates, and between the wild type and Y446A compared to Y251A which is seemingly inactive. It follows that Tyr251 in Apl17-2 may in fact be the catalytic acid of the enzyme, which is the role of its corresponding residue in Alg17c.

Considering that the enzyme is significantly more active on poly M than poly G, it is strange that it is most active on alginate which is a mixture of M and G. A possible explanation could be that the enzyme is even more active on alternating MG blocks, which is the case for the exolytic alginate lyases Atu3025 (Ochiai et al., 2006) and OalB (Jagtap et al., 2014).

Most of the progress assays seem to flatten out and stall at a yield threshold of 20 ± 5%. The reason for this is unclear. Since this threshold seems independent of the conditions used, it is likely not related to enzyme stability. Maybe glucose is a problematic standard in activity assays involving alginate. Alternatively, there may be unforeseen chemical effects that make DNS an unsuitable method for quantification of monomer products generated by alginate lyases. This possible explanation will be revisited later in the discussion. Perhaps monomers produced by the enzyme act as inhibitors at a certain concentration. No reports of product inhibition in other exolytic alginate lyases this could be found. An easy way to confirm or disprove that the enzyme is inhibited, would be to execute a reaction

with double the amount of substrate. If the enzyme is subject to product inhibition, activity would halt at the same yield as before. Conversely, if the enzyme is not inhibited, the final yield would be much higher and strongly suggest that either the DNS assay itself or the use of glucose standards is unsuited for accurate quantification of monomer products, or there could potentially be a hidden error in the product calculations and that the substrate is actually used up. In one case (Figure 12) a substrate conversion of more than 30% was observed. This is by far the highest observed conversion in any test, and is likely due to an experimental error. The high yield and low standard deviation could indicate that double amount of substrate was added to all triplets of this sample, but this is speculation. Regardless, it could imply that the enzyme is not inhibited by a product concentration corresponding to ca. 20% yield, but an overall conclusion can not be drawn.

In certain experiments where HPAEC-PAD was used (Figure 18), the enzyme seems to have degraded all the substrate, since no intermediate oligomer-peaks are observed. However, this does not prove that the enzyme is not inhibited by a certain concentration of monomers. In the progress assays, activity stopped at levels around 20% yield with 0.5% w/v substrate and 1µM enzyme. In the reactions discussed here, the substrate concentration was 0.25% w/v and enzyme concentration was 5µM which means that there may not have been enough substrate to achieve the product/enzyme ratio that potentially inhibited the enzyme in the activity assays.

5.3 The nature of the enzymatic products generated by Apl17-2

Many experiments of this study have clearly indicated that Apl17-2 produces one or more monomeric products. Given the strong indications from characterization of the enzyme's mode of action indicating that it is an exolytic oligo-alginate lyase (discussed above), it is expected that the final enzymatic products are Δ and DEHU. It is then strange to observe four electrochemical peaks that may represent monomers after analysis by HPAEC-PAD.

The 24-hour UV-monitoring at 235 nm of reaction mixtures, showed that the environment greatly affects the transition from Δ to DEHU, and likely cause chemical the formation of other, unstable products as indicated by the striking differences in absorption trends over time (Figure 23). The high UV-absorption of products in basic environment (pH > 13.0) was not anticipated. A possible explanation could be that heating and low pH induce ring-opening of Δ and cause a shift towards UV-inactive DEHU, and that the high-pH environment maintains a more normal Δ/DEHU equilibrium. However, the opposite is thought to be more likely for the following reasons: 1) It has been reported

that alkaline conditions can induce ring-opening of pyranoses and lactones (Tihlárik & Babor, 1983). This could mean that the addition of NaOH may affect the transition of circular Δ-monomer to DEHU, even though Δ is not a regular pyranose.

2) The colour change observed after addition of strong alkali-bases might be associated with this transition. There is no hard evidence for this, but Enquist-Newman and co-workers obtained a yellow solid after drying a sample of DEHU. The colour of the solution itself was not commented. The same was observed in this study, where a seemingly colourless solution of an enzymatic reaction mixture resulted a yellow/brown solid after freeze-drying. Additionally, the α-keto acid methylglyoxal, has a yellow colour and diacetyl has a bright yellow/green colour similar to what is seen after addition of alkali-bases. These compounds are very different from DEHU, and reports describing the colour of longer, more similar α-keto acids were not found, so these reports alone do not provide strong evidence for base-induced ring-opening of Δ and formation of DEHU. Still, the combination of these findings indicates that the ring-opening, at least in part, is associated with a colour change.

If the bright yellow/green colour was a property of pure DEHU, it would be expected to see at least some colour change in reaction mixtures of Apl17-2 with alginate after hours and days of standstill. It is still possible that the addition of strong alkali-bases rapidly induce the Δ/DEHU transition, but because of the lack of appearing colour in product-solutions after standstill without added base, it is believed that the addition of strong alkali bases have additional effects on the product that contribute to the colour. In the 24-hour UV-analysis, there seems to be a correlation between the intensity of UV-absorption at 235 nm and the bright colour, as both decrease over time but never reach levels equal to the samples from reactions stopped by heat- or addition of acid, but this relationship was not further investigated.

The results from the MS-analysis conducted in this study show clearly that a basic environment induces hydration of DEHU. Interestingly, this seems to go against what is expected of α-keto acids like DEHU. A small piece of background information is necessary to clarify: Cooper and co-authors point out that α-keto acids are in equilibrium with an enolic form via keto-enol tautomerization. They may also be hydrated by addition of water to the α-carbonyl. The keto-enol equilibrium is affected by the group attached to the β-carbon. If this particular group is methyl or a methylene (as in DEHU), the equilibrium is strongly shifted towards the keto-form in neutral or acidic solutions (Cooper et al., 1983). Since water is added to the carbon of the α-ketone (α-carbonyl), this goes against what was found for DEHU, unless the keto-form remains stable in the basic environment. It is not known for certain, but it seems more

likely that in the highly basic environment, water would be added to the electron poor α-keto-carbon of DEHU and not to a carbon in Δ.

Based on ^{1}H-NMR, ^{13}C-NMR and gradient correlation spectroscopy (gCOSY), Enquist-Newman and co-workers found that the majority of DEHU obtained had been hydrated and formed two cyclic hemiacetal stereoisomers. There was a possibility of four different cyclic hemiacetals (anomers) since the substituents at both C1 and C5 could adopt two different spatial arrangements, but only the most energetically favoured were observed (Enquist-Newman et al., 2014). Two hemiacetals were also observed in NMR analysis of DKI, the 2-epimer of DEHU (Hobbs et al., 2016). The exact conditions the NMR-samples from these two studies were subjected to could not be found.

In light of the results from UV/vis- and MALDI analysis of this study and NMR-results from other studies (Enquist-Newman et al., 2014; Hobbs et al., 2016), it is hypothesised that strong alkali-bases induce ring-opening of the immediate enzymatic product Δ and subsequent hydration of DEHU at the α-carbonyl. The hydrated DEHU will cyclise and give rise to four different anomers, but two low-energy forms will dominate. The elevated UV-absorption and colour change is thought to be associated with auxiliary alkali-ion and pH-effects, in addition to ring-opening.

Since the ICS operated in high NaOH conditions, the different peaks that are seen in Figure 22 might in fact be the different anomeric forms of hydrated and cyclised DEHU.

Hydration of DEHU may have important implications for the use of the DNS method for quantification of enzymatically generated monomers from alginate. Since the DNS solution is basic and contains NaOH, DEHU may more readily be hydrated than it would be to reduce 3,5-dinitrosalisylic acid (DNS). Evidence suggests that hydrated DEHU rearrange to cyclic compounds with consequential loss of its aldehyde group. Thus, its reducing potential would greatly, if not completely diminish. The reduction of DNS by aldehyde groups from the open form of reducing sugars is the working principle of the DNS assay for quantification of these sugars. This may explain the low product yields obtained from activity assays in this study because of the many implications that DEHU is in fact the enzymatic product of Apl17-2.

5.4 Concluding remarks and future perspectives

This study has shown that Apl17-2 is an exolytic, thermostable alginate lyase that is capable of depolymerising all lengths of saturated and unsaturated (pre-digested) alginate with strong indications that it follows the canonical β-elimination of PL-enzymes. Implying that it operates from the saturated or unsaturated non-reducing ends of alginate, producing Δ/DEHU and intermediate oligomers with unsaturated non-reducing ends. The enzyme was found to be active on alginate, poly M and poly G in decreasing order of measured activities, and also on substrate with unsaturated non-reducing ends. The residue Tyr251 was discovered to be important for the enzyme's activity, while Tyr446 was found not to be crucial for activity. The optimal conditions for the enzyme were: 300 mM NaCl, pH 4.8 and 60 °C. The enzyme was shown to be stable at 60 °C for 24 hours without relative loss in activity. This means that Apl17-2 is among the most thermostable alginate lyases, and has among the lowest if not the lowest pH optimum.

The final enzymatic products of Apl17-2 are expected to be 4-deoxy-L-erythro-hex-4-enopyranuronate (Δ) which eventually, spontaneously rearrange by ring opening and tautomerization to the α-keto acid 4-deoxy-L-erythro-5-hexoseulose uronic acid (DEHU). The enzymatic products of Apl17-2 are UV-active at pH 5.6 and in highly acidic, and basic conditions with very different trends of absorption over time.

The measurable product is unstable under storage, prior to quantification by the DNS method. Results of this study indicated that the Δ/DEHU equilibrium is sensitive to physicochemical inputs, and that alternative, unstable products may arise non-enzymatically under changing conditions, in the presence of enzymatic product. There is a striking colour change of reaction mixtures of Apl17-2 upon addition of strong alkali-bases. This change of colour is thought to be, at least in part, a property associated with the formation of DEHU. There are strong indications that DEHU is hydrated under highly basic conditions. From the combination of results from this study and previous reports, it is thought that hydrated DEHU readily cyclises to give four different anomers where two forms will dominate. Given the loss of the reducing aldehyde group upon cyclisation, the basic conditions of the DNS assay, this may render the DNS assay unsuitable for the accurate quantification of monomer products from alginate depolymerisation.

There are still a range of properties of Apl17-2 that remains to be investigated. A natural first step would be to determine if the enzyme is inhibited by its monomeric product, as several experiments of this study could indicate. Kinetic studies could determine how Apl17-2 performs in comparison to other exolytic alginate lyases on alginate, poly M, poly G and especially poly MG since this substrate has not been tested in this study. Kinetics could also be used to evaluate the importance of suspected active site residues by examining a range of mutants. Crystal structures of Apl17-2 with and without bound substrate, could reveal the identity and position of the residues acting as the catalytic base and -acid, and also residues involved in substrate-binding and stabilisation of the anionic charge on the substrate carboxyl. A melting curve analysis could clarify how the enzyme denatures at high temperature and could provide more insight in stability properties.

One of the primary applications for an oligo-alginate lyase such as Apl17-2, would likely be to produce DEHU for metabolic applications by microbes. Examples include production of pyruvate as a product in itself (Cesario et al., 2018) or further fermentation into bioethanol (Enquist-Newman et al., 2014; Takagi et al., 2017; Wargacki et al., 2012). Future engineered microbial platforms may be able to produce more valuable products than bioethanol from DEHU, such as 1,4-butanediol (Yim et al., 2011) and 1,3-propanediol (Nakamura & Whited, 2003) as suggested by Enquist-Newman and co-authors (Enquist-Newman et al., 2014). These compounds are used in the industrial production of plastics, polyesters, detergents, adhesives, solvents, medicines, fragrances and more (Kaur et al., 2012; Yim et al., 2011), and both may be used in the synthesis of biodegradable materials (Ahn et al., 2001; Umare et al., 2007).

By using metabolic engineering on yeast cells (Enquist-Newman et al., 2014; Takagi et al., 2017), DEHU may be used to grow yeast cells for use in aquaculture fish feed with potential health benefits and growth enhancement (Øverland & Skrede, 2017). Alginate lyases may be used in the treatment of cystic fibrosis infected with *P. aeruginosa* by breaking down the protective biofilm of which alginate is an essential component (Islan et al., 2013; Zhu & Yin, 2015).

Perhaps the colour change that occurs upon addition of base to the enzymatic product could be used to develop a novel colorimetric assay for product quantification in assays with alginate lyases.

References

Aarstad, O. A., Tondervik, A., Sletta, H. & Skjak-Braek, G. (2012). Alginate sequencing: an analysis of block distribution in alginates using specific alginate degrading enzymes. *Biomacromolecules*, 13 (1): 106-16. doi: 10.1021/bm2013026.

Ahn, B. D., Kim, S. H., Kim, Y. H. & Yang, J. S. (2001). Synthesis and characterization of the biodegradable copolymers from succinic acid and adipic acid with 1,4-butanediol. *Journal of Applied Polymer Science*, 82 (11): 2808-2826. doi: 10.1002/app.2135.

Akita, H., Nakashima, N. & Hoshino, T. (2016). Pyruvate production using engineered Escherichia coli. *AMB Express*, 6 (1): 94. doi: 10.1186/s13568-016-0259-z.

Axpe, E. & Oyen, M. L. (2016). Applications of Alginate-Based Bioinks in 3D Bioprinting. *Int J Mol Sci*, 17 (12). doi: 10.3390/ijms17121976.

Bakkevig, K., Sletta, H., Gimmestad, M., Aune, R., Ertesvåg, H., Degnes, K., Christensen, B. E., Ellingsen, T. E. & Valla, S. (2005). Role of the Pseudomonas fluorescens alginate lyase (AlgL) in clearing the periplasm of alginates not exported to the extracellular environment. *Journal of bacteriology*, 187 (24): 8375-8384. doi: 10.1128/JB.187.24.8375-8384.2005.

Bateman, A., Smart, A., Luciani, A., Salazar, G. A., Mistry, J., Richardson, L. J., Qureshi, M., El-Gebali, S., Potter, S. C., Finn, R. D., et al. (2018). The Pfam protein families database in 2019. *Nucleic Acids Research*, 47 (D1): D427-D432. doi: 10.1093/nar/gky995.

Blocker, K. M., Britton, Z. T., Naranjo, A. N., McNeely, P. M., Young, C. L. & Robinson, A. S. (2015). Chapter Eight - Recombinant G Protein-Coupled Receptor Expression in Saccharomyces cerevisiae for Protein Characterization. In Shukla, A. K. (ed.) vol. 556 *Methods in Enzymology*, pp. 165-183: Academic Press.

Braccini, I. & Pérez, S. (2001). Molecular Basis of Ca2+-Induced Gelation in Alginates and Pectins: The Egg-Box Model Revisited. *Biomacromolecules*, 2 (4): 1089-1096. doi: 10.1021/bm010008g.

Cesario, M. T., da Fonseca, M. M. R., Marques, M. M. & de Almeida, M. (2018). Marine algal carbohydrates as carbon sources for the production of biochemicals and biomaterials. *Biotechnol Adv*, 36 (3): 798-817. doi: 10.1016/j.biotechadv.2018.02.006.

Cherubini, F. (2010). The biorefinery concept: Using biomass instead of oil for producing energy and chemicals. *Energy Conversion and Management*, 51 (7): 1412-1421. doi: 10.1016/j.enconman.2010.01.015.

Chojnacki, S., Cowley, A., Lee, J., Foix, A. & Lopez, R. (2017). Programmatic access to bioinformatics tools from EMBL-EBI update: 2017. *Nucleic Acids Res*, 45 (W1): W550-W553. doi: 10.1093/nar/gkx273.

Cooper, A. J., Ginos, J. Z. & Meister, A. (1983). Synthesis and properties of the. alpha.-keto acids. *Chemical Reviews*, 83 (3): 321-358.

Cynkin, M. A. & Ashwell, G. (1960). Uronic Acid Metabolism in Bacteria: IV. PURIFICATION AND PROPERTIES OF 2-KETO-3-DEOXY-d-GLUCONOKINASE IN ESCHERICHIA COLI. *Journal of Biological Chemistry*, 235 (6): 1576-1579.

Davidson, I., Sutherland, I. & Lawson, C. (1977). Localization of O-acetyl groups of bacterial alginate. *Microbiology*, 98 (2): 603-606.

Davidson, I. W., Lawson, C. J. & Sutherland, I. W. (1977). An alginate lysate from Azotobacter vinelandii phage. *J Gen Microbiol*, 98 (1): 223-9. doi: 10.1099/00221287-98-1-223.

Enquist-Newman, M., Faust, A. M., Bravo, D. D., Santos, C. N., Raisner, R. M., Hanel, A., Sarvabhowman, P., Le, C., Regitsky, D. D., Cooper, S. R., et al. (2014). Efficient ethanol production from brown macroalgae sugars by a synthetic yeast platform. *Nature*, 505 (7482): 239-43. doi: 10.1038/nature12771.

Entner, N. & Doudoroff, M. (1952). GLUCOSE AND GLUCONIC ACID OXIDATION OF PSEUDOMONAS SACCHAROPHILA. *Journal of Biological Chemistry*, 196 (2): 853-862.

Ertesvåg, H. (2015). Alginate-modifying enzymes: biological roles and biotechnological uses. *Front Microbiol*, 6: 523. doi: 10.3389/fmicb.2015.00523.

FAO. (2018). *The global status of seaweed production, trade and utilization*, 978-92-5-130870-7. Rome, Italy: Food and Agriculture Organization of the United Nations.

Gacesa, P. (1987). Alginate-modifying enzymes: A proposed unified mechanism of action for the lyases and epimerases. *FEBS Letters*, 212 (2): 199-202. doi: https://doi.org/10.1016/0014-5793(87)81344-3.

Gacesa, P. (1988). Alginates. *Carbohydrate Polymers*, 8 (3): 161-182. doi: https://doi.org/10.1016/0144-8617(88)90001-X.

Garron, M. L. & Cygler, M. (2010). Structural and mechanistic classification of uronic acid-containing polysaccharide lyases. *Glycobiology*, 20 (12): 1547-73. doi: 10.1093/glycob/cwq122.

Gasteiger, E., Hoogland, C., Gattiker, A., Duvaud, S. e., Wilkins, M. R., Appel, R. D. & Bairoch, A. (2005). Protein Identification and Analysis Tools on the ExPASy Server. In *The Proteomics Protocols Handbook*, pp. 571-607.

Gorin, P. A. J. & Spencer, J. F. T. (1966). EXOCELLULAR ALGINIC ACID FROM AZOTOBACTER VINELANDII. *Canadian Journal of Chemistry*, 44 (9): 993-998. doi: 10.1139/v66-147.

Gouet, P. & Robert, X. (2014). Deciphering key features in protein structures with the new ENDscript server. *Nucleic Acids Research*, 42 (W1): W320-W324. doi: 10.1093/nar/gku316.

Govan, J. R. W., Fyfe, J. A. M. & Jarman, T. R. (1981). Isolation of Alginate-producing Mutants of Pseudomonas fluorescens, Pseudomonas putida and Pseudomonas mendocina. *Microbiology*, 125 (1): 217-220. doi: doi:10.1099/00221287-125-1-217.

Grant, G. T., Morris, E. R., Rees, D. A., Smith, P. J. C. & Thom, D. (1973). Biological interactions between polysaccharides and divalent cations: The egg-box model. *FEBS Letters*, 32 (1): 195-198. doi: https://doi.org/10.1016/0014-5793(73)80770-7.

Hashimoto, W., Kawai, S. & Murata, K. (2010). Bacterial supersystem for alginate import/metabolism and its environmental and bioenergy applications. *Bioengineered bugs*, 1 (2): 97-109. doi: 10.4161/bbug.1.2.10322.

Haug, A., Larsen, B., Smidsrød, O., Smidsrød, O., Eriksson, G., Blinc, R., Paušak, S., Ehrenberg, L. & Dumanović, J. (1967). Studies on the Sequence of Uronic Acid Residues in Alginic Acid. *Acta Chemica Scandinavica*, 21: 691-704. doi: 10.3891/acta.chem.scand.21-0691.

He, M., Guo, M., Zhang, X., Chen, K., Yan, J. & Irbis, C. (2018). Purification and characterization of alginate lyase from Sphingomonas sp. ZH0. *Journal of Bioscience and Bioengineering*, 126 (3): 310-316. doi: 10.1016/j.jbiosc.2018.01.017.

Heyraud, A., Colin-Morel, P., Girond, S., Richard, C. & Kloareg, B. (1996). HPLC analysis of saturated or unsaturated oligoguluronates and oligomannuronates. Application to the determination of the action pattern of Haliotis tuberculata alginate lyase. *Carbohydrate Research*, 291: 115-126. doi: https://doi.org/10.1016/S0008-6215(96)00138-3.

Hobbs, J. K., Lee, S. M., Robb, M., Hof, F., Barr, C., Abe, K. T., Hehemann, J. H., McLean, R., Abbott, D. W. & Boraston, A. B. (2016). KdgF, the missing link in the microbial metabolism of uronate sugars from pectin and alginate. *Proc Natl Acad Sci U S A*, 113 (22): 6188-93. doi: 10.1073/pnas.1524214113.

Horn, S. J., Moen, E. & Østgaard, K. (1999). Direct determination of alginate content in brown algae by near infra-red (NIR) spectroscopy. *Journal of Applied Phycology*, 11 (1): 9-13. doi: 10.1023/A:1008024009954.

Horn, S. J. (2009). *Seaweed biofuels : production of biogas and bioethanol from brown macroalgae*. Saarbrücken: VDM Verlag Dr. Müller.

Horn, S. J., Vaaje-Kolstad, G., Westereng, B. & Eijsink, V. G. (2012). Novel enzymes for the degradation of cellulose. *Biotechnology for biofuels*, 5 (1): 45. doi: 10.1186/1754-6834-5-45.

Hreggvidsson, G., Jon Oskar Jonsson, W., Bjornsdottir, B., Fridjonsson, O., Altenbuchner, J., Watzlawick, H., Dobruchowska, J. & P. Kamerling, J. (2015). *Thermostable alginate degrading enzymes and their methods of use*.

Huerta-Cepas, J., Serra, F. & Bork, P. (2016). ETE 3: Reconstruction, Analysis, and Visualization of Phylogenomic Data. *Mol Biol Evol*, 33 (6): 1635-8. doi: 10.1093/molbev/msw046.

Hulo, N., Bairoch, A., Bulliard, V., Cerutti, L., Cuche, B. A., de Castro, E., Lachaize, C., Langendijk-Genevaux, P. S. & Sigrist, C. J. (2008). The 20 years of PROSITE. *Nucleic Acids Res*, 36 (Database issue): D245-9. doi: 10.1093/nar/gkm977.

Inoue, A., Nishiyama, R., Mochizuki, S. & Ojima, T. (2015). Identification of a 4-deoxy-L-erythro-5-hexoseulose uronic acid reductase, FlRed, in an alginolytic bacterium Flavobacterium sp. strain UMI-01. *Mar Drugs*, 13 (1): 493-508. doi: 10.3390/md13010493.

Invitrogen. (2010). *One Shot® BL21(DE3) Competent Cells: Publication nr.: MAN0000662*. User Guide. Available at: https://assets.thermofisher.com/TFS-Assets/LSG/manuals/oneshotbl21_man.pdf.

Invitrogen. (2013). *One Shot® TOP10 Competent Cells: Publication nr.: MAN0000633*. User Guide. Available at: https://assets.thermofisher.com/TFS-Assets/LSG/manuals/oneshottop10_man.pdf.

Islan, G. A., Bosio, V. E. & Castro, G. R. (2013). Alginate Lyase and Ciprofloxacin Co-Immobilization on Biopolymeric Microspheres for Cystic Fibrosis Treatment. *Macromolecular Bioscience*, 13 (9): 1238-1248. doi: 10.1002/mabi.201300134.

Jagtap, S. S., Hehemann, J. H., Polz, M. F., Lee, J. K. & Zhao, H. (2014). Comparative biochemical characterization of three exolytic oligoalginate lyases from Vibrio splendidus reveals complementary substrate scope, temperature, and pH adaptations. *Appl Environ Microbiol*, 80 (14): 4207-14. doi: 10.1128/AEM.01285-14.

Jain, S. & Ohman, D. E. (2005). Role of an alginate lyase for alginate transport in mucoid Pseudomonas aeruginosa. *Infection and immunity*, 73 (10): 6429-6436. doi: 10.1128/IAI.73.10.6429-6436.2005.

Kaur, G., Srivastava, A. K. & Chand, S. (2012). Advances in biotechnological production of 1,3-propanediol. *Biochemical Engineering Journal*, 64: 106-118. doi: https://doi.org/10.1016/j.bej.2012.03.002.

Kim, H. T., Chung, J. H., Wang, D., Lee, J., Woo, H. C., Choi, I.-G. & Kim, K. H. (2012). Depolymerization of alginate into a monomeric sugar acid using Alg17C, an exo-oligoalginate lyase cloned from Saccharophagus degradans 2-40.(Report). *Applied Microbiology and Biotechnology*, 93 (5): 2233. doi: 10.1007/s00253-012-3882-x.

Kumar, A. K. & Sharma, S. (2017). Recent updates on different methods of pretreatment of lignocellulosic feedstocks: a review. *Bioresour Bioprocess*, 4 (1): 7. doi: 10.1186/s40643-017-0137-9.

Lau, M. W. & Dale, B. E. (2009). Cellulosic ethanol production from AFEX-treated corn stover using Saccharomyces cerevisiae 424A(LNH-ST). *Proc Natl Acad Sci U S A*, 106 (5): 1368-73. doi: 10.1073/pnas.0812364106.

Lee, K. Y. & Mooney, D. J. (2012). Alginate: properties and biomedical applications. *Prog Polym Sci*, 37 (1): 106-126. doi: 10.1016/j.progpolymsci.2011.06.003.

Linker, A. & Jones, R. S. (1966). A new polysaccharide resembling alginic acid isolated from pseudomonads. *Journal of Biological Chemistry*, 241 (16): 3845-3851.

Lombard, V., Bernard, T., Rancurel, C., Brumer, H., Coutinho, P. M. & Henrissat, B. (2010). A hierarchical classification of polysaccharide lyases for glycogenomics. *Biochem J*, 432 (3): 437-44. doi: 10.1042/BJ20101185.

Lunin, V. V., Li, Y., Linhardt, R. J., Miyazono, H., Kyogashima, M., Kaneko, T., Bell, A. W. & Cygler, M. (2004). High-resolution crystal structure of Arthrobacter aurescens chondroitin AC lyase: an enzyme-substrate complex defines the catalytic mechanism. *J Mol Biol*, 337 (2): 367-86. doi: 10.1016/j.jmb.2003.12.071.

May, T. B., Shinabarger, D., Maharaj, R., Kato, J., Chu, L., DeVault, J. D., Roychoudhury, S., Zielinski, N. A., Berry, A. & Rothmel, R. K. (1991). Alginate synthesis by Pseudomonas aeruginosa: a key

pathogenic factor in chronic pulmonary infections of cystic fibrosis patients. *Clinical Microbiology Reviews*, 4 (2): 191. doi: 10.1128/CMR.4.2.191.

McHugh, D. J. (2003). *A Guide to the Seaweed Industry*: Food and Agriculture Organization of the United Nations.

McKee, J. W. A., Kavalieris, L., Brasch, D. J., Brown, M. T. & Melton, L. D. (1992). Alginate content and composition ofMacrocystis pyrifera from New Zealand. *Journal of Applied Phycology*, 4 (4): 357-369. doi: 10.1007/BF02185794.

Milledge, J., Smith, B., Dyer, P. & Harvey, P. (2014). Macroalgae-Derived Biofuel: A Review of Methods of Energy Extraction from Seaweed Biomass. *Energies*, 7 (11): 7194-7222. doi: 10.3390/en7117194.

Miyake, O., Hashimoto, W. & Murata, K. (2003). An exotype alginate lyase in Sphingomonas sp. A1: overexpression in Escherichia coli, purification, and characterization of alginate lyase IV (A1-IV). *Protein Expression and Purification*, 29 (1): 33-41. doi: 10.1016/s1046-5928(03)00018-4.

Nakamura, C. E. & Whited, G. M. (2003). Metabolic engineering for the microbial production of 1,3-propanediol. *Current Opinion in Biotechnology*, 14 (5): 454-459. doi: https://doi.org/10.1016/j.copbio.2003.08.005.

Ochiai, A., Hashimoto, W. & Murata, K. (2006). A biosystem for alginate metabolism in Agrobacterium tumefaciens strain C58: molecular identification of Atu3025 as an exotype family PL-15 alginate lyase. *Res Microbiol*, 157 (7): 642-9. doi: 10.1016/j.resmic.2006.02.006.

Ochiai, A., Yamasaki, M., Mikami, B., Hashimoto, W. & Murata, K. (2010). Crystal structure of exotype alginate lyase Atu3025 from Agrobacterium tumefaciens. *J Biol Chem*, 285 (32): 24519-28. doi: 10.1074/jbc.M110.125450.

Park, D., Jagtap, S. & Nair, S. K. (2014). Structure of a PL17 family alginate lyase demonstrates functional similarities among exotype depolymerases. *J Biol Chem*, 289 (12): 8645-55. doi: 10.1074/jbc.M113.531111.

Park, H. H., Kam, N., Lee, E. Y. & Kim, H. S. (2012). Cloning and Characterization of a Novel Oligoalginate Lyase from a Newly Isolated Bacterium Sphingomonas sp. MJ-3. *Marine Biotechnology*, 14 (2): 189-202. doi: 10.1007/s10126-011-9402-7.

Peng, C., Wang, Q., Lu, D., Han, W. & Li, F. (2018). A Novel Bifunctional Endolytic Alginate Lyase with Variable Alginate-Degrading Modes and Versatile Monosaccharide-Producing Properties. *Front Microbiol*, 9: 167. doi: 10.3389/fmicb.2018.00167.

Pindar, D. F. & Bucke, C. (1975). The biosynthesis of alginic acid by <em>Azotobacter vinelandii</em&gt. *Biochemical Journal*, 152 (3): 617. doi: 10.1042/bj1520617.

Pomin, V. H. (2012). *Seaweed : Ecology, Nutrient Composition, and Medicinal Uses*. Earth Sciences in the 21st Century. New York: Nova Science Publishers, Inc.

Preiss, J. & Ashwell, G. (1962a). Alginic acid metabolism in bacteria. I. Enzymatic formation of unsaturated oligosac-charides and 4-deoxy-L-erythro-5-hexoseulose uronic acid. *J Biol Chem*, 237: 309-16.

Preiss, J. & Ashwell, G. (1962b). Alginic Acid Metabolism in Bacteria: II. THE ENZYMATIC REDUCTION OF 4-DEOXY-l-ERYTHRO-5-HEXOSEULOSE URONIC ACID TO 2-KETO-3-DEOXY-d-GLUCONIC ACID. *Journal of Biological Chemistry*, 237 (2): 317-321.

Renewable Fuels Association. (2019). *World Fuel Ethanol Production*. Available at: https://ethanolrfa.org/resources/industry/statistics/#1549569130196-da23898a-53d8.

Roesijadi, G., Jones, S. B., Snowden-Swan, L. J. & Zhu, Y. (2010). *Macroalgae as a Biomass Feedstock: A Preliminary Analysis*, PNNL-19944; Other: BM0204010; TRN: US201106%%96 United States 10.2172/1006310 Other: BM0204010; TRN: US201106%%96 PNNL English: ; Pacific Northwest National Lab. (PNNL), Richland, WA (United States).

Sabra, W., Zeng, A. P. & Deckwer, W. D. (2001). Bacterial alginate: physiology, product quality and process aspects. *Applied Microbiology and Biotechnology*, 56 (3): 315-325. doi: 10.1007/s002530100699.

Schiener, P., Black, K. D., Stanley, M. S. & Green, D. H. (2015). The seasonal variation in the chemical composition of the kelp species Laminaria digitata, Laminaria hyperborea, Saccharina latissima and Alaria esculenta. *Journal of Applied Phycology*, 27 (1): 363-373. doi: 10.1007/s10811-014-0327-1.

Sharma, S. & Horn, S. J. (2016). Enzymatic saccharification of brown seaweed for production of fermentable sugars. *Bioresource Technology*, 213: 155-161. doi: https://doi.org/10.1016/j.biortech.2016.02.090.

Shevchik, V. E., Condemine, G., Robert-Baudouy, J. & Hugouvieux-Cotte-Pattat, N. (1999). The Exopolygalacturonate Lyase PelW and the Oligogalacturonate Lyase Ogl, Two Cytoplasmic Enzymes of Pectin Catabolism in Erwinia chrysanthemi 3937. *Journal of Bacteriology*, 181 (13): 3912.

Shin, J. W., Lee, O. K., Park, H. H., Kim, H. S. & Lee, E. Y. (2015). Molecular characterization of a novel oligoalginate lyase consisting of AlgL- and heparinase II/III-like domains from Stenotrophomonas maltophilia KJ-2 and its application to alginate saccharification. *Korean Journal of Chemical Engineering*, 32 (5): 917-924. doi: 10.1007/s11814-014-0282-1.

Sikorski, P., Mo, F., Skjåk-Bræk, G. & Stokke, B. T. (2007). Evidence for Egg-Box-Compatible Interactions in Calcium−Alginate Gels from Fiber X-ray Diffraction. *Biomacromolecules*, 8 (7): 2098-2103. doi: 10.1021/bm0701503.

Skjåk-Bræk, G., Grasdalen, H. & Larsen, B. (1986). Monomer sequence and acetylation pattern in some bacterial alginates. *Carbohydrate Research*, 154 (1): 239-250. doi: https://doi.org/10.1016/S0008-6215(00)90036-3.

Skjåk-Bræk, G., Zanetti, F. & Paoletti, S. (1989). Effect of acetylation on some solution and gelling properties of alginates. *Carbohydrate Research*, 185 (1): 131-138. doi: 10.1016/0008-6215(89)84028-5.

Smidsrød, O., Haug, A., Lian, B., Huhtikangas, A., Pearson, W. B. & Meisalo, V. (1972). Properties of Poly(1,4-hexuronates) in the Gel State. II. Comparison of Gels of Different Chemical Composition. *Acta Chemica Scandinavica*, 26: 79-88. doi: 10.3891/acta.chem.scand.26-0079.

Stiger-Pouvreau, V., Bourgougnon, N. & Deslandes, E. (2016). Carbohydrates From Seaweeds. In *Seaweed in Health and Disease Prevention*, pp. 223-274.

Sumner, J. B. & Graham, V. A. (1921). DINITROSALICYLIC ACID: A REAGENT FOR THE ESTIMATION OF SUGAR IN NORMAL AND DIABETIC URINE. *Journal of Biological Chemistry*, 47 (1): 5-9.

Suzuki, H., Suzuki, K.-i., Inoue, A. & Ojima, T. (2006). A novel oligoalginate lyase from abalone, Haliotis discus hannai, that releases disaccharide from alginate polymer in an exolytic manner. *Carbohydrate Research*, 341 (11): 1809-1819. doi: https://doi.org/10.1016/j.carres.2006.04.032.

Szekalska, M., Puciłowska, A., Szymańska, E., Ciosek, P. & Winnicka, K. (2016). Alginate: Current Use and Future Perspectives in Pharmaceutical and Biomedical Applications. *International Journal of Polymer Science*, 2016: 1-17. doi: 10.1155/2016/7697031.

Takagi, T., Sasaki, Y., Motone, K., Shibata, T., Tanaka, R., Miyake, H., Mori, T., Kuroda, K. & Ueda, M. (2017). Construction of bioengineered yeast platform for direct bioethanol production from alginate and mannitol. *Appl Microbiol Biotechnol*, 101 (17): 6627-6636. doi: 10.1007/s00253-017-8418-y.

Thomas, F., Lundqvist, L. C. E., Jam, M., Jeudy, A., Barbeyron, T., Sandström, C., Michel, G. & Czjzek, M. (2013). Comparative characterization of two marine alginate lyases from Zobellia galactanivorans reveals distinct modes of action and exquisite adaptation to their natural substrate. *The Journal of biological chemistry*, 288 (32): 23021. doi: 10.1074/jbc.M113.467217.

Tihlárik, K. & Babor, K. (1983). Determination of carboxyl groups in the starch oxidized by nitrogen dioxide.

Trifinopoulos, J., Nguyen, L. T., von Haeseler, A. & Minh, B. Q. (2016). W-IQ-TREE: a fast online phylogenetic tool for maximum likelihood analysis. *Nucleic Acids Res*, 44 (W1): W232-5. doi: 10.1093/nar/gkw256.

Umare, S. S., Chandure, A. S. & Pandey, R. A. (2007). Synthesis, characterization and biodegradable studies of 1,3-propanediol based polyesters. *Polymer Degradation and Stability*, 92 (3): 464-479. doi: https://doi.org/10.1016/j.polymdegradstab.2006.10.007.

USDA. (2019). *USDA Agricultural Projections to 2028*. Agriculture, U. S. D. o.

von Heijne, G. (1990). The signal peptide. *The Journal of Membrane Biology*, 115 (3): 195-201. doi: 10.1007/BF01868635.

Vuoristo, K. S., Fredriksen, L., Oftebro, M., Arntzen, M. Ø., Aarstad, O. A., Stokke, R., Steen, I. H., Hansen, L. D., Schüller, R. B., Aachmann, F. L., et al. (2019). Production, Characterization, and Application of an Alginate Lyase, AMOR_PL7A, from Hot Vents in the Arctic Mid-Ocean Ridge. *Journal of Agricultural and Food Chemistry*, 67 (10): 2936-2945. doi: 10.1021/acs.jafc.8b07190.

VWR. (2013). *VWR Red Taq DNA Polymerase Master Mix: Cat. No.: 733-2131*. User Guide. Available at: https://dk.vwr.com/assetsvc/asset/da_DK/id/12367515/contents.

Wang, D., Kim, D. H. & Kim, K. H. (2016). Effective production of fermentable sugars from brown macroalgae biomass. *Applied Microbiology and Biotechnology*, 100 (22): 9439-9450. doi: 10.1007/s00253-016-7857-1.

Wang, D., Aarstad, O. A., Li, J., McKee, L. S., Saetrom, G. I., Vyas, A., Srivastava, V., Aachmann, F. L., Bulone, V. & Hsieh, Y. S. (2018). Preparation of 4-Deoxy-L-erythro-5-hexoseulose Uronic Acid (DEH) and Guluronic Acid Rich Alginate Using a Unique exo-Alginate Lyase from Thalassotalea crassostreae. *J Agric Food Chem*, 66 (6): 1435-1443. doi: 10.1021/acs.jafc.7b05751.

Wang, L., Li, S., Yu, W. & Gong, Q. (2015). Cloning, overexpression and characterization of a new oligoalginate lyase from a marine bacterium, Shewanella sp. *Biotechnol Lett*, 37 (3): 665-71. doi: 10.1007/s10529-014-1706-z.

Wang, M., Chen, L., Zhang, Z., Wang, X., Qin, S. & Yan, P. (2017). Screening of alginate lyase-excreting microorganisms from the surface of brown algae. *AMB Express*, 7 (1): 74. doi: 10.1186/s13568-017-0361-x.

Wargacki, A. J., Leonard, E., Win, M. N., Regitsky, D. D., Santos, C. N., Kim, P. B., Cooper, S. R., Raisner, R. M., Herman, A., Sivitz, A. B., et al. (2012). An engineered microbial platform for direct biofuel production from brown macroalgae. *Science*, 335 (6066): 308-13. doi: 10.1126/science.1214547.

Wong, T. Y., and, L. A. P. & Schiller, N. L. (2000). Alginate Lyase: Review of Major Sources and Enzyme Characteristics, Structure-Function Analysis, Biological Roles, and Applications. *Annual Review of Microbiology*, 54 (1): 289-340. doi: 10.1146/annurev.micro.54.1.289.

Xiao, W., Wang, R.-S., Handy, D. E. & Loscalzo, J. (2018). NAD(H) and NADP(H) Redox Couples and Cellular Energy Metabolism. *Antioxidants & redox signaling*, 28 (3): 251-272. doi: 10.1089/ars.2017.7216.

Yim, H., Haselbeck, R., Niu, W., Pujol-Baxley, C., Burgard, A., Boldt, J., Khandurina, J., Trawick, J. D., Osterhout, R. E., Stephen, R., et al. (2011). Metabolic engineering of Escherichia coli for direct production of 1,4-butanediol. *Nat Chem Biol*, 7 (7): 445-52. doi: 10.1038/nchembio.580.

Yip, V. L. & Withers, S. G. (2006). Breakdown of oligosaccharides by the process of elimination. *Curr Opin Chem Biol*, 10 (2): 147-55. doi: 10.1016/j.cbpa.2006.02.005.

Yoon, H. J., Hashimoto, W., Miyake, O., Okamoto, M., Mikami, B. & Murata, K. (2000). Overexpression in Escherichia coli, purification, and characterization of Sphingomonas sp. A1 alginate lyases. *Protein Expr Purif*, 19 (1): 84-90. doi: 10.1006/prep.2000.1226.

Zhu, B. & Yin, H. (2015). Alginate lyase: Review of major sources and classification, properties, structure-function analysis and applications. *Bioengineered*, 6 (3): 125-31. doi: 10.1080/21655979.2015.1030543.

Zhu, X.-H., Lu, M., Lee, B.-Y., Ugurbil, K. & Chen, W. (2015). In vivo NAD assay reveals the intracellular NAD contents and redox state in healthy human brain and their age dependences. *Proceedings of the National Academy of Sciences of the United States of America*, 112 (9): 2876-2881. doi: 10.1073/pnas.1417921112.

Zhu, Y., Wu, L., Chen, Y., Ni, H., Xiao, A. & Cai, H. (2016). Characterization of an extracellular biofunctional alginate lyase from marine Microbulbifer sp. ALW1 and antioxidant activity of enzymatic hydrolysates. *Microbiol Res*, 182: 49-58. doi: 10.1016/j.micres.2015.09.004.

Øverland, M. & Skrede, A. (2017). Yeast derived from lignocellulosic biomass as a sustainable feed resource for use in aquaculture. *Journal of the Science of Food and Agriculture*, 97 (3): 733-742. doi: 10.1002/jsfa.8007.

Appendix

Appendix A: Multiple sequence alignment

Figure 25 shows an alignment of Apl17-2 and all characterized PL17, subfamily 2 enzymes from the CAZY database (March 31, 2019). The residues that are mutated inY251A and Y446A are indicated by blue dots on the underside of the alignment. The sties of mutation do not correspond with the numbers in the alignment because of gaps in the alignment.

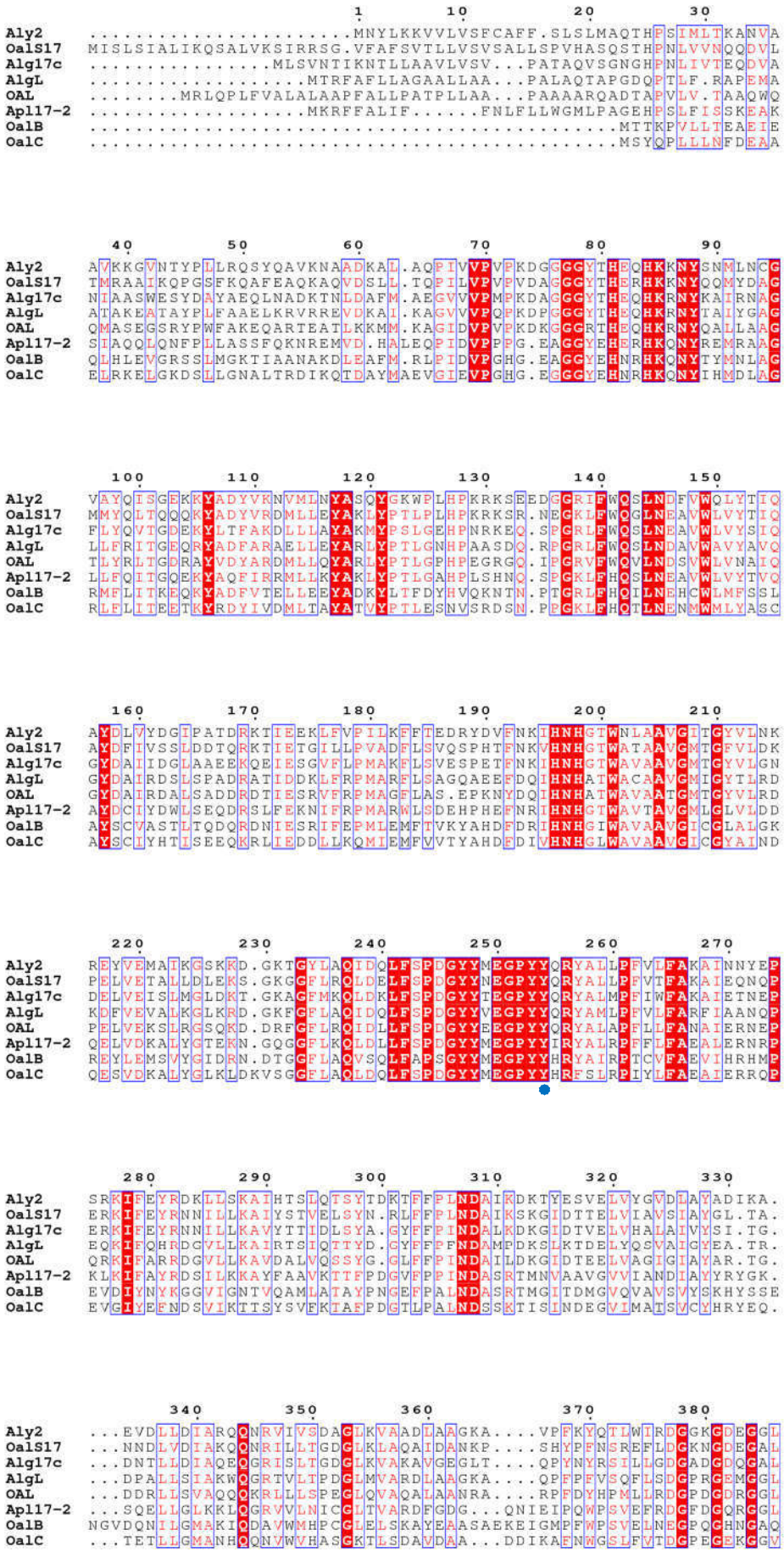
Aly2
OalS17
Alg17c
AlgL
OAL
Apl17-2
OalB
OalC

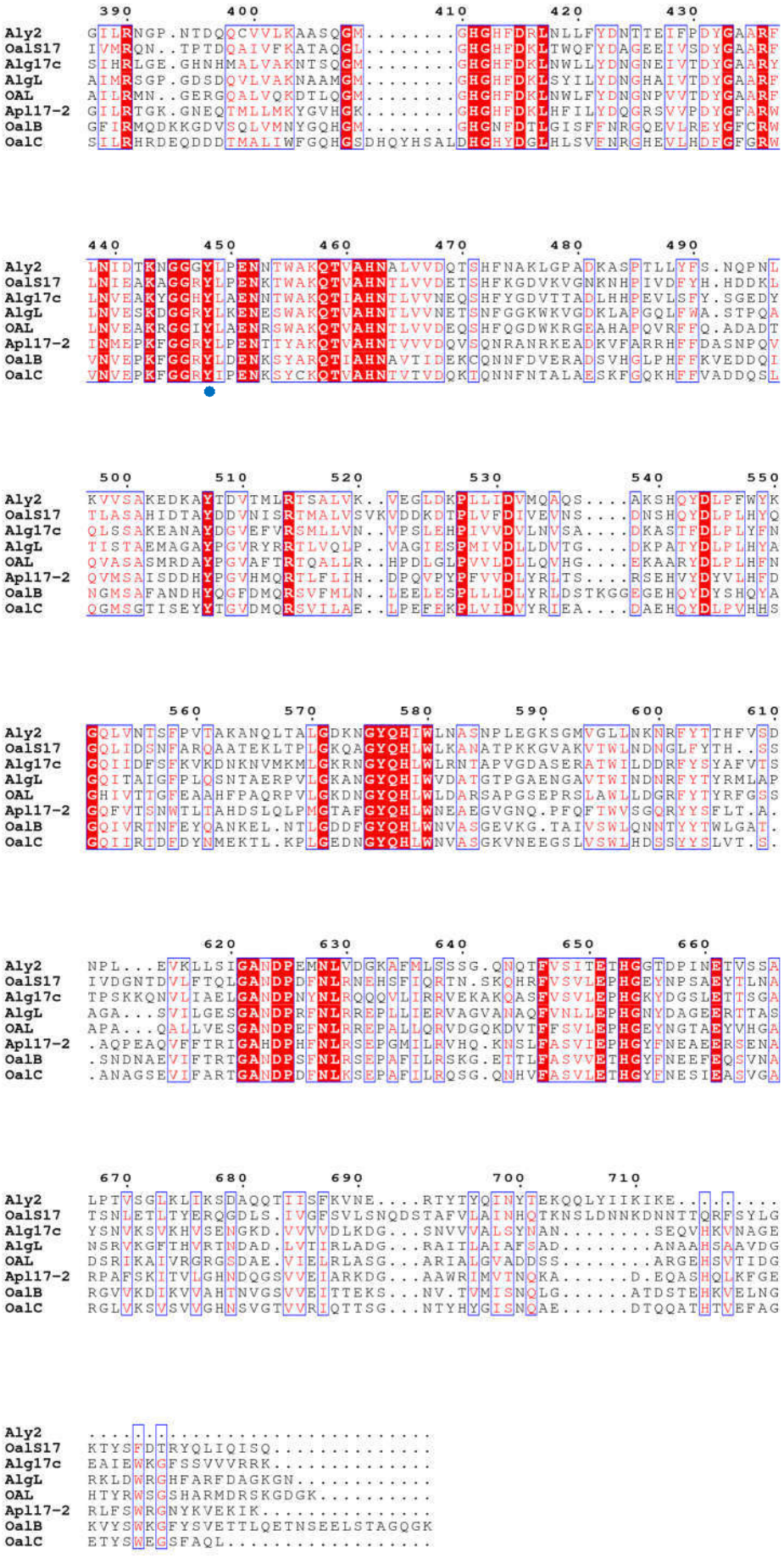
390 400 410 420 430
Aly2 GILRNGP.NTDQQCVVLKAASQGM.....GHGHFDRLNLLFYDNTTEIFPDYGAARF
OalS17 IVMRQN..TPTDQAIVFKATAQGL.....GHGHFDKLTWQFYDAGEEIVSDYGAARF
Alg17c SIHRLGE.GHNHMALVAKNTSQGM.....GHGHFDKLNWLLYDNGNEIVTDYGAARY
AlgL AIMRSGP.GDSDQVLVAKNAAMGM.....GHGHFDKLSYILYDNGHAIVTDYGAARF
OAL AIIRMN..GERGQALVQKDTLQGM.....GHGHFDKLNWLFYDNGNPVVTDYGAARF
Apl17-2 GIIRTGK.GNEQTMLLMKYGVHGK.....GHGHFDKLHFILYDQGRSVVPDYGFARW
OalB GFIRMQDKKGDVSQLVMNYGQHGM.....GHGNFDILGISFFNRGQEVLREYGFCRW
OalC SILRHRDEQDDDTMALIWFGQHGSDHQYHSALDHGHYDGLHLSVFNRGHEVLHDFGFGRW
440 450 460 470 480 490
Aly2 LNIDTKNGGGYLPENNTWAKQTVAHNALVVDQTSHFNAKLGPADKASPTLLYFS.NQPNL
OalS17 LNIEAKAGGRYLPENKTWAKQTVAHNTLVVDETSHFKGDVKVGNKNHPIVDFYH.HDDKL
Alg17c LNVEAKYGGHYLAENNTWAKQTIAHNTLVVNEQSHFYGDVTTADLHHPEVLSFY.SGEDY
AlgL LNVESKDGGRYLKENESWAKQTVAHNTLVVNETSNFGGKWKVGDKLAPGQLFWA.STPQA
OAL LNVEAKRGGIYLAENRSWAKQTVAHNTLVVDEQSHFQGDWKRGEAHAPQVRFFQ.ADADT
Apl17-2 INMEPKFGGRYLPENTTYAKQTVAHNTVVVDQVSQNRANRKEADKVFARRHFFDASNPQV
OalB VNVEPKFGGRYLDENKSYARQTIAHNAVTIDEKCQNNFDVERADSVHGLPHFFKVEDDQI
OalC VNVEPKFGGRYIPENKSYCKQTVAHNTVTVDQKIQNNFNTALAESKFGQKHFFVADDQSL
500 510 520 530 540 550
Aly2 KVVSAKEDKAYTDVTMLRTSALVK..VEGLDKPLLIDVMQAQS....AKSHQYDLPFWYK
OalS17 TLASAHIDTAYDDVNISRTMALVSVKVDDKDTPLVFDIVEVNS....DNSHQYDLPLHYQ
Alg17c QLSSAKEANAYDGVEFVRSMLLVN..VPSLEHPIVVDVLNVSA....DKASTFDLPLYFN
AlgL TISTAEMAGAYPGVRYRRTLVQLP..VAGIESPMIVDLLDVTG....DKPATYDLPLHYA
OAL QVASASMRDAYPGVAFTRTQALLR..HPDLGLPVVLDLLQVHG....EKAARYDLPLHFN
Apl17-2 QVMSAISDDHYPGVHMQRTLFLIH..DPQVPYPFVVDLYRLTS....RSEHVYDYVLHFD
OalB NGMSAFANDHYQGFDMQRSVFMLN..LEELESPLLLDLYRLDSTKGGEGEHQYDYSHQYA
OalC QGMSGTISEYYTGVDMQRSVILAE..LPEFEKPLVIDVYRIEA....DAEHQYDLPVHHS
560 570 580 590 600 610
Aly2 GQLVNTSFPVTAKANQLTALGDKNGYQHIWLNASNPLEGKSGMVGLLNKNRFYTTHFVSD
OalS17 GQLIDSNFARQAATEKLTPLGKQAGYQHLWLKANATPKKGVAKVTWLNDNGLFYTH..SS
Alg17c GQIIDFSFKVKDNKNVMKMLGKRNGYQHLWLRNTAPVGDASERATWILDDRFYSYAFVTS
AlgL GQITAIGFPLQSNTAERPVLGKANGYQHIWVDATGTPGAENGAVTWINDNRFYTYRMLAP
OAL GHIVTTGFEAAHFPAQRPVLGKDNGYQHLWLDARSAPGSEPRSLAWLLDGRFYTYRFGSS
Apl17-2 GQFVTSNWTLTAHDSLQLPMGTAFGYQHLWNEAEGVGNQ.PFQFTWVSGQRYYSFLT.A.
OalB GQIVRTNFEYQANKEL.NTLGDDFGYQHLWNVASGEVKG.TAIVSWLQNNTYYTWLGAT.
OalC GQIIRTDFDYNMEKTL.KPLGEDNGYQHLWNVASGKVNEEGSLVSWLHDSSYYSLVT.S.
620 630 640 650 660
Aly2 NPL...EVKLLSIGANDPEMNLVDGKAFMLSSSG.QNQTFVSITEIHGGTDPINETVSSA
OalS17 IVDGNTDVLFTQLGANDPDFNLRNEHSFIQRTN.SKQHRFVSVLEPHGEYNPSAEYTLNA
Alg17c TPSKKQNVLIAELGANDPNYNLRQQQVLIRRVEKAKQASFVSVLEPHGKYDGSLETTSGA
AlgL AGA...SVILGESGANDPRFNLRREPLLIERVAGVANAQFVNLLEPHGNYDAGEERTTAS
OAL APA...QALLVESGANDPEFNLRREPALLQRVDGQKDVTFFSVLEPHGEYNGTAEYVHGA
Apl17-2 .AQPEAQVFFTRIGAHDPHFNLRSEPGMILRVHQ.KNSLFASVIEPHGYFNEAEERSENA
OalB .SNDNAEVIFTRTGANDPSFNLRSEPAFILRSKG.ETTLFASVVETHGYFNEEFEQSVNA
OalC .ANAGSEVIFARTGANDPDFNLKSEPAFILRQSG.QNHVFASVLETHGYFNESIEASVGA
670 680 690 700 710
Aly2 LPTVSGLKLIKSDAQQTIISFKVNE....RTYTYQINYTEKQQLYIIKIKE..........
OalS17 TSNLETLTYERQGDLS.IVGFSVLSNQDSTAFVLAINHQTKNSLDNNKDNNTTQRFSYLG
Alg17c YSNVKSVKHVSENGKD.VVVVDLKDG...SNVVVALSYNAN.........SEQVHKVNAGE
AlgL NSRVKGFTHVRTNDAD.LVTIRLADG...RAITLAIAFSAD.........ANAAHSAAVDG
OAL DSRIKAIVRGRGSDAE.VIELRLASG...ARIALGVADDSS.........ARGEHSVTIDG
Apl17-2 RPAFSKITVLGHNDQGSVVEIARKDG...AAWRIMVTNQKA.......D.EQASHQLKFGE
OalB RGVVKDIKVVAHTNVGSVVEITTEKS...NV.TVMISNQLG.......ATDSTEHKVELNG
OalC RGLVKSVSVVGHNSVGTVVRIQTTSG...NTYHYGISNQAE.......DTQQATHTVEFAG
Aly2 ....
OalS17 KTYSFDTRYQLIQISQ..............
Alg17c EAIEWKGFSSVVVRRK..............
AlgL RKLDWRGHFARFDAGKGN............
OAL HTYRWSGSHARMDRSKGDGK..........
Apl17-2 RLFSWRGNYKVEKIK..............
OalB KVYSWKGFYSVETTLQETNSEELSTAGQGK
OalC ETYSWEGSFAQL................

Figure 25: **Multiple sequence alignment of Apl17-2 and other PL17 enzymes.** The figure shows the alignment of Apl17-2 and all characterized PL17 subfamily 2 enzymes from the CAZY database (31.3.2019). Clustal Omega and ESPript were used to create the alignment.

Appendix B: Enzyme production and purification

Figure 27 displays gels from SDS-PAGE analysis of purified WT- and mutant proteins of Apl17-2.

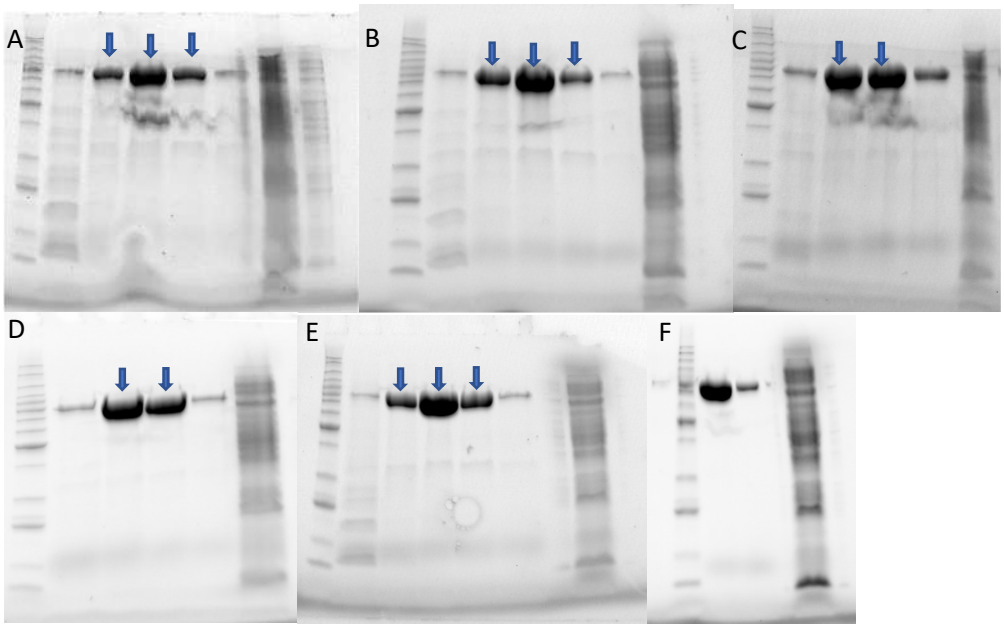

Figure 26: **SDS-PAGE of purified WT Apl17-2, Y251A and Y446A.** All parts of the figure except for part F show SDS-PAGE of fractions of purified protein. The ladder is in the leftmost column and the flow-through from sample application during purification is on rightmost column in every picture. Arrows indicate what fractions were selected. (A) Part 1 of 2 of the first WT enzyme purification. (B) Part 2/2 of the first enzyme purification. A and B were combined into a single solution. (C) The second batch of purified WT enzyme. (D) Third batch of purified WT enzyme. (E) Purified Y251A. (F) Purified Y446A that had already been fractionated and collected. The two bars of samples are different dilutions.

Appendix C: Calculations of enzymatic products

Method 1)

The method shown in this section was used to calculate product yields from activity assays. It is based on first determining the #mol of monomer units in the available substrate, which equals the theoretical #mol of potential glucose equivalents (GE) and converting #mol glucose to mass of glucose, and finally relate the obtained GE value (mg/mL) from a measured sample to the theoretical maximum amount of glucose (mg/mL):

The glucose-based standard curve was always used to convert from measured absorption (540 nm) of the samples to glucose equivalents (GE). The following is an example of a yield calculation:

Example values:

Substrate in reaction mix = 5 mg/mL * 0.1mL = 0.5 mg

Obtained GE from measured sample = 0.85 mg/mL * 0.1 mL = 0.085 mg

#mol monomer units in the substrate = $n_{\Delta} = \frac{m}{M_{w,\Delta}} = \frac{5*10^{-4}\ g}{175.03\ g/mol} = 2.857 * 10^{-6}\ mol$

Mass of the theoretical glucose: $m_{glucose} = 2.857 * 10^{-6}\ mol * 180.156\ g/mol = 5.1 * 10^{-4}\ g$

Maximal amount of obtainable GE 5 mg/mL substrate = 0.51 mg

Given for example GE = 0.085 mg, this equates to 0.085/0.51 *100% = 16.7% yield.

Method 2)

Method 2 determines the mass of the amount of product produced and compares it to the mass of the available substrate. This is possible without further adjustments, since the mass of the product and the mass of the monomeric units within the polymer chain is the same: 173.03 g/mol.

Given an example value of 0.85 mg/mL GE and 0.5% (w/v) available substrate, the conversion from GE to the immediate enzymatic product Δ would be done as follows:

Substrate in reaction mix = 5 mg/mL * 0.1mL = 0.5 mg

Obtained GE from measured sample = 0.85 mg/mL * 0.1 mL = 0.085 mg

$n_{gluc} = \frac{m}{M_{w,gluc}} = \frac{0.085 * 10^{-3}\ g}{180.156\ g/mol} = 4.72 * 10^{-7}$ mol glucose, assumption: $n_{gluc} = n_{\Delta}$

$m_{\Delta} = n_{\Delta} * M_{w,\Delta} = 4.72 * 10^{-7}$ mol * 175.03 g/mol $= 8.26 * 10^{-5}$ g Δ = 0.0826 mgΔ.

converted substrate/available substrate = $\frac{0.0826mg}{0.5mg} * 100\% = \underline{16.5\%}$

Appendix E: Protparam for WT and mutants

Theoretical parameters for all enzyme variants was estimated by protparam (Gasteiger et al., 2005). Selected parameters are listed in Table 18 for all enzyme variants of Apl17-2.

Table 18: Protparam for all proteins used in this study in addition to the wild-type sequence of Apl17-2. *Please note that the protein that is called WT Apl17-2 here is the actual WT, while the enzyme often referred to as WT Apl17-2 elsewhere in this thesis is the PRC-product with His-tag and no signal peptide.*

Protein	#Residues	M_w [kDa]	Extinction coeff. (ε)	pI
WT Apl17-2	729	83.6	116785	8.57
Apl17-2 PCR-product	719	82.3	111285	8.18
Y251A	719	82.3	109795	8.18
Y446A	719	82.3	109795	8.18

Appendix F: Base-induced colour change of reaction mixtures of Apl17-2 with sodium alginate

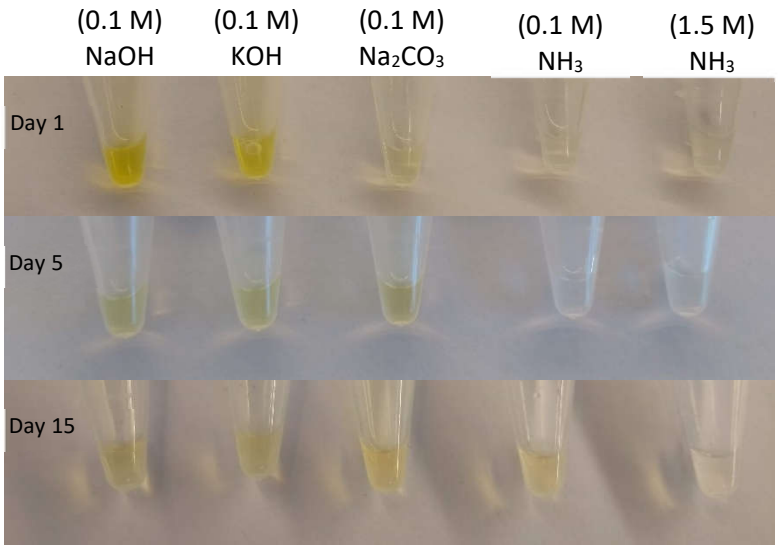

Figure 27: **Photographs of reaction mixtures of Apl17-2 with sodium alginate containing different bases.** Each reaction mixture contained one base as indicated over the photographs. The concentrations of the bases after being added to the reaction solutions are shown in parenthesis over the respective bases. The pH values of the reaction mixtures after addition of base were: 13.5, 13.5, 11.5, 10.0 and 11.5 from left to right. The panel labelled "day 1" show the reaction mixtures ca. 5 minutes after addition of the bases. The reaction conditions were 1 µM Apl17-2, 0.5% (w/v) sodium alginate, 25 mM NaOAc, 300 mM NaCl, pH 5.6 and 50 °C. Reaction mixtures were incubated for 1 hour before adding the respective bases to terminate the reactions.

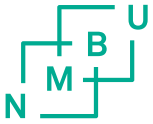

Norges miljø- og biovitenskapelige universitet
Noregs miljø- og biovitskapelege universitet
Norwegian University of Life Sciences

Postboks 5003
NO-1432 Ås
Norway